THE EFFECTS OF RUBBER MODIFICATION ON FRICTION AND WEAR OF EPOXY NETWORKS

by

Majid R. Chitsaz-Zadeh

Dissertation submitted to the Faculty of the
Virginia Polytechnic Institute and State University
in partial fulfillment of the requirements for the degree of

DOCTOR OF PHILOSOPHY

in

Mechanical Engineering

APPROVED:

N. S. Eiss, Jr., Chairman

C. W. Smith

H. H. Mabie

R. A. Heller

R. G. Mitchiner

August, 1987
Blacksburg, Virginia

THE EFFECTS OF RUBBER MODIFICATION ON FRICTION AND WEAR OF EPOXY NETWORKS

by

Majid R. Chitsaz-Zadeh

Committee Chairman: N. S. Eiss, Jr.
Mechanical Engineering

(ABSTRACT)

An epoxy resin (Epon 828) was chemically modified with two different elastomers, poly(dimethyl-co-diphenyl) siloxane (PSX) and carboxyl-terminated butadiene-acrylonitrile (CTBN), to enhance its fracture toughness. The friction and wear of specimens modified with different amounts of elastomer were investigated in a pin-on-disk wear machine. An attempt was made to correlate the fracture toughness of the epoxy material to its fatigue wear rate for experiments in which a steel ball was sliding on a modified epoxy disk. A different type of experiment, modified epoxy pin sliding on abrasive disk, was performed to detect whether abrasive wear of modified epoxies responds differently than fatigue wear to the fracture toughness. Other experiments were performed in which the wear debris produced during sliding was blown out of the interface to study its influence on friction and wear behavior. The effect of surface morphology on friction and wear was also studied.

The results indicated that a marked improvement in fracture toughness was achieved for samples with higher elastomer content. Regardless of the type of the experiment, epoxy pin-on-abrasive disk or

steel ball-on-epoxy disk, wear rates correlated positively with inverse of fracture toughness. Both friction coefficient and wear rate were found to be influenced by the removal of the wear debris, especially for samples with higher elastomer content. The friction coefficient was reduced for samples with higher elastomer content and this was attributed to the low surface energy of the elastomer. CTBN-modified epoxies exhibited lower friction coefficient than epoxies modified with polysiloxane. It was found that sample morphology had significant effect on both friction coefficient and wear rate; the sample with approximately the same domain size but the least number of elastomeric domains exhibited the highest friction coefficient and the highest wear rate.

DEDICATION

This dissertation is dedicated to the memory of my dear father

.

ACKNOWLEDGEMENT

I am indebted to thank Dr. Norman Eiss, chairman of my committee and employer for the past five years. His patience, availability, and guidance exceeded all reasonable expectations. It is through him that I have learned the proper techniques and methods of scientific research.

I express my deep appreciation to Drs. H. H. Mabie, C. W. Smith, R. A. Heller, and R. G. Mitchiner for serving on my advisory committee. I am grateful to Dr. L. D. Mitchell for his time and service on my final defense. Special thanks goes to Drs. G. L. Wilkes and J. E. McGrath, co-principal investigators of the modified epoxy research, for their valuable advice and suggestions concerning the chemical aspects of this research. I sincerely thank J. E. Cecere for preparation and supply of the epoxy specimens. Dr. G. T. Adel is also thanked for his help and suggestions concerning the image processing system.

This research would have not been possible without the financial support of the Office of Naval Research. I am also grateful for the financial support of the National Aeronautics and Space Administration and the U.S. Army Research Office for other projects throughout my graduate studies.

A fond thanks to my mother for her continued support and encouragement throughout my college career. Last but not certainly the least, I extend my special thanks to my wife, Parivash, for the support, encouragement and endurance of this endeavor.

TABLE OF CONTENTS

TABLE OF CONTENTS (Con't)

LIST OF FIGURES

LIST OF FIGURES (Con't)

LIST OF FIGURES (Con't)

LIST OF TABLES

LIST OF TABLES (Con't)

1. INTRODUCTION

Since the first epoxy resin patents were granted in the 1930's and 1940's, properties of epoxy resins such as excellent chemical and corrosion resistance, good adhesion, high modulus and strength, and good electrical insulation have been utilized in many applications [1,2].* These include coatings, adhesives, and laminates.

Current demands for so-called high performance materials has heightened interest in epoxy resins as structural adhesives and as matrix resins for high-strength composites. Both of these applications take advantage of the outstanding strength and modulus and generally good adhesion of the resins. However, such uses also require good fracture resistance and impact strength, properties which epoxy resins do not generally exhibit [3].

The use of epoxy materials is not limited to structural adhesives, coatings, and laminates. Because of their good dimensional stability, high mechanical strength, and good corrosion resistance, epoxy resins are good candidates for mechanical components in which sliding occurs such as bushings and bearings, which were previously made of metals. In these applications, the tribological performance of epoxies is of great importance.

Mechanical components, in which two contacting surfaces are smooth and loaded cyclically, sometimes wear and eventually fail by a process known as delamination wear [4]. Cyclic loading causes either subsurface

*Numbers in brackets refer to references at the end of the dissertation.

or surface cracks or both to nucleate and propagate through the material. The subsurface crack propagation can lead to the formation of a sheet which delaminates from the material. Since the crack growth per stress cycle and the number of stress cycles are features which control the rate of particle delamination, one can expect that increasing resistance to crack growth increases the wear life of a given material.

Although epoxy resins have many good properties, they have poor resistance to crack propagation since they are highly cross-linked thermosets. In order to suppress this undesirable property, elastomeric modifiers can be introduced into the final glassy matrix to enhance their fracture toughness. Extensive body of literature shows that two popular types of elastomers, carboxyl- and amine-terminated butadiene acrylonitrile (CTBN and ATBN) have been used to toughen epoxy without causing appreciable loss in the mechanical properties [5-10].

CTBN and ATBN elastomers have relatively high glass transition temperatures which limits their low temperature flexibility; their highly unsaturated structure makes them unsuitable for use at elevated temperatures [11,12]. Siloxane elastomers present a rather attractive alternative to the butadiene acrylonitrile (BTN) elastomers most often used for epoxy modification. Poly(dimethyl-co-diphenyl siloxane) elastomers exhibit glass transition temperatures well below those of BTN modifiers (-120°C vs. -40°C) and also display very good thermal stability [13,14]. Other favorable and potentially useful properties include good weatherability, oxidative stability, and moisture resistance.

The non-polar nature and low surface energy of polysiloxanes constitute a thermodynamic driving force which causes migration of the polysiloxane to the air-polymer surface during curing. Such migration is believed to lead to the formation of a hydrophobic and chemically bound surface coating [15]. Knowledge of this slippery surface layer has led to the investigation of the tribological properties of siloxane-modified epoxy resins [16,17].

Friction and wear are known to be functions of surface energy, toughness, and fatigue [18]. Fatigue itself is a function of contact stress and elastic modulus. Surface energy and toughness depend on various factors such as percent of siloxane in the epoxy and sample morphology.

Although fatigue wear generally takes place at the surface, it is somewhat influenced by the fatigue properties of the bulk [19]. Fatigue involves crack formation and crack propagation, therefore, it is a fracture process.

One of the purposes of this research is to study the effects of fracture toughness on fatigue wear of modified epoxies. Another purpose of this research is to investigate whether the effect of fracture toughness on wear will be the same, if a different type of test is performed. A third objective is to perform experiments in which the produced wear debris is blown out of the wear track to test the hypothesis that the debris changed the predominant wear mechanism from fatigue to abrasive thereby caused a higher wear rate.

Researchers have shown that friction coefficient is influenced by surface energy. Siloxane modifiers have very low surface energy. Thus, tests are performed to determine the effect of siloxane content in the epoxy on friction behavior of modified epoxy networks. Finally, the effect of surface morphology on tribological responses of the modified epoxies is to be determined.

2. LITERATURE REVIEW

2.1 General Properties

The use of structural adhesives and fiber composites in aircraft, guided weapons, ships, and vehicle construction has increased markedly in the last decade and this dramatic growth rate shows every sign of continuing in the future. Epoxy resins, one type of thermosetting polymer, is widely employed as an adhesive and as the matrix material for glass and carbon-fiber composites.

Preparation of an epoxy resin consists of mixing the resin and hardener, usually at low temperatures, to form a homogeneous solution. The curing time depends on the compositions of the epoxy and hardener and the temperature. Once cured, epoxy resins are highly cross-linked, amorphous thermoset polymers. In spite of their favorable mechanical and structural properties, epoxy resins are usually brittle (because of their high cross-link density) and consequently have limited utility in applications requiring high impact and fracture toughness.

Several methods have been proposed to increase the fracture toughness of epoxies and one of the most successful involves the incorporation of elastomeric modifiers into the uncured epoxy resins. The incorporation of elastomers is done in a two step procedure. First, a solution of elastomer-epoxy is synthesized by reacting the epoxy resin with the elastomer under vacuum (elastomer is dissolved in the epoxy). A curing agent is then added to this solution. The mixture of epoxy/elastomer/hardener is then poured into a mold and is cured in an

oven. The cured rubber-modified epoxy will then exhibit a two-phase microstructure consisting of relatively small rubbery particles dispersed in, and bonded to, a matrix of an epoxy. This microstructure causes an increase in toughness compared to that of the unmodified matrix. Because the matrix contains relatively little rubber (5-15%), there is only a minimal reduction in other important properties such as modulus and mechanical strength.

2.2 Fracture Toughness

The primary objective of rubber modification is the enhancement of fracture toughness with little sacrifice in other properties.

The first progress towards a fundamental understanding of rubber toughening epoxies came in the late 1960's. At that time McGarry [5,6] demonstrated that fracture toughness could be improved significantly by incorporating 5 to 15 percent CTBN (carboxyl-terminated butadiene) in epoxy resin. In this early work, Sultan and McCarry [7] claimed that a small particle size induced shear yielding while a larger particle size encouraged crazing. Riew, Row, and Siebert [8] agreed with this view in rubber-toughened epoxies, although they did not observe "fibrous" crazes similar to those identified in thermoplastics.

Only a few reports of crazing in epoxies published in literature have been supported by microscopic evidence. On the whole, it is now accepted that crazing, at least as it occurs in thermoplastics, is not active in failure mechanisms of structural epoxy resins. Donald and Kramer [9] have suggested that limited crazing occurs in thermoplastics

that have a low molecular weight between chain entanglements. On the basis of Donald and Kramer's proposal, crazing is not to be expected in fully cured epoxy resins which also have low molecular weight constituents between cross-links [10].

Kinloch, Shaw, Tod, and Hunston [20] investigated the fracture behavior of bisphenol A diglycidyl ether (DGEBA) epoxy resin modified with CTBN rubber. They determined the critical stress intensity factor, K_{Ic}, for the initiation of crack growth from compact tension specimens machined from molded sheet of materials (ASTM E399-72). Figure 1 demonstrates the compact tension and three-point bend specimens, two common LEFM (Linear Elastic Fracture Mechanics) sample geometries. Their experiments were conducted over a broad range of temperature from -80°C to 60°C. Their data shows that at 20°C the critical stress intensity factor, K_{Ic}, for the unmodified epoxy is about 1 $MN \cdot m^{-3/2}$. Upon modification with 15 percent (by weight) of CTBN rubber, K_{Ic} increases significantly to 2.7 $MN \cdot m^{-3/2}$. The increase in fracture toughness is much higher at elevated temperatures.

Levita, Marchetti, and Butta [21], have studied the effect of the temperature of cure on the fracture toughness and mechanical properties of the ATBN-modified epoxies. They reported that at a curing temperature of 10°C the addition of rubber, up to 4 percent, does not make any significant change in the fracture toughness. However, when curing temperature was raised to 120°C, there was a significant increase in fracture toughness even at 5 percent rubber. Typical values of critical stress intensity factors, for 10 percent rubber, range from

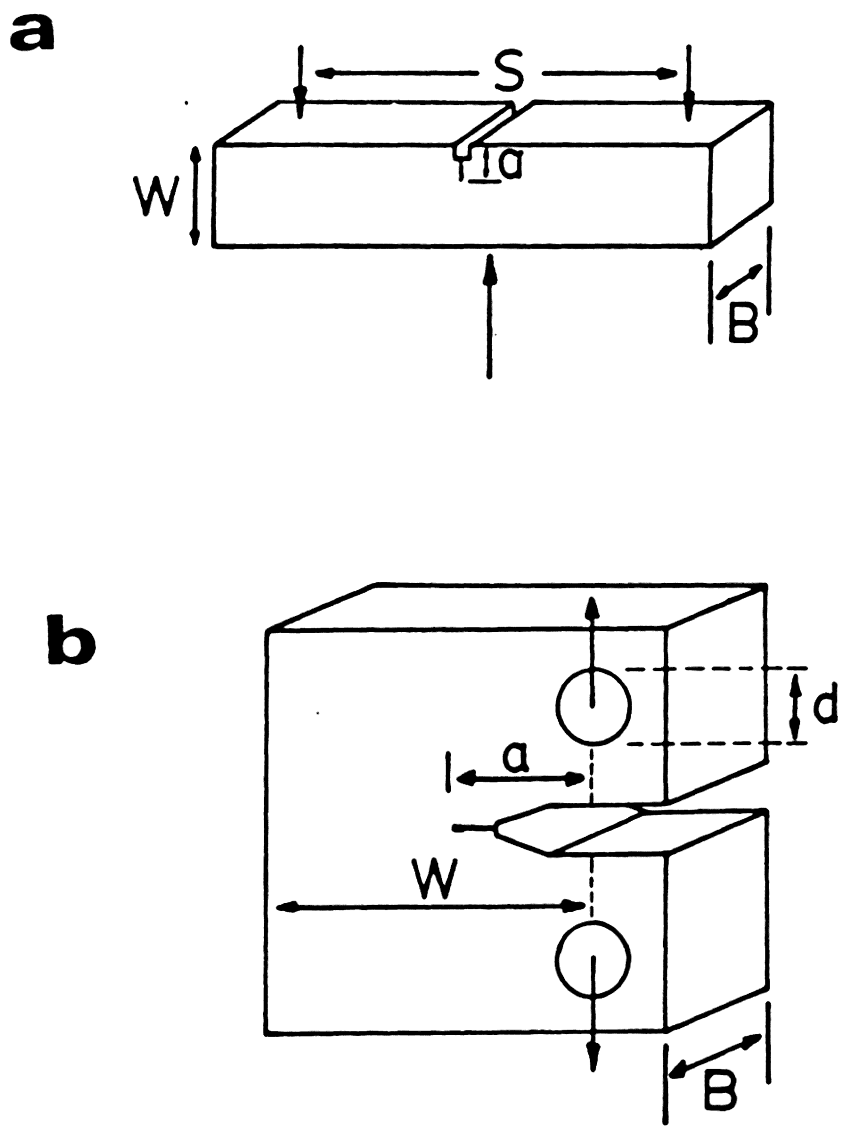

Figure 1: Fracture mechanics testing geometries: a) three-point bend and b) compact tension.

0.8 $MN \cdot m^{-3/2}$ at 10°C to 2.2 $MN \cdot m^{-3/2}$ at 120°C [22]. It can be observed that by varying the cure conditions fracture toughness changes by a factor of 2.7 and addition of rubber **does not** necessarily cause an increase in fracture resistance. Thus, to a certain extent, the cure conditions are more important than the amount of added rubber. Several other investigators [23-27] have reported the same trend; fracture toughness increased at least by a factor of 4 by incorporation of 15 percent CTBN or ATBN rubber.

2.3 Toughening Mechanism

It is not yet entirely clear how the elastomeric domains in an epoxy network act to increase the fracture resistance. McGarry [5] and Bucknall [28] initially proposed that these modified glassy networks absorb mechanical energy through crazing, much like high-impact polystyrene. This view was later found to be inadequate, particularly when applied to highly crosslinked thermosets, such as those used for structural laminates. Further work towards an understanding of mechanisms is described by Yee [29] and, Pearson [30]. Yee and Pearson propose a toughening mechanism of cavitation and shear band deformation. They did not ascertain any significant effect of particle size.

Kinloch et al. [20] proposed a mechanism for the onset of unstable crack growth. Intrinsic to this mechanism is the generation of a triaxial stress ahead of the crack tip which provokes void formation either inside the rubber particles or between the particles and the

matrix. The stress concentration produced at the equators of the rubber particles is said to nucleate shear deformations in the matrix surrounding each particle. It is suggested that shear yielding begins at one particle and terminates at another one. Kinloch et al [20], found that void formation is more important in the early stages of fracture and is closely involved with shear deformations, however, it is the shear yielding that is the main source of energy dissipation. They pointed out that the interplay between these two mechanisms ultimately determines the contribution of each.

In a second part of the previous study, Kinloch et al. [31], extended their investigation to studies of crack blunting in CTBN-modified epoxies and introduced the critical values of the applied stress and the crack tip radius as a unique failure criterion which consists of two parameters, $\sigma(t_c)$ and c. The parameter c denotes the critical distance ahead of a sharp crack at which critical stress for crack propagation, $\sigma(t_c)$, must be attained for crack to propagate. For a quantitative derivation of this criterion, Ref. [31] may be consulted. The basis of their formulation is the ability of shear deformation at the loaded crack tip to blunt the crack tip.

The matrix itself is given a lot of importance in the theories just described. A rather different approach was taken by Sayre, Kunz, and Assink [32]. They derived a model for the toughness of rubber-modified epoxies based on the observation that a crack propagation through the brittle epoxy matrix and leaves rubber particles bridging the crack as it opens. These rubber ligaments are observed in the optical microscope

to fail by tearing at critical strains. This is shown in Fig. 2. The elastic energy stored in the particles during straining is dissipated irreversibly (as heat) during the tear failure. Sayre et al. [32] proposed that change in the fracture toughness could be expressed as:

$$\Delta G_{IC} = \left(1 - \frac{6}{\lambda^2 + \lambda + 4} \right) 4\Gamma V_P$$

where Γ is the rubber tear energy, V_P is the volume fraction of rubber, and λ is the critical extension ratio of the rubber. This model, which has qualitatively good agreement with experiments, predicts that toughness will increase with tear energy and volume fraction of the elastomeric phase. For further theoretical development of crack tip mechanisms in epoxies, the reader might consult Kinloch and Williams [33] and Yamini and Young's work [34] on plastic deformation mechanisms in unmodified epoxies.

2.4 Morphology

As pointed out before, during the curing process, the rubber will separate out in the form of dispersed rubber particles. The extend of solubility of rubber with epoxy, at initial stages of curing process, is an important factor in determining the size of the rubbery particles. There are various other factors which influence the morphology of a sample such a miscibility, curing temperature, percent of rubber content, and molecular weight of both resin and rubber [21].

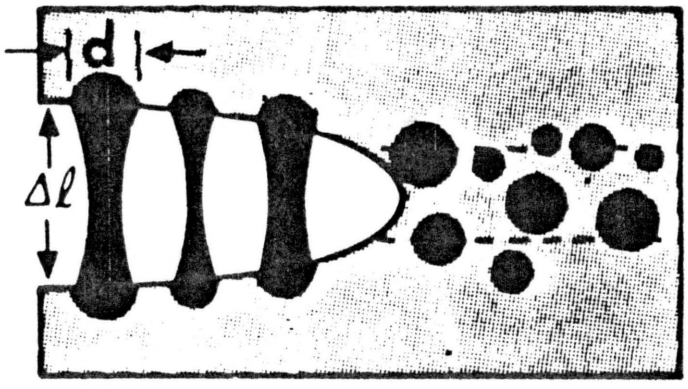

(a)

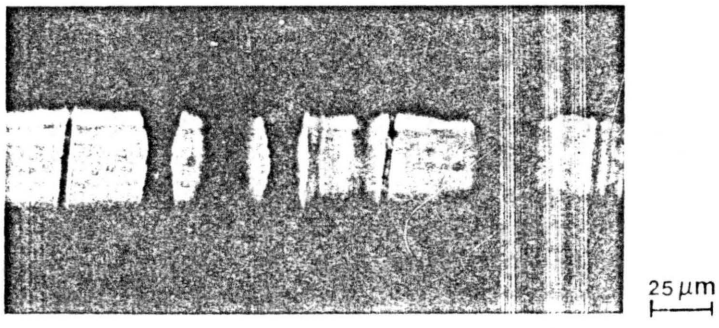

(b)

Figure 2: Model of crack propagation in a rubber-modified epoxy. b) Optical micrograph of crack in rubber-modified epoxy showing strained rubber particles bridging open crack. After Ref. 32.

Several investigators [22] have reported that with more rubber content, the size of the rubbery particles increases and the spacing between these particles decreases, i.e., they are more closely packed. Nae et al. [35], reported that the average diameter size of the particles increased from 3 μm at 2 percent rubber to 8.5 μm at 8 percent rubber, while the average number of the particles decreased from 15 to 7 per one hundred square micrometer. Kirshenbaum [36] reported the same trends in regard to the domain size and number.

It is important to realize that the rubber content is not the only governing factor with respect to morphology. The phase separation and morphology are also controlled by thermodynamic and kinetic parameters. The driving force is loss of compatibility due to the increase in average molecular weight during polymerization. The resisting force is high viscosity of solution which controls the formation and growth of the domains. These parameters have been analyzed by Manzione, Gillham, and McPherson [37] who proposed a morphology map that predicts the formation of many small particles at low temperature and of a limited number of large particles at high temperature. Butta, et al. [22] studied the effect of cure temperature on morphology and their experimental data agree with this generalization. Their Scanning Electron Microscope (SEM) micrographs showed that at 15°C no particles could be observed. At high magnifications (~ 20kx) a pattern resembling a nodular structure was visible. At 60°C a large number of small domains (~ 2 μm) formed. Whereas at 160°C the number of domains was more than one order of magnitude smaller and the domains were larger

(~ 8 μm). Their data show a strong dependence of toughness on the domain size. Yorkgitis and co-authors [16] suggested that increasing the molecular weight of the rubber would result in very large domains (as big as 40 μm) on the surface.

The question of the relative importance of particle size, and more importantly particle size distribution, to the toughness is still a matter of debate. The work of Sultan and McGarry [7], suggests that large particles (~ 1 μm) cause crazing and are five times more effective toughening than shear band producing small ones (0.01 μm). In contrast, a rubber particle tear energy model [3,32] predicts no substantial size dependence when particles are less than 1 μm but predicts a decrease in toughness for larger particle sizes.

2.5 Friction and Wear of Polymers

Friction and wear research at Virginia Polytechnic Institute and State University has been conducted under direction of Dr. N. S. Eiss, Jr. since 1973. Investigations have been made on several different polymers such as low-density polyethylene (LDPE), poly(vinyl chloride) (PVC), and polychlorotrifluoroethylene (PCTFE), etc. Major variables, investigated include the effects of counterface asperity penetration, degree of crystallinity, molecular weight, and surface roughness. Recent research at VPI&SU has been concerned with polyimides and rubber-modified epoxies.

Chitsaz-Zadeh and Eiss [38] investigated the effects of structure, sliding speed, and temperature on the friction and wear of polyimide

thin films. They found that wear rate was significantly lower for the structure which had the most flexible molecular chains as indicated by its glass transition temperature. They observed higher friction and wear for higher sliding velocities. A fatigue wear mechanism was deduced and a positive correlation was found for a power law relationship between wear rate and elastic modulus. They also reported a marked reduction in wear for tests at elevated temperatures.

Hanmin et al. [39] studied tribological properties of a thermoplastic, poly(phenylene sulphide) reinforced with carbon fibers. They ran composite pins on a carbon steel ring and reported that friction coefficient dropped moderately, up to a fiber content of 30 percent and then increased significantly to a value of 1.5 at a carbon content of 70 percent. Their data shows a rather complicated variation in wear rate. Wear rate of the samples with up to 20 percent fiber content is lower than that of the control sample, but it rises dramatically and shows a maximum at 50 percent fiber content and drops again with higher percentages of fiber content. They believe that such a behavior is associated with changes in wear mechanism for different fiber content.

Thomas [40] has studied wear properties of blends of plasticized poly(vinyl chloride) and thermoplastic copolyester elastomer. He has adapted an abrasive wear mode with samples running against abrasive paper of grit size of 320. The data reveals that elastomer-modified PVC exhibits much higher impact strength than the unmodified PVC. When percent modifier in PVC was 75, both tear strength and tensile strength

increased significantly. Upon observation of wear results, one can conclude that wear volume decreased by at least a factor of 2 at higher percent of modifier (75 percent). Although it is not mentioned, it is interesting to note that there is a good inverse linear correlation between wear volume and impact strength. These parameters have been analyzed by Omar, Atkins, and Lancaster [41]. They showed that for an abrasive wear mode, the wear rate was inversely proportional to the square of critical stress intensity factor. They reported a correlation coefficient of 0.97. Impact strength is a measure of fracture toughness and toughness is directly proportional to K_{Ic}^2, with a constant of proportionality being $\frac{1}{E}$. Thomas' experimental results are in good agreement with these findings.

Friction and wear of graphite-modified epoxy resin has been investigated by Subramanian and co-workers [42]. They have conducted experiments on modified epoxy pins and loaded them against a hardened steel. The pins contained graphite ranging from 0.5 to 30 weight percent. The friction coefficient drops significantly with addition of graphite as little as 0.5 percent. The reduction in wear loss is drastic, by introducing 3 percent graphite, wear loss drops from 0.3 mg for unmodified sample, to almost zero. There is almost no wear for samples containing more than 3 percent graphite. They attributed the reduction in friction and wear to the formation of film on the counterface.

Not many leading tribologists have conducted any research in the relatively new area of rubber-modified epoxies. Eiss and Czichos [17],

Hu et al. [43] are among the first pioneers who have studied the effects of elastomeric polysiloxanes on the tribological behavior of epoxies.

Eiss and Czichos investigated the effects of various factors such as percent polysiloxane, normal load, and test configuration. The main effect of increasing the normal load was to increase both coefficient of friction and wear. They reported that the earlier stages of wear of modified epoxy pins on steel, was an abrasive mode. It is further reported that wear rates correlated with the inverse of fracture toughness. This is in agreement with findings of Omar, et al. [41]. The friction coefficients of modified epoxy pins rubbing against steel were found to be higher than those on glass. However, after completion of wear-in, the friction coefficients were comparable on steel and glass. In the other test configuration, where a steel ball was slid on modified epoxy plates, wear rate generally decreased with higher rubber content up to a rubber content of 15 percent polysiloxane which had 20 percent trifluoropropylmethylsiloxane (TFP). For samples of 10 percent PSX with TFP contents higher than 20 percent, the wear rate increased.

Eiss and Czichos proposed that when elastomeric domains were small and widely dispersed, the domains were debonded from the epoxy wall. When the domains were closely packed, wear was initiated at the sites of thin epoxy walls between the domains where stress concentration was high. After being cracked these walls were removed as loose wear particles [17].

Lee [44] has found that for fatigue wear resistance, "fracture energy is the most important property." He also believes that most wear

mechanisms, eventually lead to fatigue wear of polymers. Lee has taken the Archard's equation and derived a relationship between the wear volume and the stress intensity factor. This relationship shows that wear volume is inversely proportional to the square of stress intensity factor. This is the same relation that Omar, et al. [41] suggested by their experimental data. Lee believes that the reduction in the wear of polysiloxane-modified epoxies, reported by Eiss and Potter [45], is not only due to the reduction in elastic modulus, but also due to the increase of fracture toughness.

In another study, Yorkgitis et al. [46] studied friction and wear properties of ATBN and CTBN rubbers-modified epoxies. The increase in weight percent of rubber from 0 to 15 resulted in 50 percent increase in K_{Ic}. Their data shows that for CTBN-modified epoxies, the wear rates are about 12, 6, and 3 μm^2 per cycle for samples with 5, 10, and 15 percent rubber, respectively. The wear rates have a negative correlation with stress intensity factors. This is in good agreement with the theoretical model proposed by Lee [44]. The wear of ATBN-modified epoxies, however, did not seem to have any correlation with K_{Ic}. Yorkgitis, et al. reported that the friction coefficient did not change significantly as a function of percent rubber.

3. EXPERIMENTAL PROGRAM

3.1 Sample Preparation

Siloxane-modified epoxy networks were synthesized and supplied by J. A. Cecere of the Chemistry Department at VPI&SU. The control epoxy resin utilized was a diglycidyl ether-based bisphenol A resin (Epon 828). The poly(dimethyl-co-diphenyl siloxane) oligomers were used as the elastomeric modifiers with having two different ratios of diphenyl and dimethyl (1:4, 2:3) monomers. The amount of these then added to the epoxy resin was 0, 5, 10, to 15 weight percent. After the linear epoxy-siloxane precursor was synthesized, it was reacted with the crosslink curing agent, bis(4-aminocyclohexyl) methane (PACM-20).

The epoxy/siloxane/PACM-20 mixture was poured into a hot RTV-silicon mold of precise shapes to be used for solid-state testing. The mixture was cured at 160°C for 2.5 hours. The cured samples were stored in a dessicator to prevent deterioration and hydrolysis by atmosphere moisture.

In addition to the control epoxy sample, three series of modified epoxies were synthesized. Series I samples contained a siloxane modifier, poly(dimethyl-co-diphenyl), whose DP content was 20 percent. Series II samples contained the same siloxane as the modifier with a different molecular weight and a DP content of 40 percent. The modifier for Series III samples was a CTBN rubber with 18 percent AN (acrylonitrile). All samples were designated by three numbers; the first is the weight percent of the total modifier in the epoxy network,

the second is the molecular weight of the modifier, and the third number is the percent of copolymer DP (AN) in the siloxane (CTBN) modifier. For example, 5-2500-20DP is the sample with 5 percent siloxane modifier at a molecular weight of 2500 and the DP content of the modifier is 20 percent, 15-4000-18AN is a sample with 15 percent CTBN modifier whose molecular weight is 4000 and the AN content of the modifier is 18 percent.

3.2 Fracture and Modulus Testing

For tensile tests, standard (cf. ASTM D632) dog-bone samples (3.5 mm widths, 2 mm thickness, 13 mm gauge length) were machined out of the molded plates. The samples were tested in an Instron testing machine at a cross-head speed of 5 mm/min (procedure and a typical load-elongation curve are given in Appendix A.) At least 5 samples of each composition were used for tensile tests, except control and 15-2500-20DP, for which two samples were used. Table 1 shows average mechanical properties of the samples.

Flexural modulus and fracture tests utilized a three-point bend geometry. For fracture toughness tests, a thin saw notch approximately 1 mm deep was cut into the center of the sample. Into this notch a sharp one-sided razor blade was placed and tapped lightly to make a sharp pre-crack. The cross-head speed for flexural testing was 1.0 mm/min and that for fracture testing was 0.5 mm/min. For the complete procedure and sample dimensions of flexural and fracture testing refer to Appendix B.

Fracture toughness for modified epoxies was monitored through the

TABLE 1

Average Mechanical Properties

Sample	Elong. (%)	S_{ult} (MPa)	S*Elong (MPa)	Modulus (MPa)
control	**15**	**61**	**9.2**	**490**
5-2500-20DP	19 ± 4 †	58 ± 7	11.1 ± 5	451 ± 26
10-2500-20DP	18 ± 3	66 ± 4	11.6 ± 2	509 ± 10
15-2500-20DP	18 ± --	55 ± --	9.7 ± --	454 ± --
5-5000-40DP	18 ± 3	64 ± 12	11.6 ± 4	447 ± 35
10-5000-40DP	17 ± 3	58 ± 5	9.8 ± 2	456 ± 19
15-5000-40DP	15 ± 6	51 ± 10	8.0 ± 5	437 ± 29

† Mean values and 95% confidence range.

plane-strain stress intensity factor, K_{Ic}; the subscript I denoting that the crack is stressed in a tensile-opening mode (the most critical and important mode) and the subscript c that it refers to failure condition. K_{Ic} is a measure of material property and is independent of the geometry of the cracked body.

K_{Ic} values of at least five samples of each material composition were calculated according to ASTM E399 [47]:

$$K_{Ic} = \frac{6\ P_c}{BW^{1/2}}\ f\left(\frac{a}{w}\right)$$

where P_c is the critical load, B is the sample's width, W is its thickness, and a is the length of the pre-crack (See Fig. 60b in App. B). Letting $R = \frac{a}{w}$, the geometry factor $Y = f\left(\frac{a}{w}\right)$ is given as:

$$Y = 1.93\ R^{1/2} - 3.07\ R^{3/2} + 14.53\ R^{5/2} - 25.11\ R^{7/2} + 25.90\ R^{9/2}$$

For validity of K_{Ic} values, the criteria of ASTM E399 were followed as closely as possible. The sample size requirements were met. The only criterion which could not always be satisfied was that for a straight pre-crack front, ± 5%.

After obtaining K_{Ic} values, the critical strain energy release rate, G_{Ic}, which is commonly referred to as fracture toughness, was calculated from the following formula:

$$G_{Ic} = \frac{K_{Ic}^2}{E_f}\ (1 - \nu^2)$$

where, E_f = flexural modulus and ν = poisson's ratio (assumed to be 0.34 for all samples). The values of flexural modulus, plane-strain stress intensity factors, and fracture toughness are revealed in Table 2.

3.3 Friction and Wear Apparatus

For friction and wear testing, a pin-on-disk machine, shown in Fig. 3, was used. The pin, depending on the type of wear test, was either a 3.2 mm diameter 52100 chromium steel sphere or a cylinder (4.7 mm dia.) cast from modified epoxies. A pneumatic loading system was used to press the pin against the disk. The loading assembly for the pin was attached to a cantilever beam whose horizontal traversing mechanism could provide any desired radius of circular wear tracks. Thus, several tests could be conducted on each disk. The wear machine was equipped with a variable speed transmission driven by an induction motor and a timing belt-pulley system.

For the purpose of friction measurements a proximity sensor detected the horizontal deflection of the cantilever beam caused by frictional force. The output signal from the proximity sensor was recorded on an x-y plotter providing a continuous measure of frictional force. The friction measurement system was calibrated for each test. The calibration procedure is given in Appendix C.

TABLE 2

Fracture Results

Sample	E_f (GPa)	K_{Ic} ($MN.m^{-3/2}$)	G_{Ic} (J/m^2)
control	**2.00**	**0.77**	**261.8**
05-2500-20DP	1.65	0.82	**360.8**
10-2500-20DP	1.90	0.87	**352.0**
15-2500-20DP	1.44	0.83	**422.7**
05-5000-40DP	1.90	0.91	**358.6**
10-5000-40DP	1.73	0.93	**442.2**
15-5000-40DP	1.83	1.34	**867.6**
5-4000-18AN †	2.00	0.94	**380.3**
10-4000-18AN	1.75	1.05	**557.2**
15-4000-18AN	1.52	1.12	**729.6**

E_f = Flexural Modulus
K_{Ic} = Plane − strain Stress Intensity Factor
G_{Ic} = Fracture Toughness
† *Data adapted from Reference* 46

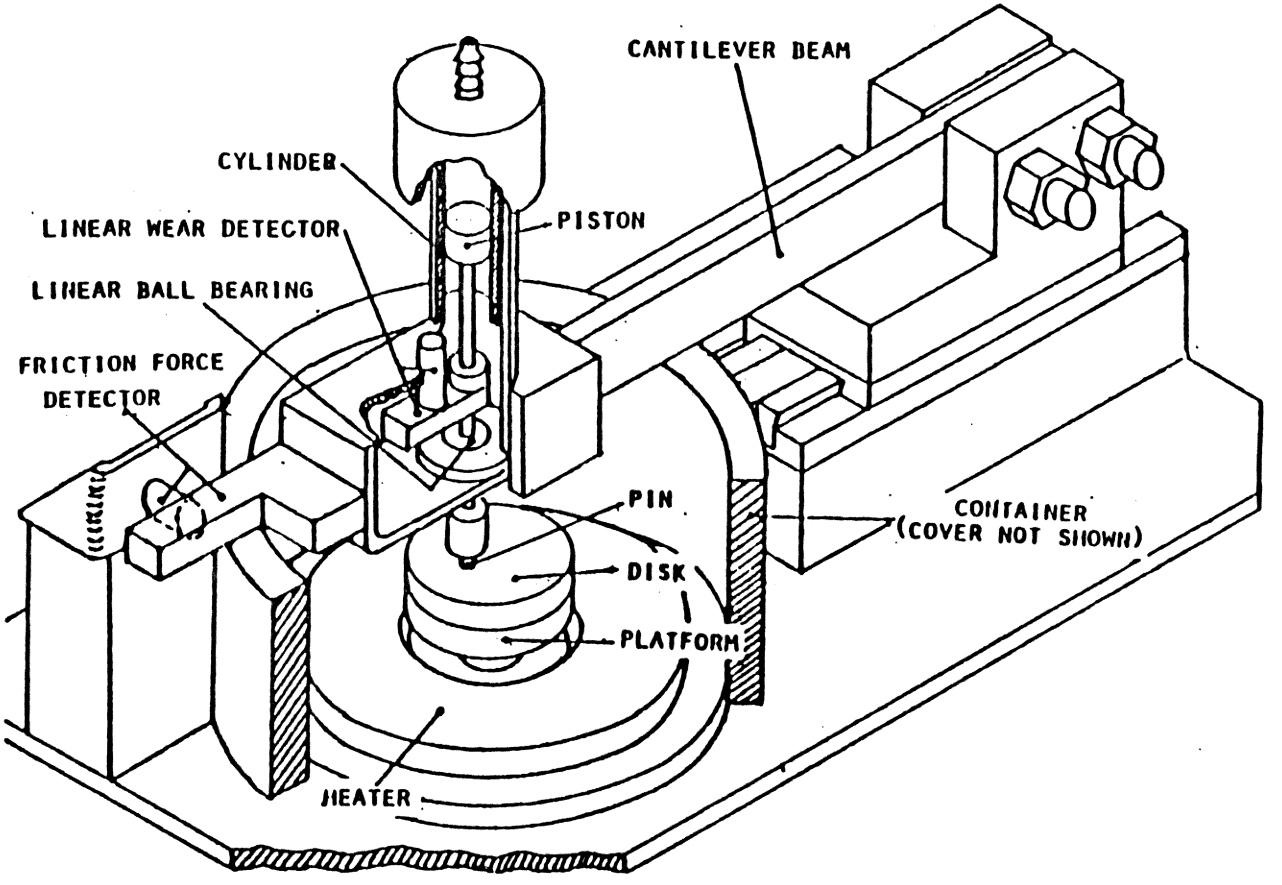

Figure 3: Pin-on-disk wear machine. After [48].

3.4 Friction and Wear Testing

For friction and wear testing two test configurations were adopted. In the first, a steel spherical pin was brought in contact with the smooth surface of the modified epoxy disk. A normal load of 10N was chosen so that the calculated Hertzian elastic stresses at the interface were below the fracture strength of the sample. The calculated contact stresses will be reported in the following chapter. Hence, the operating conditions were in favor of a fatigue wear mode.

An attempt was made to change the test geometry, i.e., modified-epoxy pin on steel disk, to determine if the modified epoxies would rank differently based on the wear rates. Therefore, modified epoxies were cast into cylindrical pins (4.7 mm dia.). The flat end of the pin was then loaded against a smooth steel disk at a load of 10 N with a sliding speed of 63 cm/s. However, preliminary tests of this geometry (flat-epoxy pin-on-steel disk) revealed that no wear occurred after 35,000 cycles even when the sliding speed was doubled. Since neither load nor speed could be increased (higher sliding speeds were not desired because frictional heating was to be kept to a minimum), this configuration was discarded. This led to the adoption of a second test configuration in which abrasive wear was the predominant wear mechanism.

3.4.1 Fatigue Wear Testing

Fatigue wear tests were conducted on all specimens which had different siloxane content in the epoxy. In addition, some tests were run on CTBN-modified epoxies for purposes of comparison. All fatigue

tests were run at a sliding speed of 63 cm/s and a load of 10N. The complete operating conditions are reported in Table 3.

For each test a new steel pin was used and the surface of the epoxy disk was cleaned with acetone. To achieve the desired sliding speed, an arbitrary radius was chosen, then the rotational speed was calculated. Because changes in fricton caused changes in rotating speed, the rotational speed was continuously monitored, by means of a Strobotac, and adjusted during the test. A thermocouple was fastened to the pin in order to monitor the heat generated by friction force at the interface. The friction measuring system was then calibrated and the test was started.

In all tests, wear did not occur until after a few thousand rotations of the disk. During all testing the initiation of wear track was accompanied by a sudden increase in the friction force. The representative friction plot seen in Fig. 4 shows this effect. For the purpose of comparison, the friction coefficient was calculated at the beginning μ_o, just after initiation of wear track μ_{after}, after 4000 cycles μ_{4000}, and after 14,000 cycles μ_{14000}.

After wear began the sphere generated a groove in the epoxy disk. To measure the wear of the epoxy specimen, the test was halted after each 2000 cycles of sliding. The disk was removed from the wear machine and four surface profiles of the groove were taken using a Talysurf 4 stylus profile meter with a skid sliding along the surface as a reference datum. These traces were 90 degrees apart on the circular wear track as shown in Fig. 5. The disk was then placed back into the

TABLE 3

Operating Conditions for Friction and Wear Testing

Number of tests under each set of conditions †

	Abrasive	Fatigue Wear		
	L = 5 N	L = 10 N, V = 62.83 cm/s		
	V = 27 cm/s	W/o Debris	Partial tests	fully worn
control	6	---	7	5
05-2500-20DP	---	---	3	5
10-2500-20DP	---	---	4	5
15-2500-20DP	---	---	2	4
05-5000-40DP	5	3	3	4
10-5000-40DP	---	2	3	3
15-5000-40DP	5	2	4	4
05-4000-18AN	---	---	3	2
10-4000-18AN	---	---	2	1
15-4000-18AN	---	---	2	3

† All tests were run at 24 ° C with relative humidity of 40-70 percent

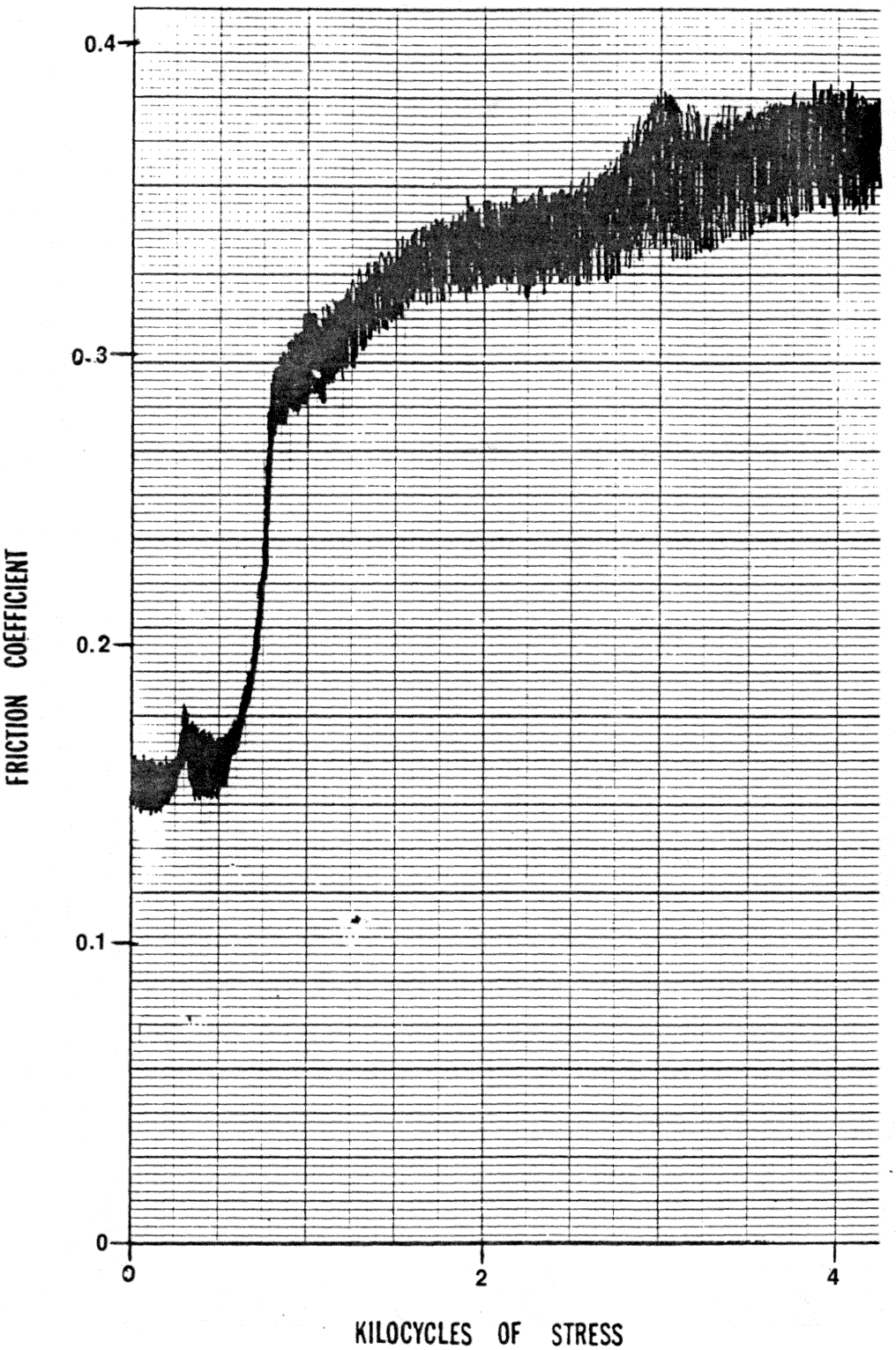

Figure 4: Representative friction plot.

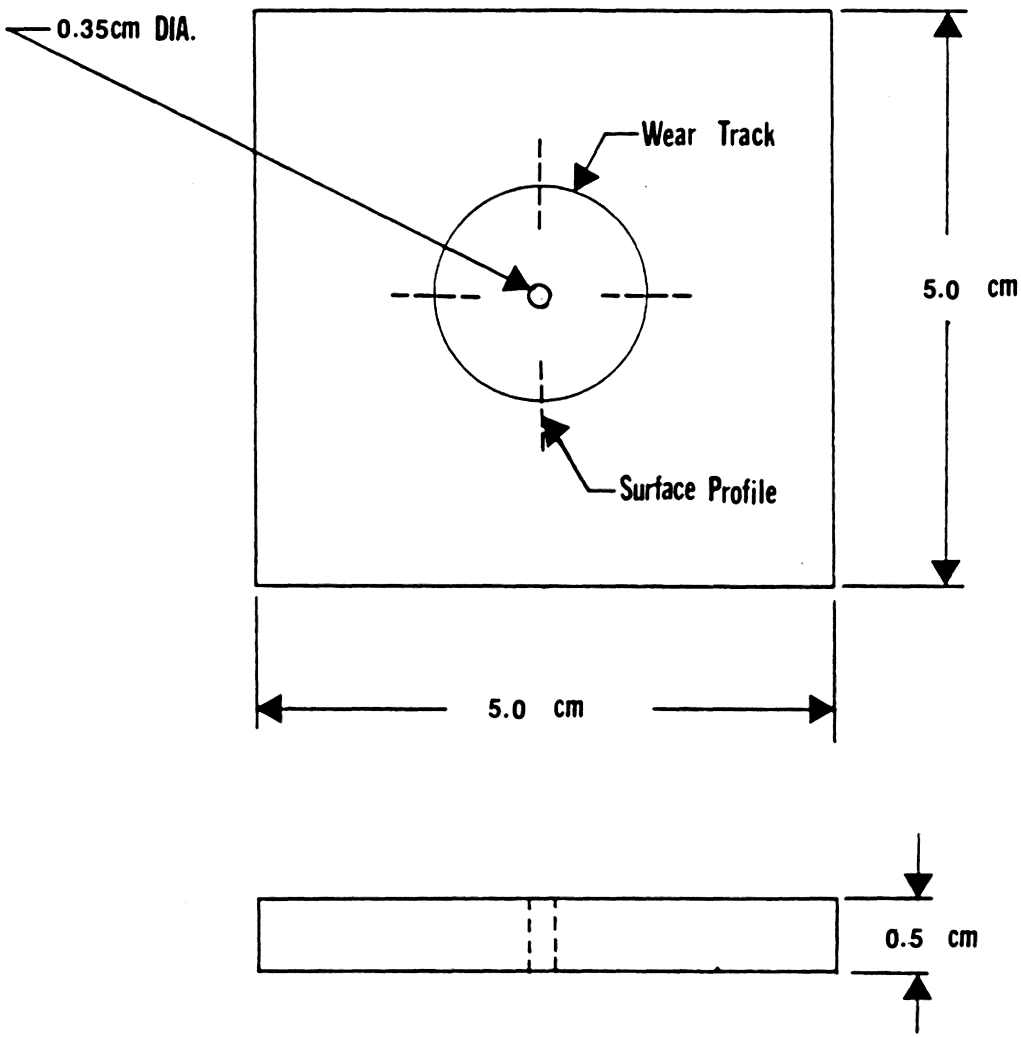

Figure 5: Epoxy disk geometry and profile trace location.

wear machine and previous procedure were repeated until 14,000 cycles were completed. The cross sectional area of the wear track was approximated by the area of a trapezoid. Figure 6 shows the wear track profile before and after trapezoidal modeling. In order to quantify the wear process, specimen wear was calculated by averaging the four cross sectional areas of the wear track (from the surface profiles) after each sliding interval. The slope of the wear vs. cycles curve, as calculated by a linear regression analysis is the wear rate.

In order to observe the response of the system to the wear debris, tests were conducted with the wear debris blown out of the wear track before they could interact with the steel pin. Pressurized air, discharging from an air tank was used to do this. A hose connected to the air tank had a 2 mm diameter nozzle attached to it. The nozzle was placed just above the wear track of the epoxy disk diametrically opposite to the pin. Blowing started before the ball was brought in contact with the rotating epoxy disk and was continued throughout the test. Friction and wear were measured in the same manner as before.

A series of partial wear tests were performed on different sample compositions to observe the progression of the wear track formation. These tests were conducted in the same manner as explained above except that each test was suspended at different stages of initiation and formation of the wear track. These specimens were then observed in an Scanning Electron Microscope (SEM) in order to reveal the progression of crack formation and wear and the role of the siloxane particles with respect to the wear process.

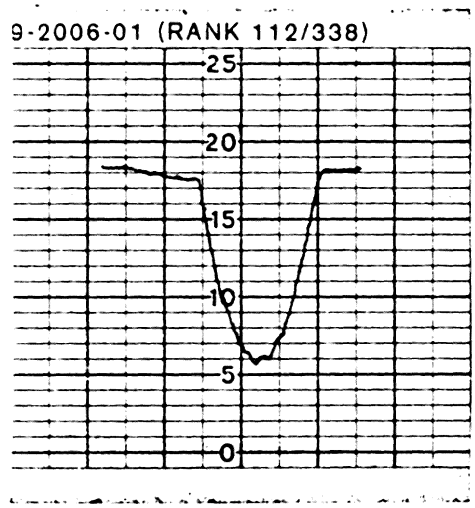

Before trapezoidal modeling

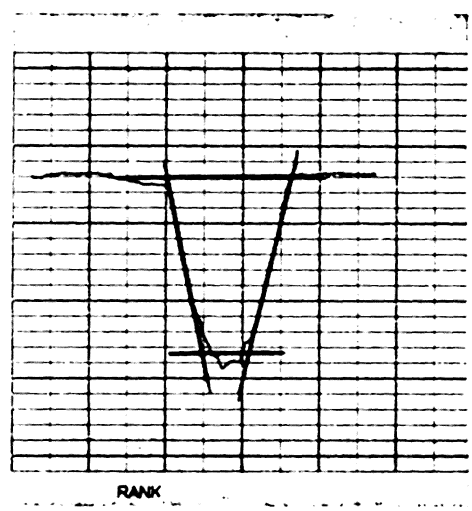

after trapezoidal modeling

Figure 6: Wear track profile.

3.4.2 Abrasive Wear Testing

A selected compositions of modified epoxies were used to cast cylindrical pins (4.7 mm dia.). These included six unmodified epoxy (control) samples and 10 siloxane-modified epoxy samples, of which five had 5 percent siloxane content and the other five, 15 percent. For abrasive wear testing, the epoxy pin was loaded against 320 grit abrasive paper which was glued to a rotating steel disk. Before each test started the contacting surface of the epoxy pin was abraded against a rotating abrasive disk for about 100 cycles. The abrasive disk then was replaced with a new one. This was done to make sure that the surface of the pin was in conformity with that of the disk.

The wear of the pin was measured by the mass loss of the pin at 50 cycle intervals. The mass measurements were done using a Cahn21 digital electrobalance whose sensitivity was 1 microgram. The wear rate is reported in mg/m. For each wear rate calculation at least seven mass measurements were obtained. Friction was measured as before. A normal load of 5N and a sliding speed of 27 cm/s was used for these tests. At higher loads or velocities the pin wore too rapidly and not more than two or three mass measurements could be made.

4. RESULTS

4.1 Fracture Toughness

The experimentally obtained values of flexural modulus, E_f, critical plane-strain stress intensity factor, K_{Ic}, and calculated values of fracture toughness, G_{Ic}, were reported in Table 2 in the previous chapter. The data show that with incorporation of elastomer into the epoxy resin, stress intensity factor increased with little reduction in flexural modulus. For all samples, with the exception of 10-20DP sample, an increase in the rubber content resulted an increase in the fracture toughness. The incorporation of 15 percent diphenyl siloxane in the epoxy resin raised the fracture toughness from 262 to 868 J/m^2, an increase of 231 percent.

4.2 Friction

Friction coefficient, for all samples, at zero cycle, just after initiation, after 4000 cycles, and after 14,000 cycles were averaged, tablulated, and are listed in Tables 4, 5, and 6.

For series I epoxies, 20 percent DP, at zero cycle there was almost no difference at different percentages of modifier. However, at higher number of cycles, friction coefficient decreased significantly with increasing percent rubber, except for sample with 10 percent siloxane. Note that in Fig. 7, the pure epoxy sample has the highest coefficient of friction followed by 10, 5, and 15 percent siloxane.

TABLE 4

Friction Coefficient Values for Epoxies of Series I, 20DP

Friction coefficient	Percent modifier 5-20DP	10-20DP	15-20DP
μ_o	0.132 ± 0.015 †	0.124 ± 0.01	0.135 ± 0.05
μ_{after}	0.26 ± 0.05	0.298 ± 0.04	0.230 ± 0.03
μ_{4000}	0.304 ± 0.02	0.350 ± 0.007	0.225 ± 0.02
μ_{14000}	0.310 ± 0.05	0.358 ± 0.014	0.245 ± 0.05

† Mean values and 95% confidence limits.

TABLE 5

Friction Coefficient Values for Epoxies of Series II, 40DP

Friction coefficient	Percent modifier 5-40DP	10-40DP	15-40DP
μ_o	0.127 ± 0.05 †	0.170 ± 0.001	0.212 ± 0.10
μ_{after}	0.257 ± 0.05	0.273 ± 0.03	0.250 ± 0.04
μ_{4000}	0.320 ± 0.025	0.293 ± 0.03	0.237 ± 0.04
μ_{14000}	0.322 ± 0.03	0.320 ± 0.001	0.247 ± 0.007

† Mean values and 95% confidence limits.

TABLE 6

Friction Coefficient Values for Epoxies of Series III, CTBN

Friction coefficient	Percent modifier 5-18AN	10-18AN	15-18AN
μ_0	0.055 ± 0.005 †	0.080 ± ---	0.080 ± 0.001
μ_{after}	0.155 ± 0.005	0.150 ± ---	0.175 ± 0.025
μ_{4000}	0.235 ± 0.015	0.200 ± ---	0.200 ± 0.001
μ_{14000}	0.245 ± 0.005	0.210 ± ---	0.160 ± 0.02

† Mean values and 95% confidence limits.

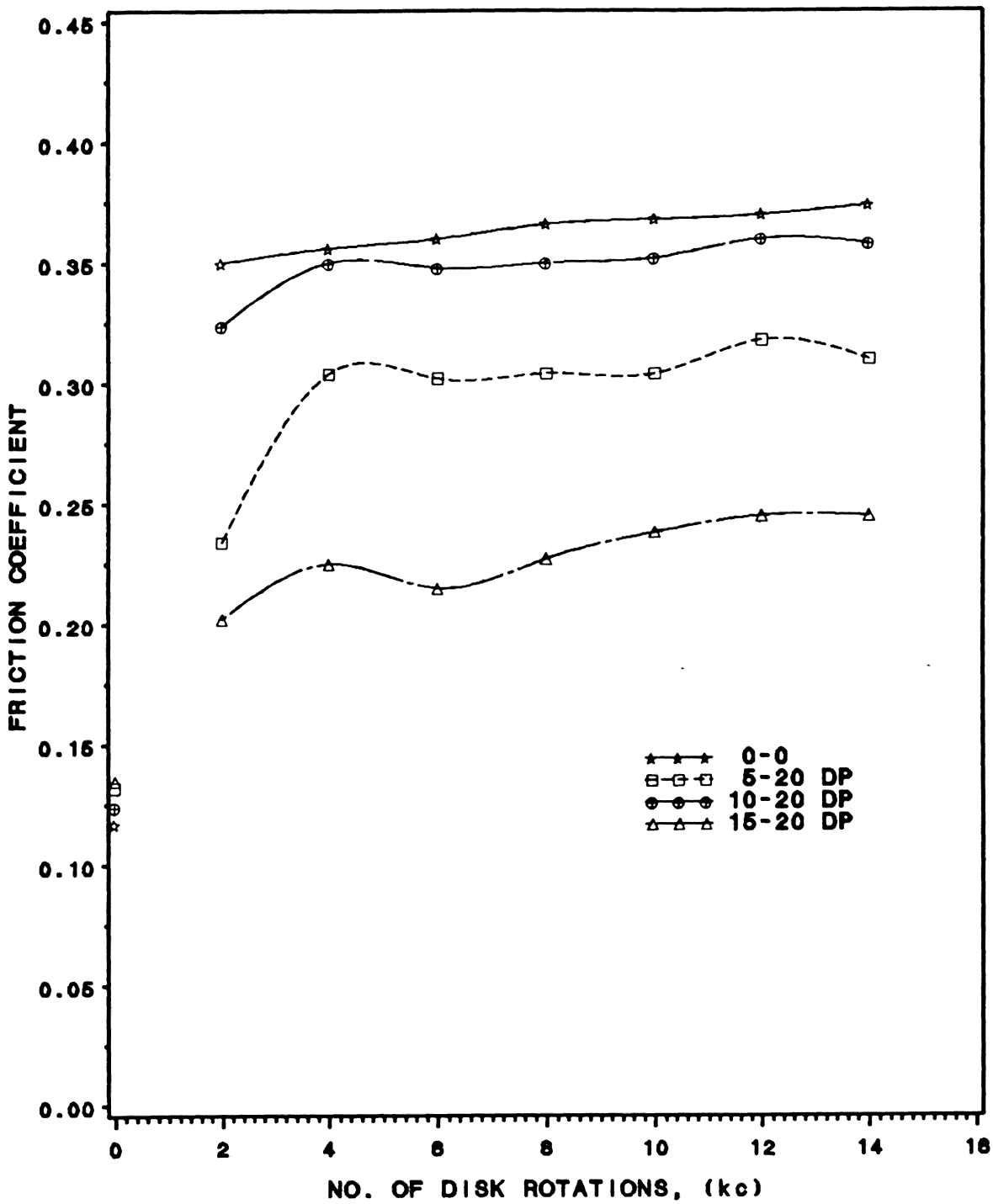

Figure 7: Effect of percent siloxane on friction, 20DP.

Upon observing the initial friction values for 40DP samples (Table 5) it is noticed that, considering 95 percent confidence limits, there is statistically no change. However, after the wear track has initiated and friction reaches to a steady state, the pure epoxy sample has the highest friction coefficient of 0.37 at 14,000 cycles and is higher than that of 15-40 DP by 50 percent. This can be seen in Fig. 8. There is no significant different between the friction values of 10-40 DP and 5-40 DP samples, however, they still both have lower friction values than the control sample. For all samples (pure epoxies and modified epoxies), the coefficient of friction increased markedly during the initiation and formation of wear track. This, most of the time occurred between 1000 to 4000 cycles of disk rotation.

Table 7 shows friction values for tests with no debris. Again at zero cycles friction increased with increasing percent in modifier. After initiation, considering the 95 percent confidence limits, there is statistically no difference between the values at different percentages of the modifier. Comparing the values of Table 7 with those of Table 5, it is revealed that friction values of tests without debris is higher than those with the debris. At 5 and 10 percent modifier this increase in friction is not very significant, but at 15 percent siloxane, there is a marked increase if the wear debris is removed. Figure 9 shows the effect of wear debris on friction at 15 percent siloxane.

For the second test configuration, flat epoxy pin on abrasive disk, the friction coefficients had a steady value throughout the test. The friction values for the control samples as well as those for the

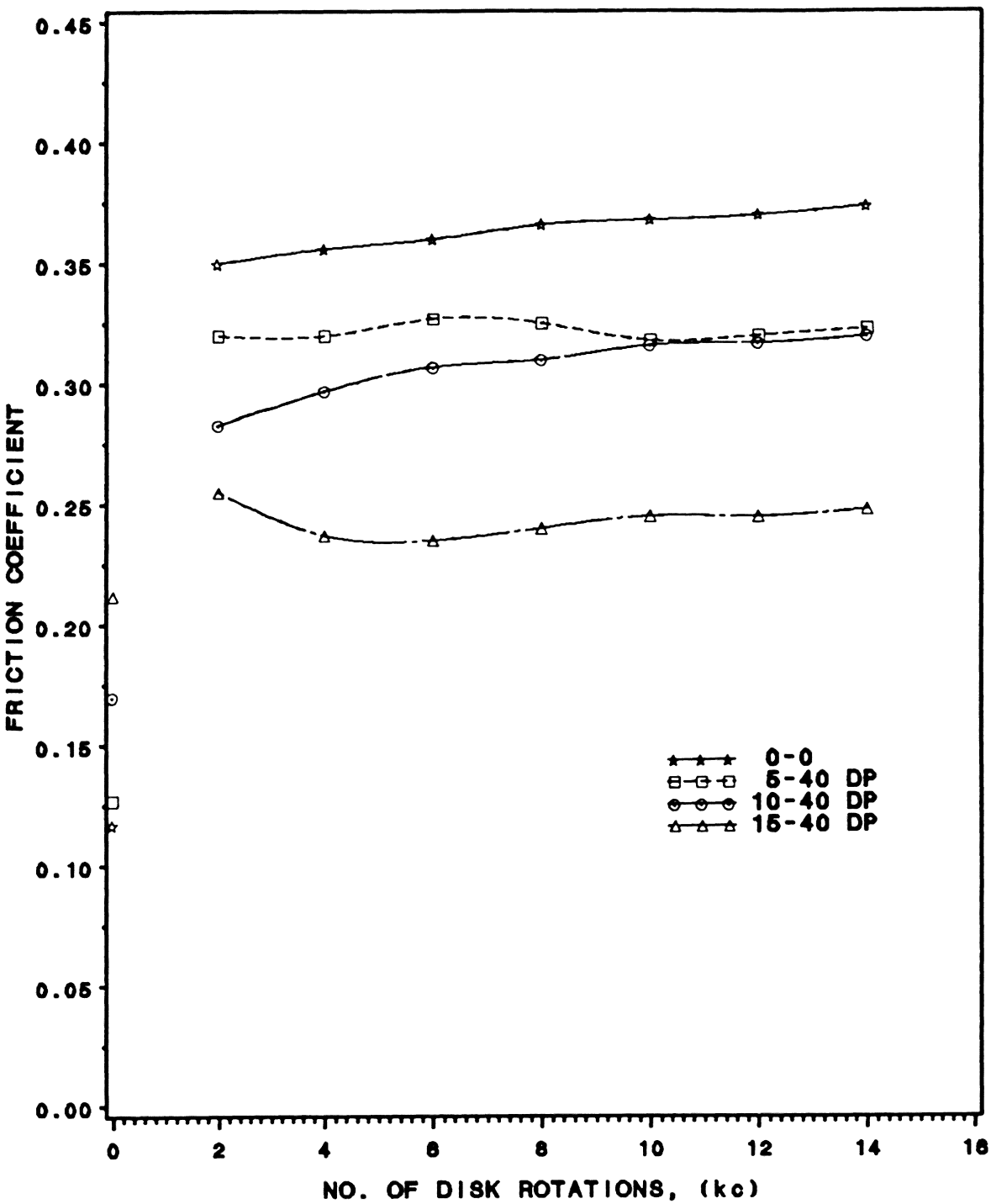

Figure 8: Effect of percent siloxane on friction, 40DP.

TABLE 7

Friction Coefficient Values for Tests w/o Debris

Friction coefficient	Percent modifier 5-40DP	10-40DP	15-40DP
μ_0	0.153 ± 0.06 †	0.180 ± 0.09	0.225 ± 0.06
μ_{after}	0.30 ± 0.05	0.285 ± 0.10	0.295 ± 0.06
μ_{4000}	0.323 ± 0.01	0.315 ± 0.06	0.315 ± 0.06
μ_{14000}	0.337 ± 0.015	0.330 ± 0.04	0.34 ± 0.15

† Mean values and 95% confidence limits.

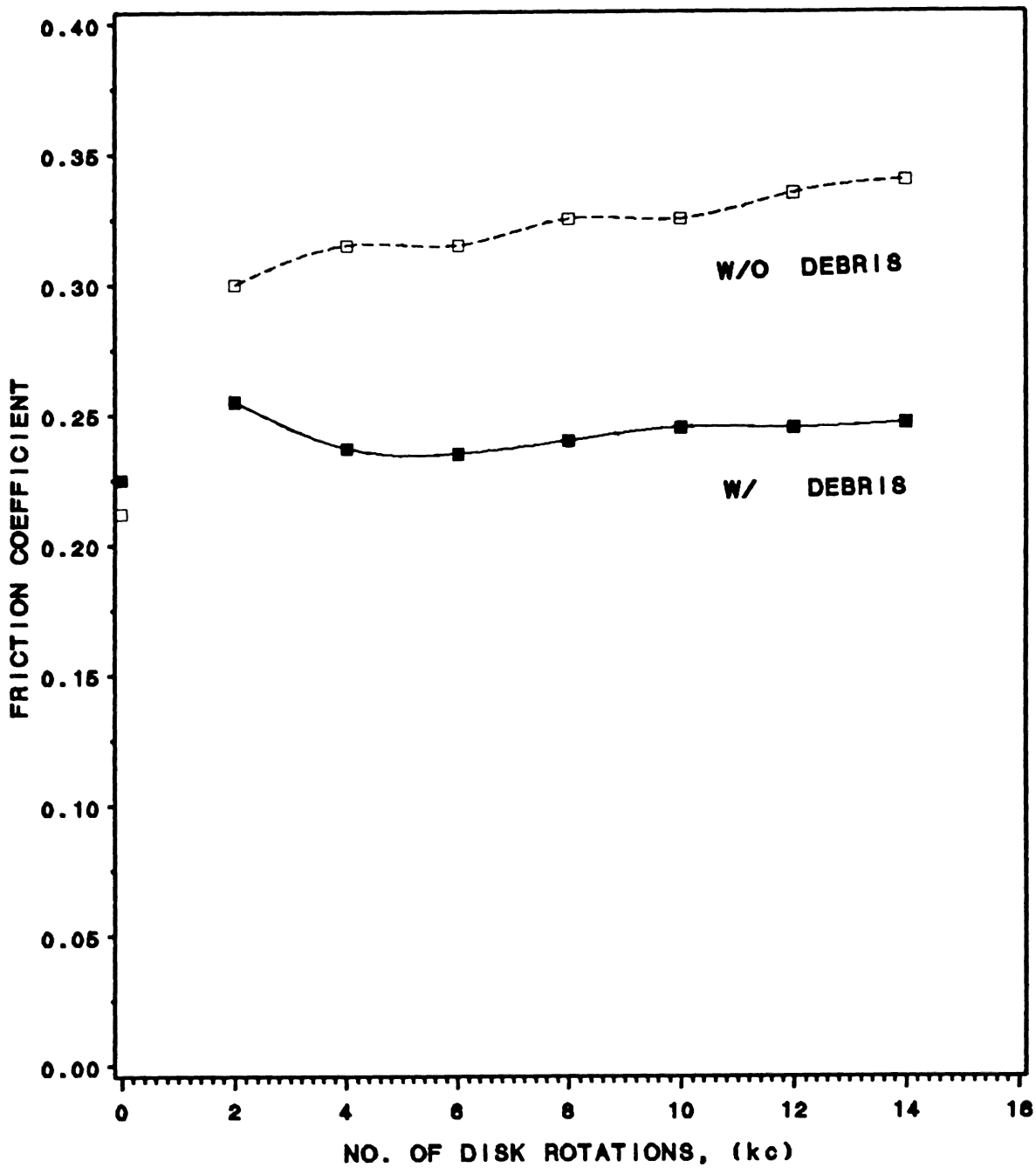

Figure 9: Effect of wear debris on friction.

modified epoxies are plotted in Fig. 10. Upon examination of this figure it is observed that with increasing the percent modifier from 0 to 15, friction decreased by 15 prcent. However, the reduction in friction for abrasive wear tests is not as much as that for the fatigue wear tests. Generally speaking, raising the amount of modifier in the epoxy resulted in lower coefficient of friction. As expected, coefficient of friction for abrasive tests is much higher (about 2 times higher) than that for the fatigue tests.

4.3 Wear

4.3.1 Fatigue Wear Testing

For each test, the average cross-sectional areas of wear tracks were plotted versus the number of cycles. A least square linear regression was performed for each set of data points. The slope of this line was taken as the wear rate. In all tests of the first configuration (steel ball on epoxy disk), the sample experienced a period of no wear followed by sudden initiation and formation of wear track and thereafter the wear was linear with number of cycles (correlation coefficients of 0.95 - .99). Figure 11 is typical of general wear trends and was chosen to show representative dispersion of data points.

The wear rates and the wear track initiation periods for specimens of 20 percent DP, 40 percent DP, and 40 percent DP without debris are reported in Tables 8, 9, and 10, respectively. The values were averaged, tabulated, and are listed in Table 11.

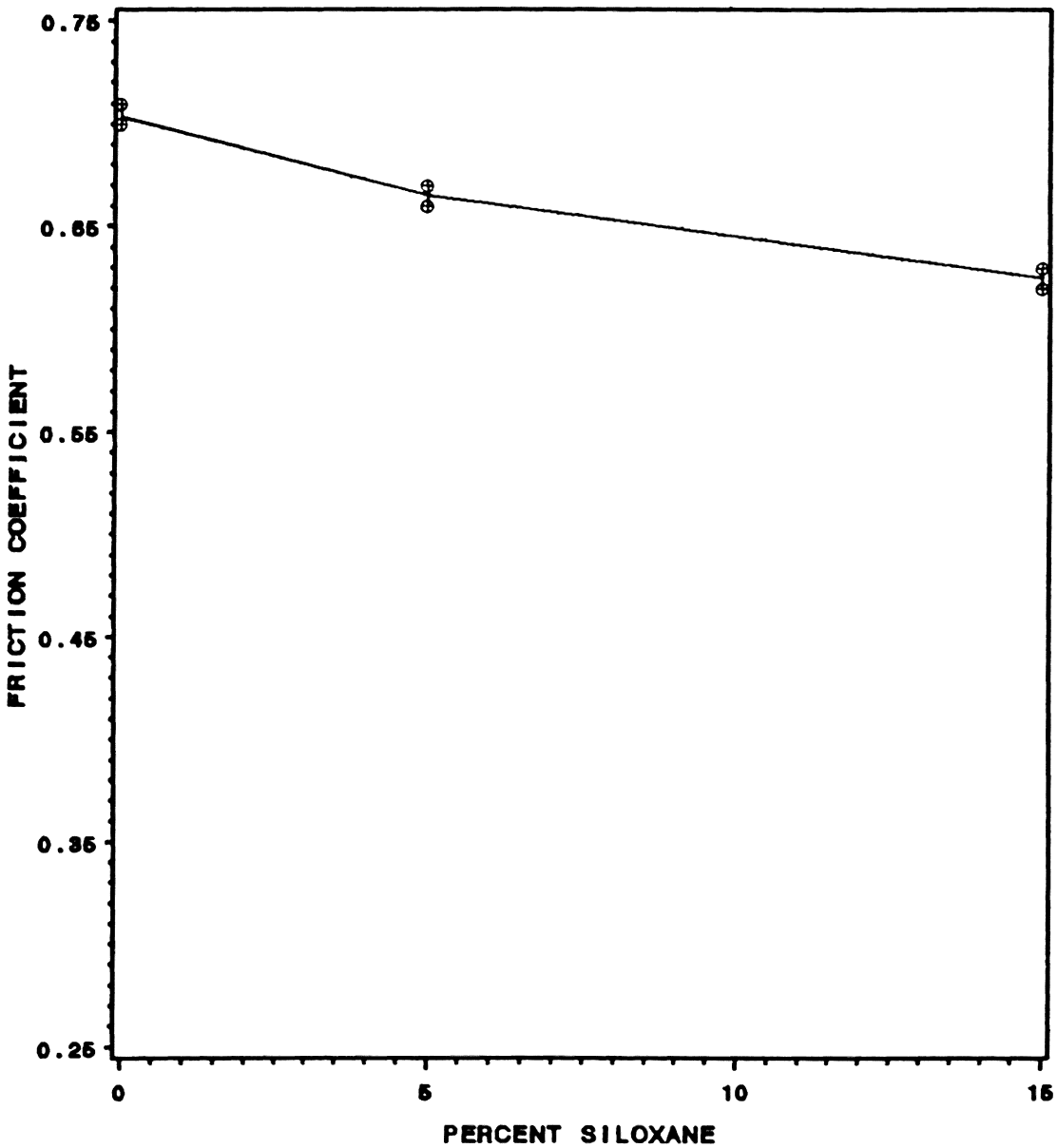

Figure 10: Effect of percent siloxane on friction, abrasive tests.

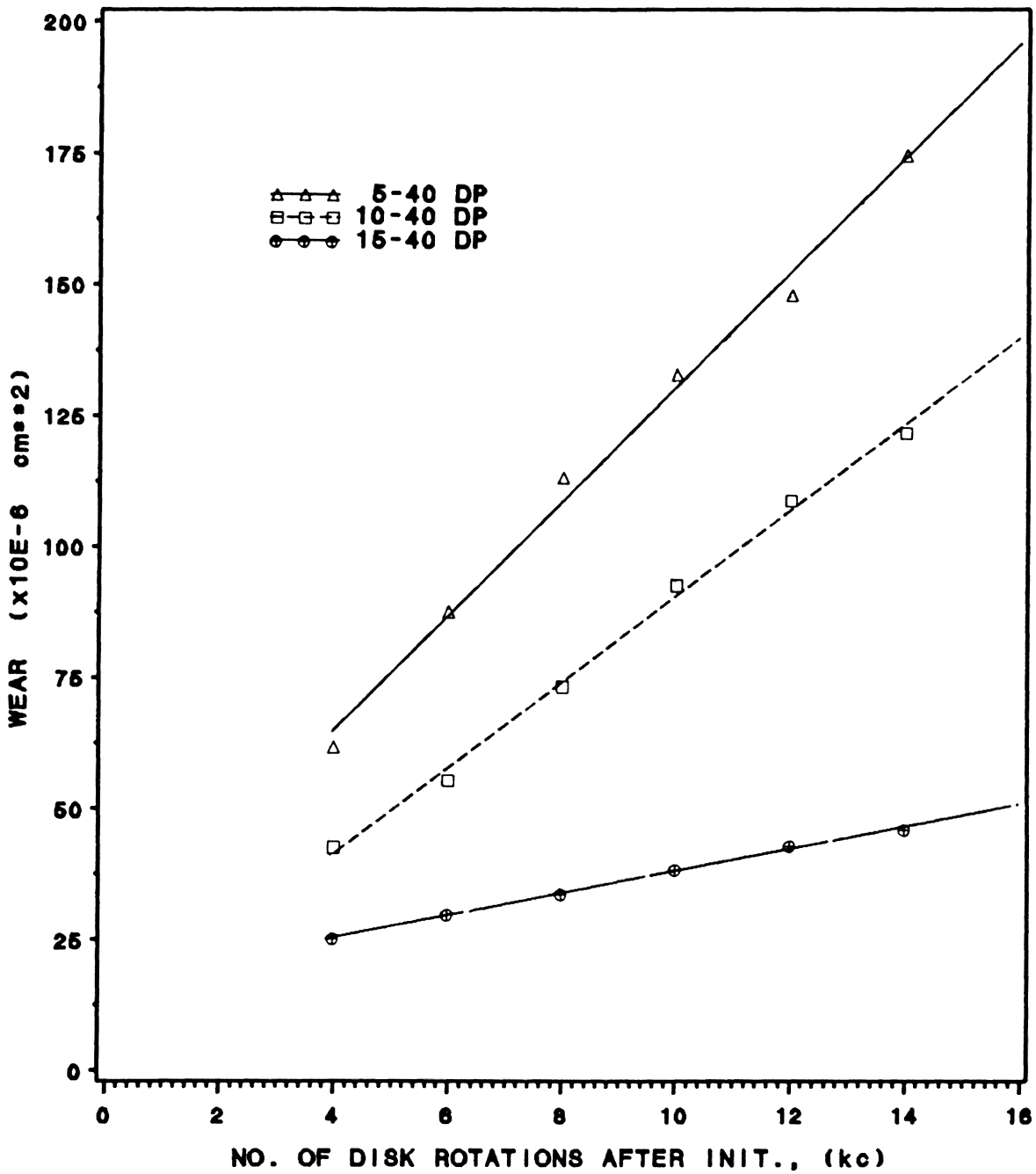

Figure 11: Effect of percent siloxane on wear, 40DP.

TABLE 8

Wear Rates and Wear Track Initiation Periods, 20DP

5-20DP		10-20DP		15-20DP	
Init. (cycles)	wear rate (cm^2/kc)	Init. (cycles)	wear rate (cm^2/kc)	Init. (cycles)	wear rate (cm^2/kc)
1200	5.9×10^{-6}	600	15.8×10^{-6}	1300	0.80×10^{-6}
3000	6.2	1500	12.6	200	5.60
2000	5.2	1050	7.8	14000	2.20
1800	8.6	1000	10.3	8000	1.66
----	10.4	1000	12.7	10000	----

TABLE 9

Wear Rates and Wear Track Initiation Periods, 40DP

5-40DP		10-40DP		15-40DP	
Init. (cycles)	wear rate (cm^2/kc)	Init. (cycles)	wear rate (cm^2/kc)	Init. (cycles)	wear rate (cm^2/kc)
900	6.9×10^{-6}	12000	5.7×10^{-6}	1600	1.3×10^{-6}
900	12.9	2800	10.0	1200	2.4
600	13.2	6900	9.5	900	2.5
800	9.5	10000	---	750	3.5
650	---	6000	---	2000	---

TABLE 10

Wear Rates and Wear Track Initiation Periods, 40DP w/o debris

5-40DP		10-40DP		15-40DP	
Init. (cycles)	wear rate (cm^2/kc)	Init. (cycles)	wear rate (cm^2/kc)	Init. (cycles)	wear rate (cm^2/kc)
1500	$11.5x10^{-6}$	1000	$14.0x10^{-6}$	600	$9.0x10^{-6}$
200	12.7	600	15.7	1100	9.7
455	13.0	—	—	—	—

TABLE 11

Average Wear Results

Sample	Init. (kc)	Wear Rate cm^2/kc	Wear Rate w/o debris
control	**0.81 ± 0.16**	**12.7(10.7-14.7)x10^{-6}**	—
5-20DP	2 ± 1.2	7.3 (4.6-10)	—
10-20DP	1 ± 0.40	11.8 (8.1-15.5)	—
15-20DP	6.70 ± 6.70	2.6 (0.0-5.9)	—
5-40DP	0.78 ± 0.14	10.6 (5.9-15.4)	12.4 (10.4-14.4)
10-40DP	7.50 ± 4.40	8.4 (4.4-12.5)	14.8 (13-17)
15-40DP	2.40 ± 2.40	2.4 (1.6-3.2)	9.35 (8-10.7)
5-18AN	4.20	10.5	—
10-18AN	3.00	6.7	—
15-18AN	1.72	2.4	—

95% confidence limits are given in parentheses

Upon examining the wear rates of the 20 percent DP samples, it is noted that the modified epoxy samples have a lower wear rate than the control (pure epoxy) sample. With the exception of 10-20 DP sample, an increase in siloxane content resulted in a decrease in the wear rate. The wear rates of 5-20 DP and 15-20 DP were 42 and 80 percent lower than that of the control sample, respectively. The average wear rate of 10-20 DP sample is also lower than the control sample but considering the 95 percent confidence limits, their difference is not significant. Figure 12 shows the effect of percent siloxane on wear, for 20 percent DP samples.

Figure 11 exhibits the effect of percent siloxane on wear, for 40 prcent DP samples. Although the wear range of 5-40 DP sample partly overlapped that of the control epoxy, it still had a lower wear rate (see Table 11). At higher siloxane content the reduction of wear rate with respect to the control sample was more; the wear rates of 10-40 DP and 15-40 DP were 34 and 81 percent lower than that of pure epoxy, respectively.

The CTBN-modified epoxies, shown in the bottom of Table 11, exhibit the same trend as the siloxane-modified epoxies did, as far as the percent rubber is concerned. The sample with the highest percent rubber has the lowest wear rate.

Wear rates for tests without wear debris in the wear track are listed in Table 11. Upon comparing the values of wear rates with and without the debris, one can notice that the effect of removal of the debris on wear rate was dependent on the amount of the siloxane in the

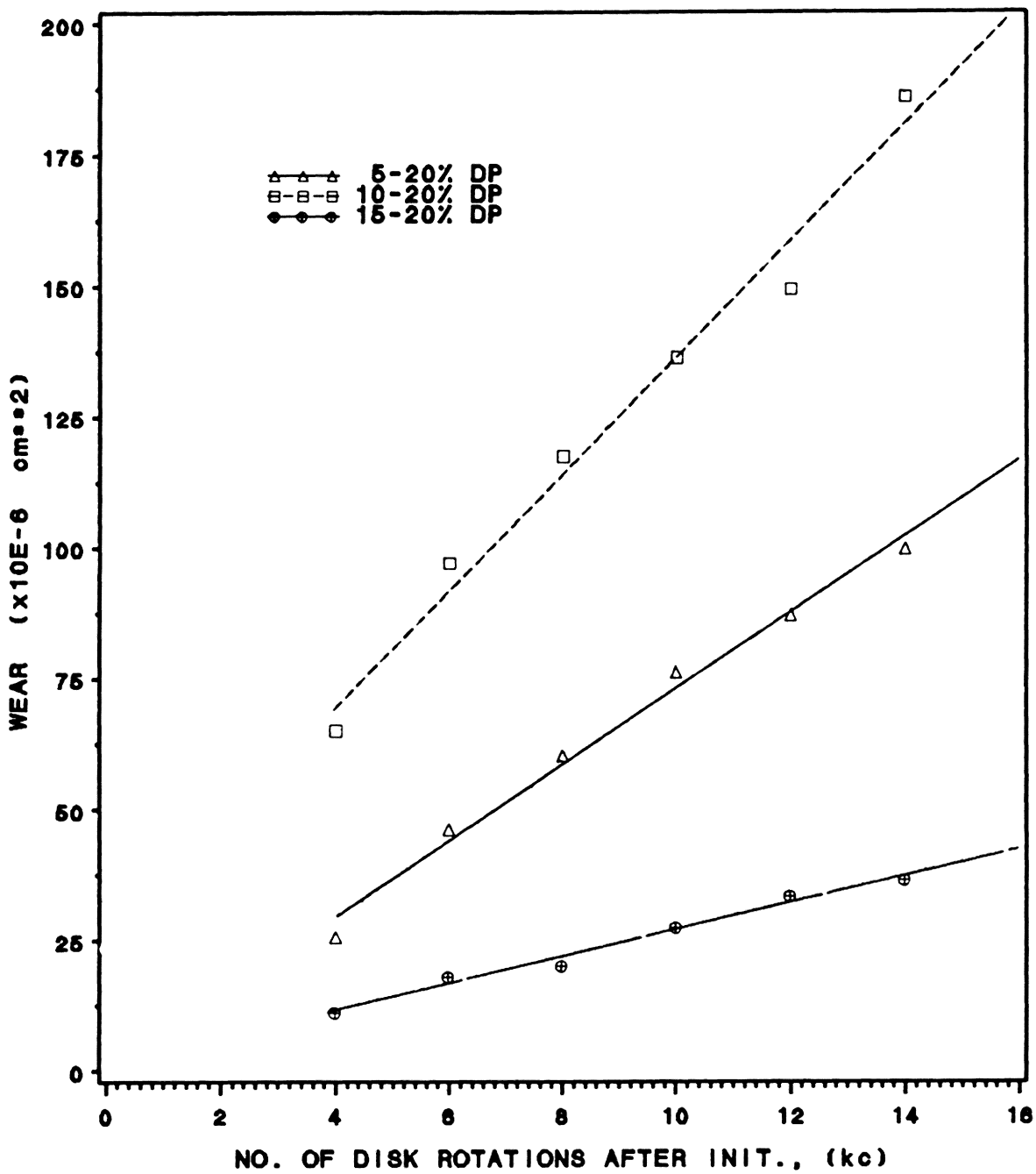

Figure 12: Effect of percent siloxane on wear, 20DP.

epoxy. At 5 percent there was no difference in wear rates; at 10 and 15 percent removing the debris increased the wear rate by 76 and 290 percent, respectively. Figure 13 shows the strong dependence of wear on the debris.

4.3.2 Abrasive Wear Tests

Abrasive wear tests were conducted on pure epoxy, 5-40 DP, and 15-40 DP samples. Figure 14 shows the effect of percent siloxane on the wear rate of these samples. For the abrasive tests, wear occurred as soon as the epoxy pin was brought in contact with the abrasive disk. From Fig. 14 it is noted that the ranking of the samples was the same as before, based on the wear rates. Therefore, it can be stated that the type of the wear mode or test geometry did not change the tribological responses of the material relative to its siloxane content.

4.4 Scanning Electron Micrographs

The surfaces of the modified epoxy specimens were examined in a Scanning Electron Microscope (SEM). All specimens were coated with gold palladium to a thickness of 75 Angstrom to prevent charging by the electron beam which had an accelerating voltage of 15 kV. Several representative SEM micrographs of the partially worn wear tracks as well as fully developed wear tracks were taken. In addition to the SEM micrographs, a few optical micrographs were taken at lower magnifications.

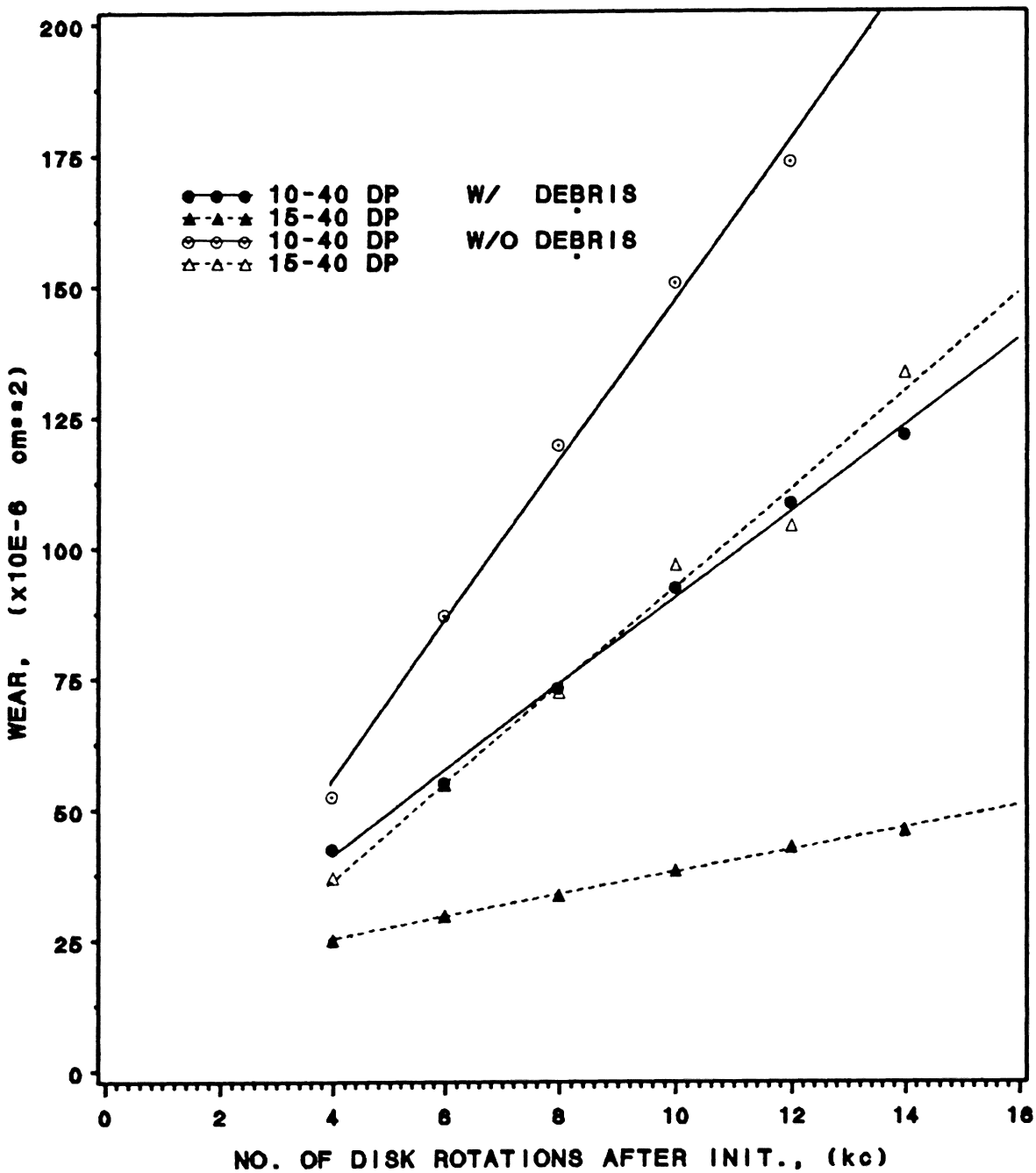

Figure 13: Effect of wear debris on wear.

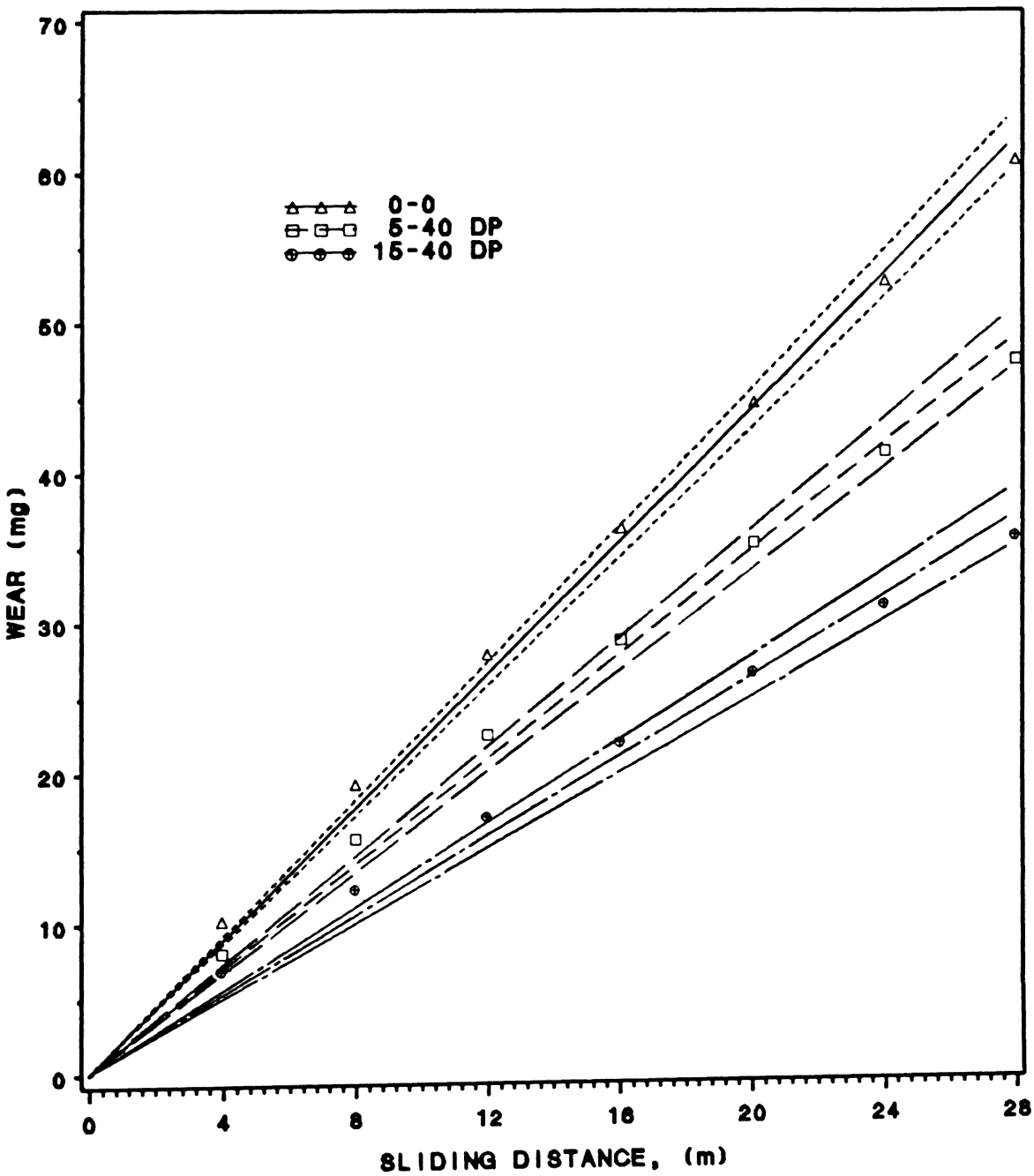

Figure 14: Effect of percent siloxane on abrasive wear.

(a)

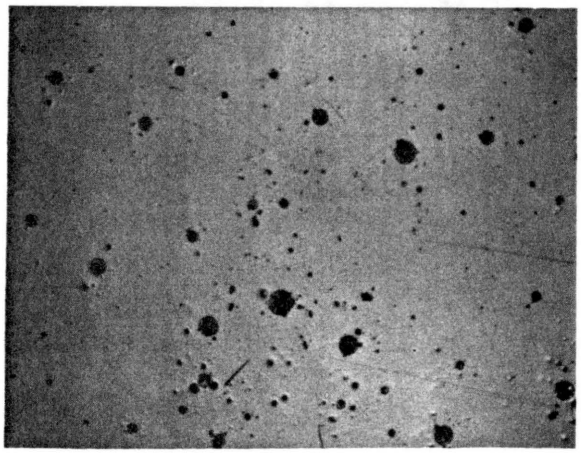

(b)

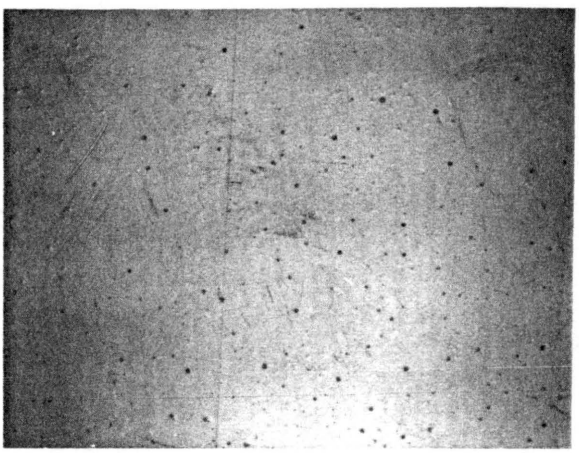

(c)

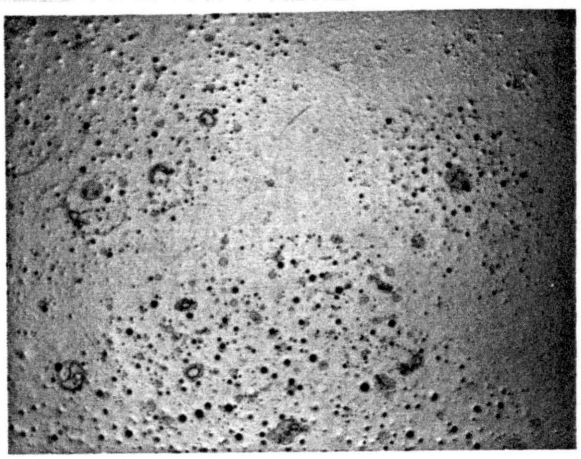

Figure 15: Optical micrographs of 20DP samples at magnification factor of 275: a) 5-20DP, b) 10-20DP, and c) 15-20DP.

(a)

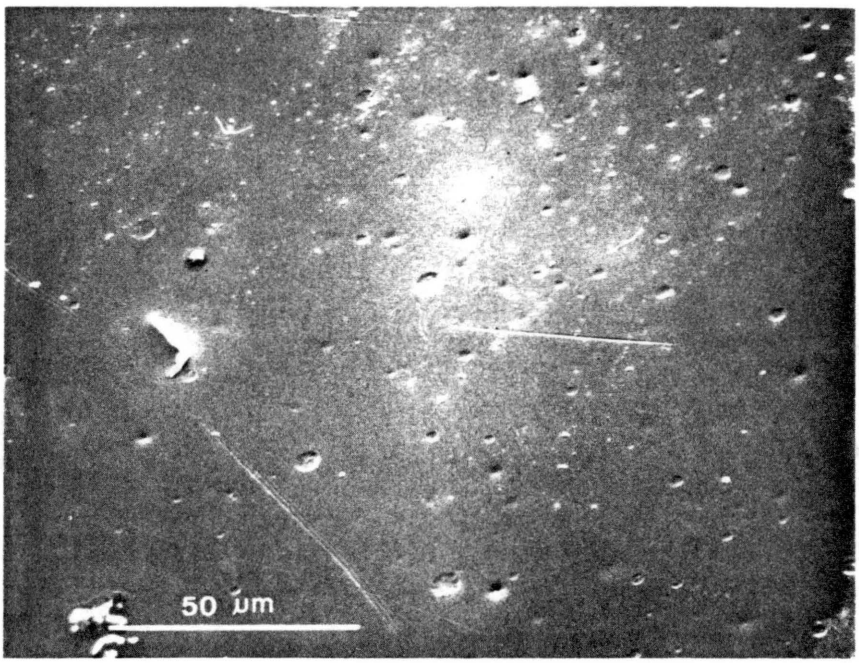

(b)

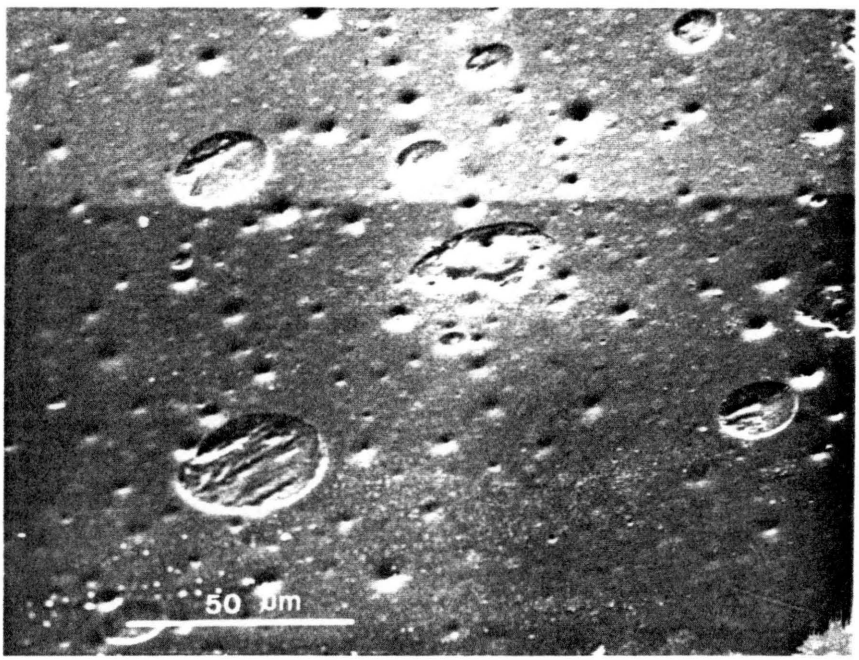

Figure 16: SEM micrographs of 20DP samples: a) 10-20DP and b) 15-20DP.

(a)

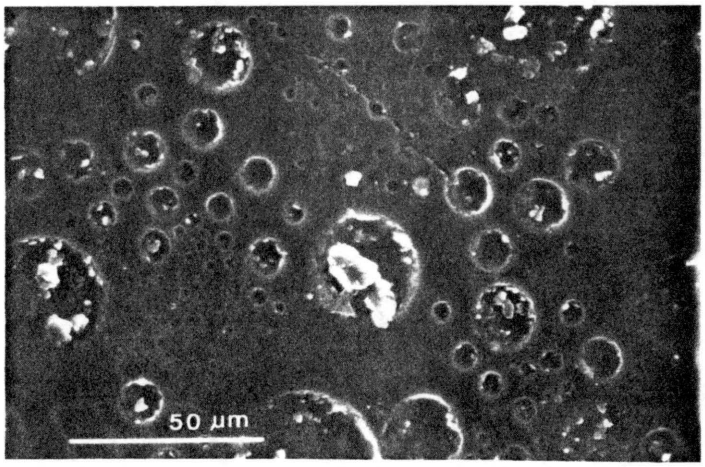

(b)

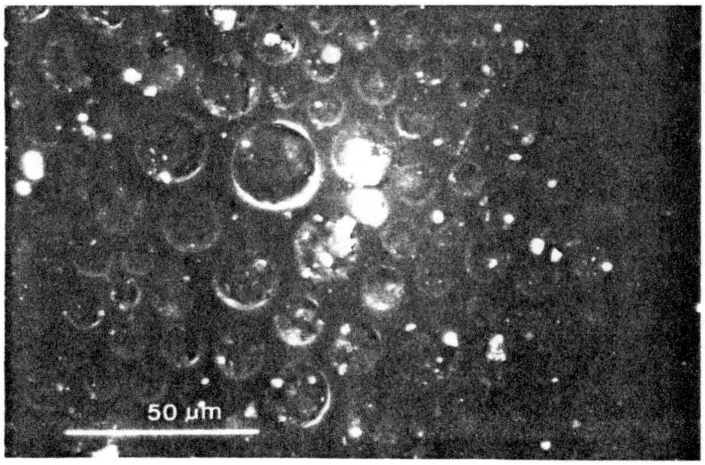

(c)

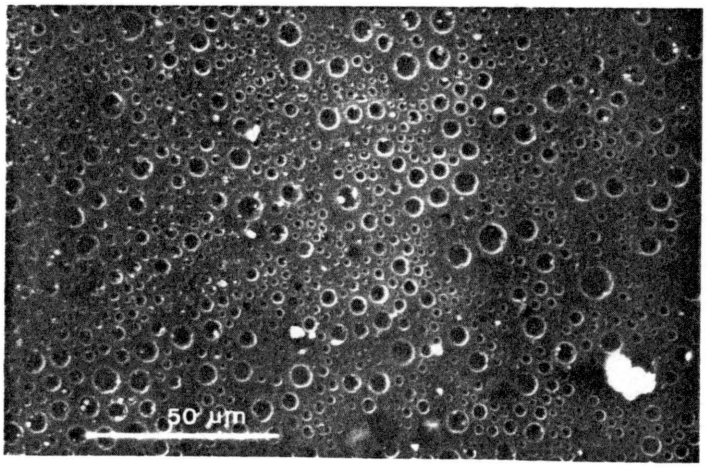

Figure 17: SEM micrograph of 40DP samples: a) 5-40DP, b) 10-40DP, and c) 15-40DP.

The surface of the siloxane-modified epoxies of different compositions are shown in Figs. 15 through 17. The pictures illustrated in Fig. 15 show the surface of 20DP samples viewed through an optical macroscope. Figure 15 shows the outstanding difference in morphology of 10-20DP surface compared to that of 5-20DP and 15-20DP. The SEM micrographs of 10-20DP and 15-20DP are shown in Fig. 16. The domain distribution of the samples with 40 percent DP are shown in Fig. 17. Upon comparing the three micrographs in Fig. 17, it is observed that with increasing percent siloxane the number of the elastomeric domains increases. There is also more uniformity with respect to size for higher siloxane content. It should be mentioned that these micrographs show the typical morphology of the surfaces and there are a few regions, for example, on 15-40DP surface that have extremely large domains; ten times larger than the domains shown in Fig. 17(c).

Surfaces of wear track after they were fully worn (14000 cycles) for the 40DP samples are represented in Figs. 18-21. An overview of the wear track of 5-40DP sample is depicted in Fig. 18. Evidence of plastic flow and drawing of the material is observed by the chevron marks in Figs. 20-21.

The wear tracks of the specimens for tests which had the wear debris blown out of the interface are shown in Figs. 22-24. Wear tracks of tests without debris, for 10-40DP sample, showed occasional cracks as shown in Figs. 23-24. The difference in surface texture of 15-40DP samples with and without debris is shown in Fig. 25. The samples of no-debris tests show cavitated circular domains where the elastomer resided

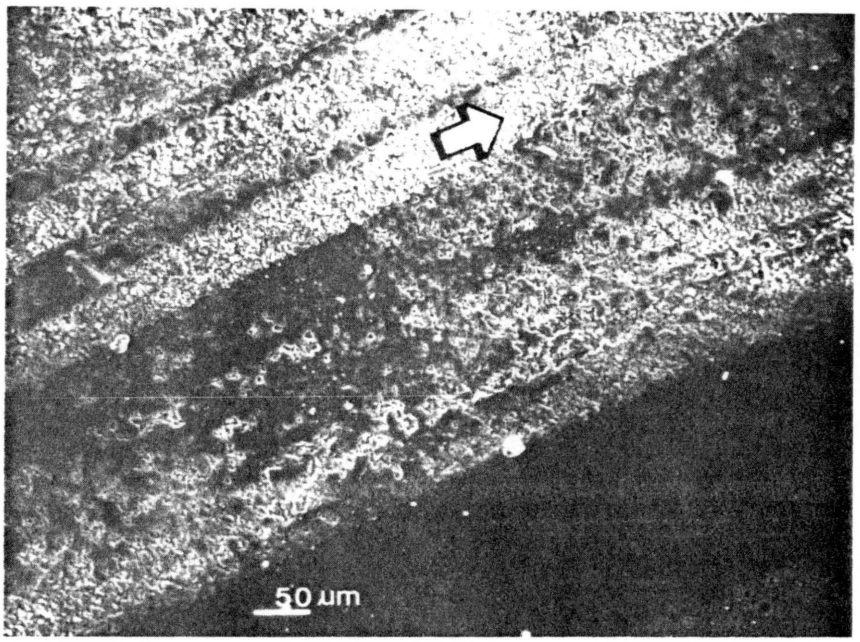

Figure 18: Wear track of 5-40DP at 14000 cycles. Arrow indicates direction of sliding.

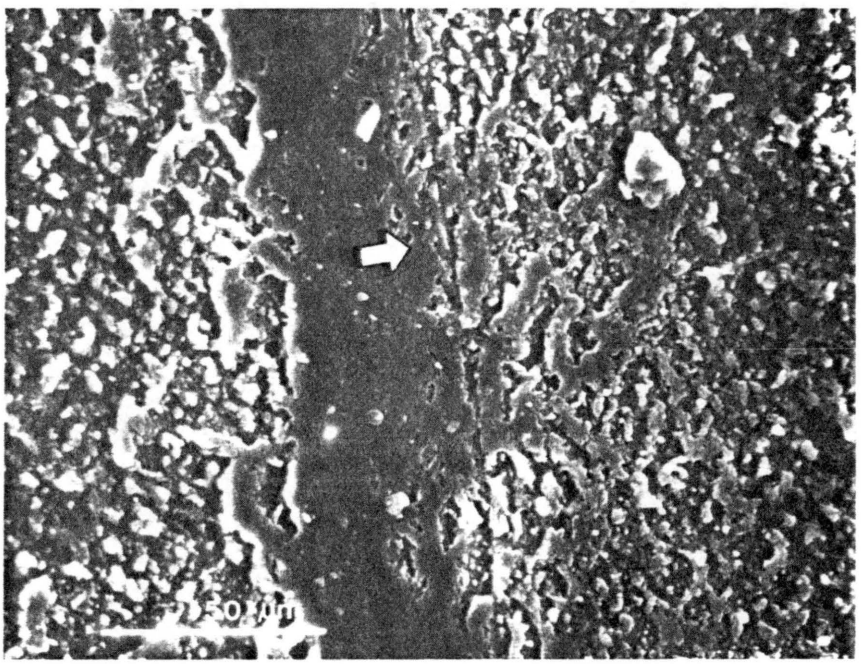

Figure 19: Wear Track of 5-40DP at 14000 cycles. Arrow indicates direction of sliding.

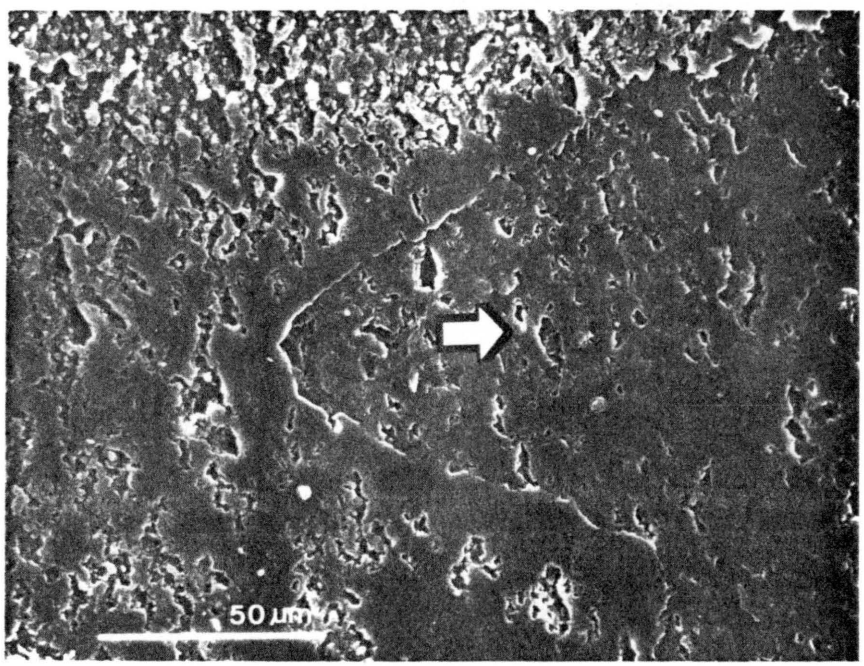

Figure 20: Wear track of 5-40DP at 14000 cycles. Arrow indicates direction of sliding.

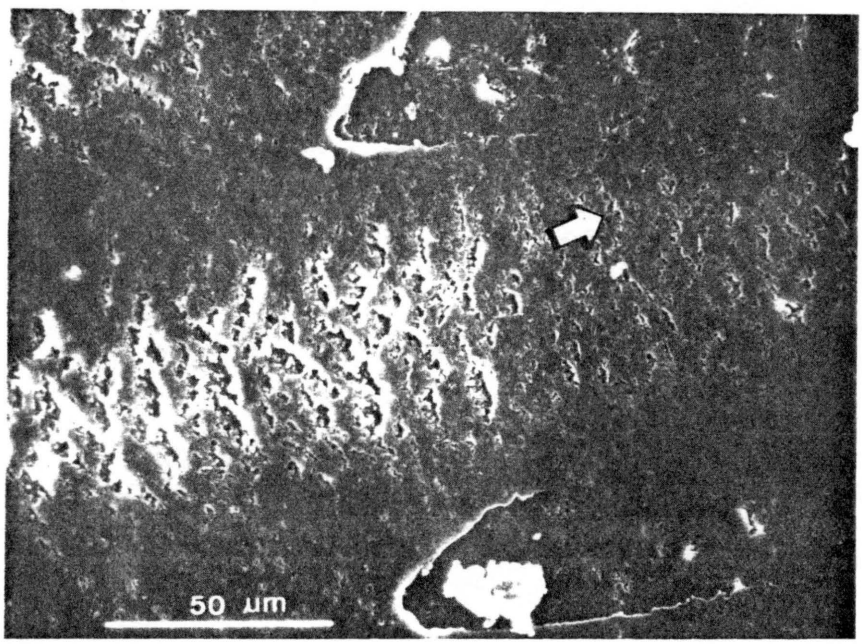

Figure 21: Wear track of 10-40DP at 14000 cycles. Arrow indicates direction of sliding.

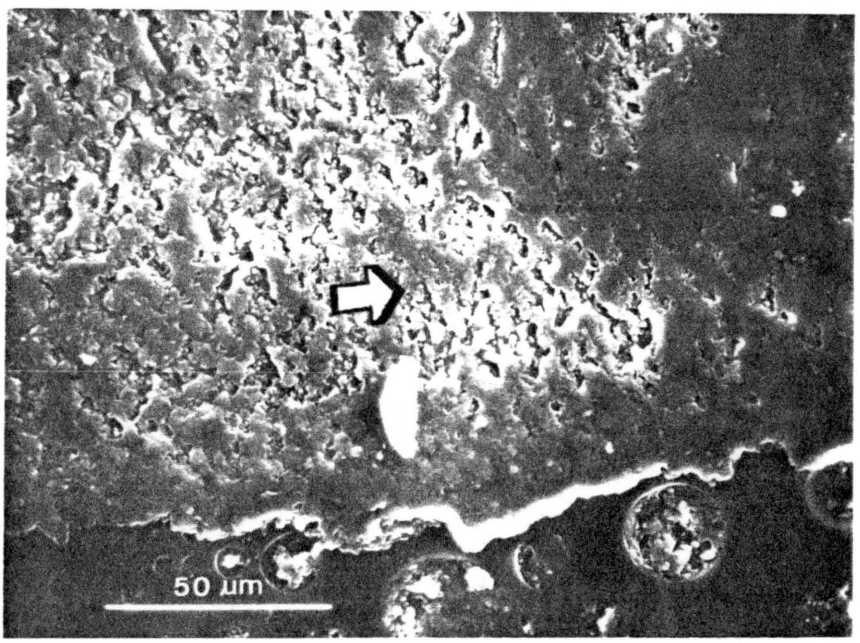

Figure 22: Wear track of 5-40DP, w/o debris after 14000 cycles. Arrow indicates direction of sliding.

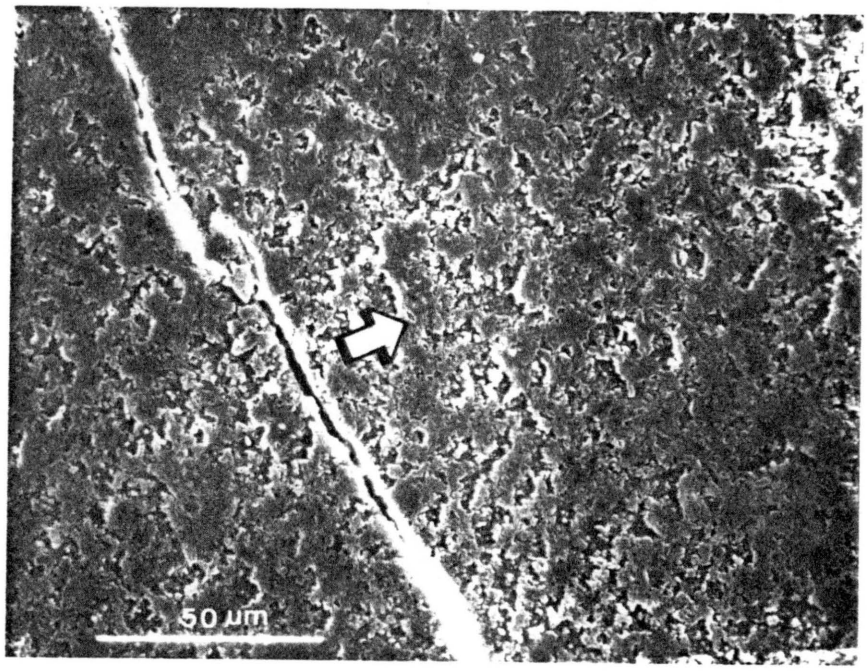

Figure 23: Wear track of 10-40DP, w/o debris after 14000 cycles. Arrow indicates direction of sliding.

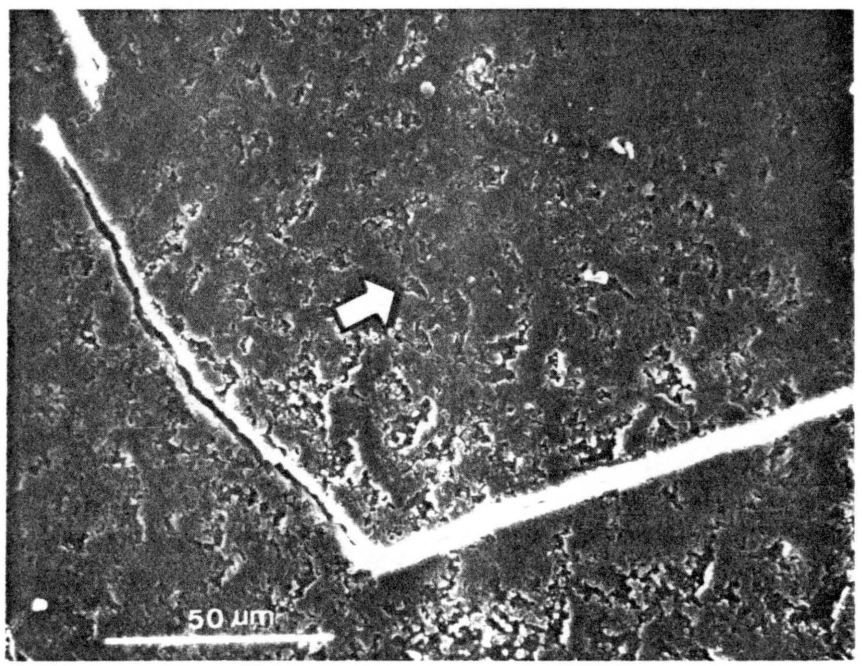

Figure 24: Wear track of 10-40DP w/o debris after 14000 cycles. Arrow indicates direction of sliding.

(a)

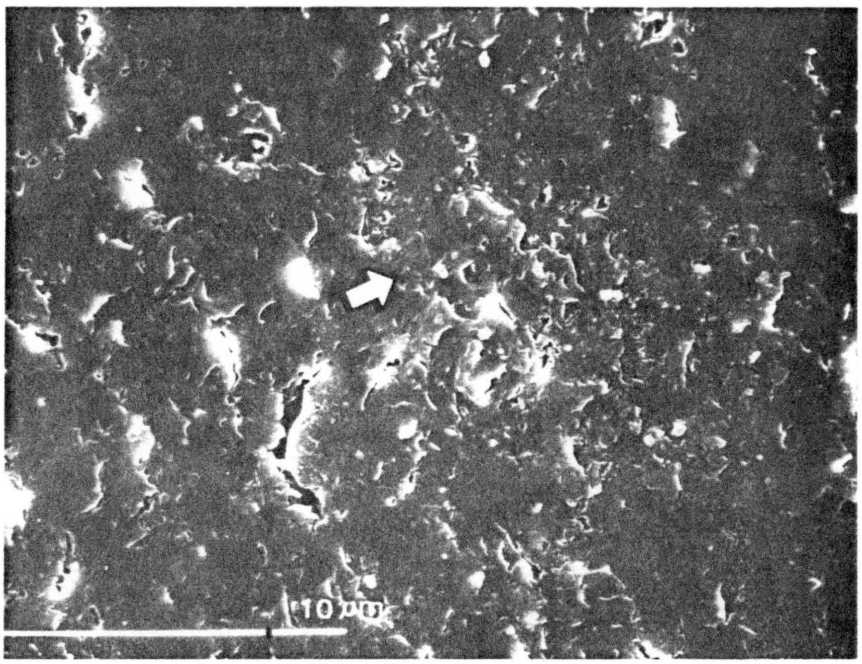

(b)

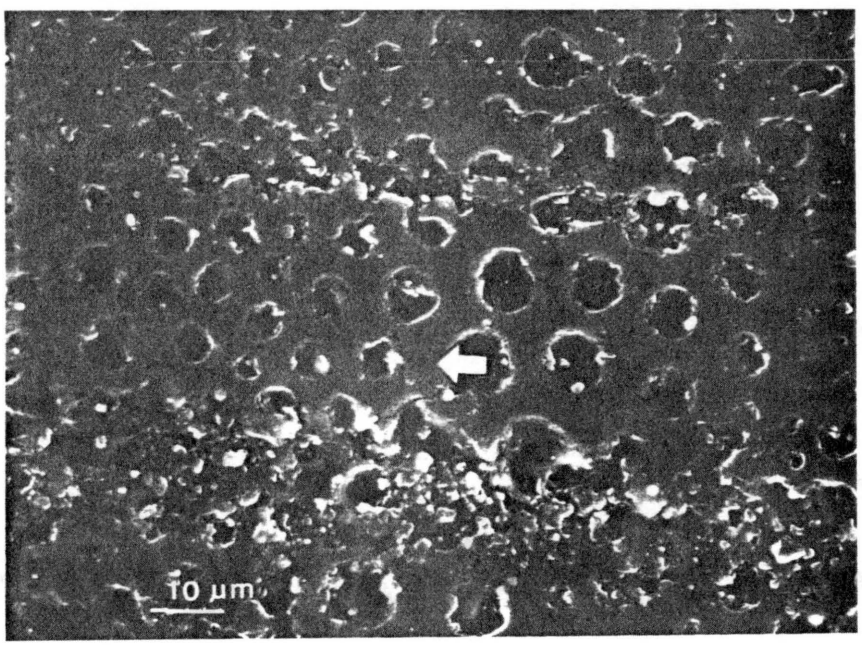

Figure 25: Wear track of 15-DP after 14000 cycles. a) with debris. b) without debris. Arrow indicates direction of sliding.

before it was removed (Fig. 25b), while samples of tests with debris show a much smoother surface (Fig. 25a). None of the micrographs of tests without debris showed any chevron marks on the surface as shown in Figs. 20-21.

Changes in the wear debris for different compositions were observed. Wear debris of each sample showed flake-like particles which were composed of smaller particles. Figure 26 shows the wear debris of each composition. Wear debris of 15-40DP seems finer than those of 5-40DP and 10-40DP (compare micrograph c with a and b in Fig. 26).

Several SEM micrographs of the samples which were partially worn were taken to reveal more evidence as to how the wear track formed. The mechanism of initiation of cracks and the formation of wear track will be discussed in the next chapter.

4.5 Morphology

The modified epoxy disks of different compositions were examined in a Ziess SEM Image Processing System (IPS). The sample was placed in the microscope which produced an image onto the image processor. The image was then analyzed by the IPS to give the domain size distribution and the statistical quantities as shown in Fig. 27. All of the samples were coated with gold-palladium to give a better contrast for image processing.

With a few exceptions, for a given specimen, the distribution of the domains was not different from one region of the surface to another. The exception mentioned above was for the samples with 40

(a)

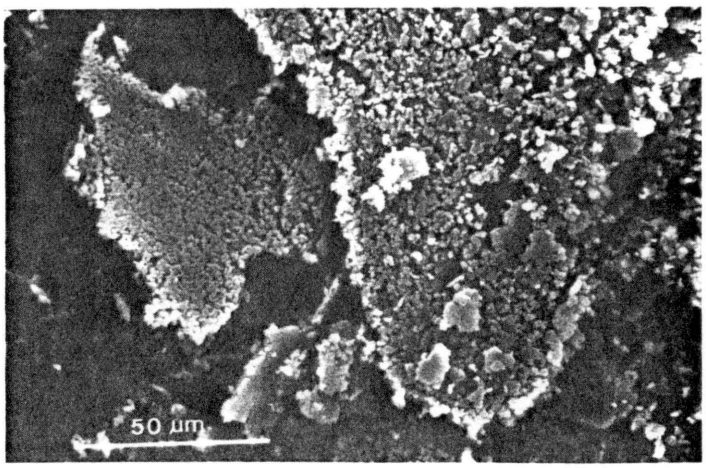

(b)

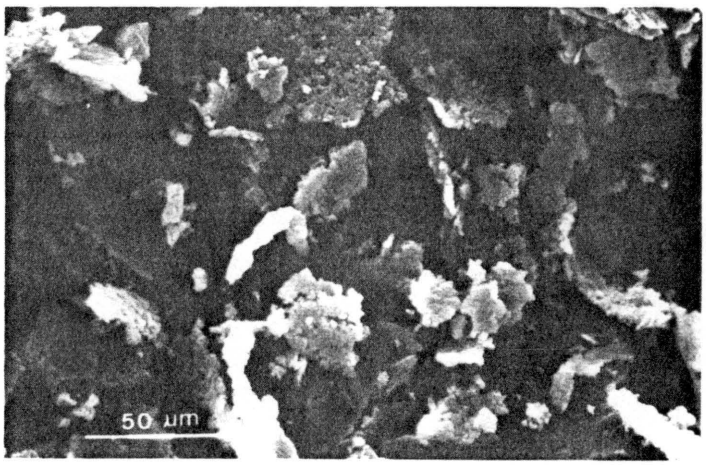

(c)

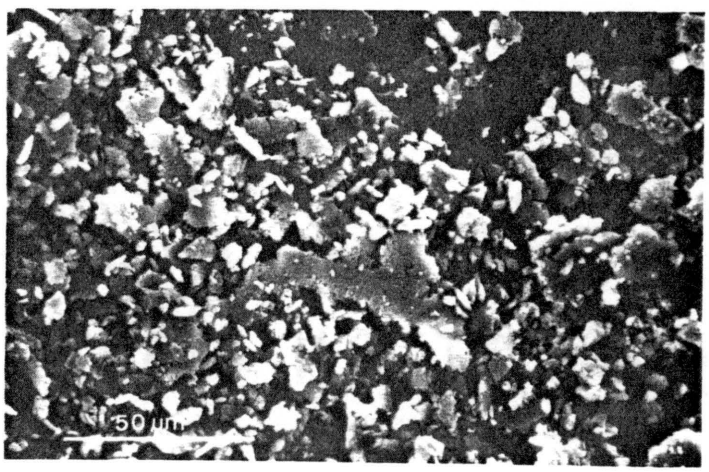

Figure 26: Wear debris of 40DP samples: a) 5 percent siloxane, b) 10 percent siloxane, and c) 15 percent siloxane.

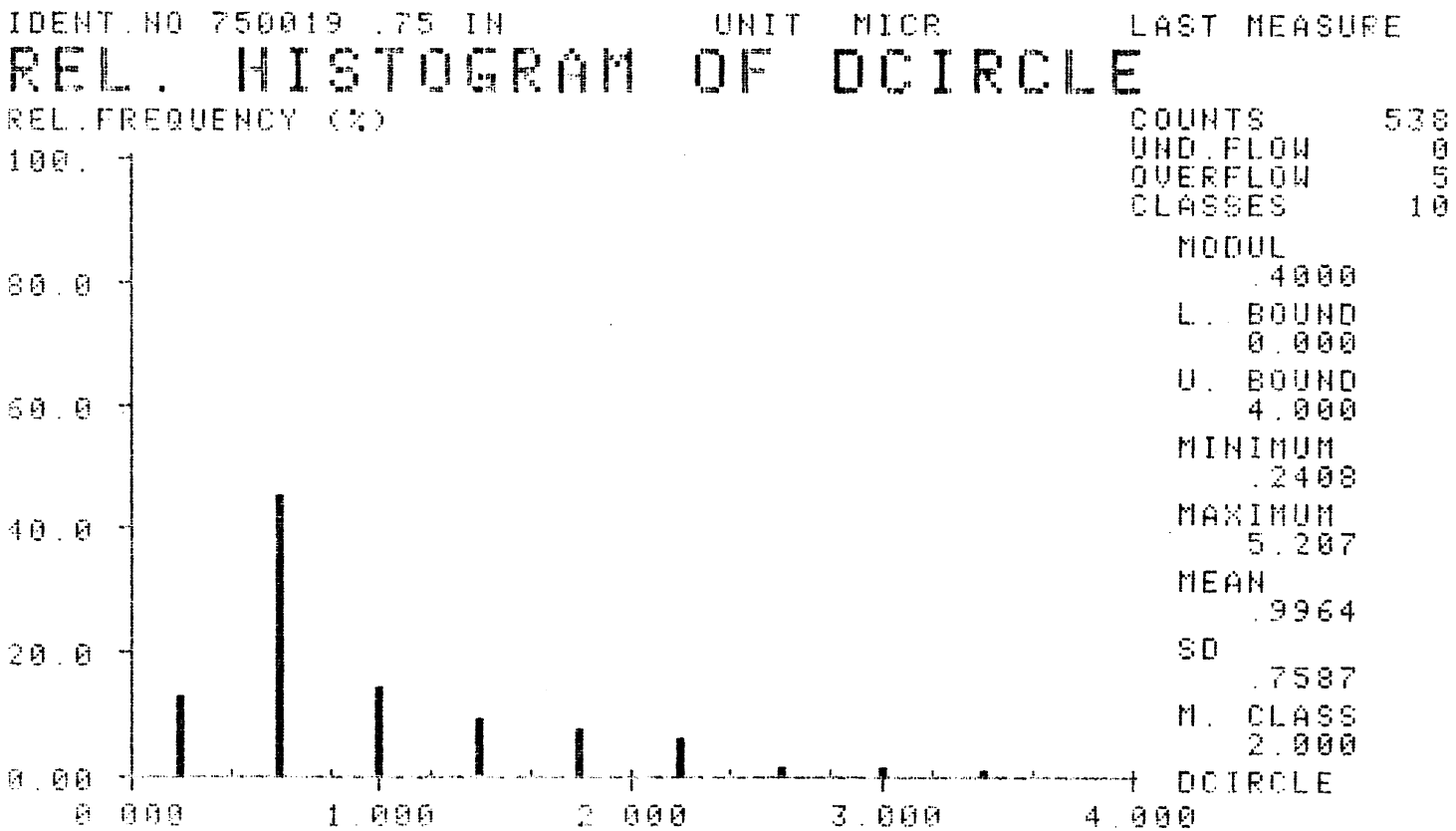

Figure 27: Representative domain size distribution

percent diphenyl which had a few extremely large domains as big as 100 μm. Since this was not a typical feature of the surface these larger domains were not included in the distribution of domain sizes.

For each specimen composition, three regions which had typical surface morphology were selected and analyzed. Results of each analysis is given in Appendix D. They were then averaged to give the values shown in Table 12. Having the average diameter and number of domains, the percentages of the total area occupied by the domains was also calculated and reported in Table 12.

The values of Table 12 show that for 40 percent DP samples, increase of percent siloxane tends to decrease the average size of the domains while for 20 percent DP samples no trend is observed with the change in percent siloxane. The main effect of the increase of percent siloxane is on the number of the domains. For all samples, except 10-20DP, the number of domains on the surface increased when more siloxane was present in the sample. It is also observed that the percent DP in the siloxane and the molecular weight had a marked influence on morphology.

TABLE 12

Morphology Results

Sample	avg. diam. (μm)	domains no. per mm^2	% area of domains
05-2500-20DP	0.78 ± 0.22 †	16,400	0.8 ± 0.45
10-2500-20DP	1.0 ± 0.34	6,700	0.6 ± 0.38
15-2500-20DP	0.89 ± 0.09	100,000	6.4 ± 1.3
05-5000-40DP	1.46 ± 0.36	55,000	9.2 ± 4.4
10-5000-40DP	0.86 ± 0.05	240,000	13.1 ± 1.6
15-5000-40DP	0.88 ± 0.05	245,000	14.9 ± 1.7

† Mean values and 95% confidence limits

5. DISCUSSION

5.1 Friction

Whenever two bodies with relative motion are brought in contact energy is dissipated as a consequence of work done by the frictional force. The frictional work is equal to the deformation losses in the softer material at the contact interface which mostly arise from plastic deformation in metals and viscoelelastic-plastic losses in polymers. The frictional force at the interface results from the adhesive forces between the surfaces at the contact points and the plowing force required to the displace the softer material from the front of the slider. The adhesion component of the friction force between the two surfaces is equal to he product of the real area of contact and shear strength of the junctions over this area. The coefficient of friction is dependent on both the adhesion of the surfaces and the deformation losses in the material.

In all tests of the steel ball on epoxy disk, friction coefficient increased abruptly as soon as wear track was formed (see Tables 4 and 5) and thereafter remained almost constant. To ascertain if the growth of real area of contact was responsible for this behavior, the radius of wear groove was calculated, based on the wear track dimensions. Using Hertzian contact equations, the contact area was calculated. The contact area equations are presented in Appendix E. A correlation analysis revealed that the radii of the grooves were constant as a function of number of cycles required to produce the grooves (cor-

relation coefficients are reported in Appendix F). Therefore, it was assumed that the contact area was constant after the wear track was formed. It should be mentioned that the calculation of area of contact for ball in groove is only an estimation because Hertzian theory assumes that contact occurs only in the groove area. However, SEM micrographs show that the ball contacted also a small surface outside the groove. Therefore, even though the groove radii are very similar as the groove increases in width, the real area may continue to increase in size.

Upon examination of the contact areas, shown in Table 13, the contact areas before wear track initiation are substantially smaller than those after the wear track was formed. For example, the contact area of 5-40 DP sample increased by 56 percent but its coefficient of friction after initiation, μ_{after} increased by 100 percent. Therefore, the increase in the area of contact partially explains the friction transition associated with wear track initiation. Hence, the additional increase in the coefficient of friction must have been a result of the deformation losses. To account for this, it can be assumed that an increase in the area of contact results in an increase in the volume of material which is plastically deformed as the slider passes over it (the deformed volume is assumed to be a hemisphere with a diameter equal to that of the area of contact). If it is assumed that the volume is proportional to the 3/2 power of the area and friction coefficient is proportional to the deformed volume, then the measured friction changes are consistent with the calculated area changes.

Madakson [49] and Friedrich [50] have shown that there is a direct

TABLE 13

Calculated contact areas, (m^2)

Sample	A_0 †	A_z ‡
control	**24.32×10^{-8}**	**38.36×10^{-8}**
05-2500-20DP	25.70	36.65
10-2500-20DP	23.71	38.2
15-2500-20DP	25.60	34.87
05-5000-40DP	24.75	38.70
10-5000-40DP	25.50	37.53
15-5000-40DP	26.20	36.20

†*ball on plane*

‡*ball in groove*

correlation between friction coefficient and surface energies of the sliding bodies. Friedrich states that adhesion depends on the surface energies of the sliding bodies and energy of the new interface between these bodies. Czichos [51] has investigated the friction coefficient of different polymers with different surface energies. Using the Dupré equation to calculate the work of adhesion, he proposed an exponential relationship between the work of friction and work of adhesion which is in good agreement with the experimental data. This equation suggests the strong dependency of friction on the surface energy.

Figures 7 and 8 show that, in general, friction coefficient after the wear track was formed was lower for epoxy samples with more siloxane content and the reduction in friction was more pronounced at higher siloxane contents. This is in complete agreement with the adhesion model of friction which depends on the surface energy. Surface energy is an indication of the strength of adhesive bonds formed between the two contacting surfaces. If surface energy is low, the adhesive bonds are weak, less shear stress can be transmitted over the interface, and the deformed volume decreases resulting in a lower energy loss and lower frictional work. The surface energy of the siloxane modifiers is significantly lower than that of the epoxies, a modified epoxy sample which has more siloxane content should possess a lower surface energy, thereby a lower coefficient of friction. Morphology results (given in Table 12) indicated that, except for 10-20 DP sample, the number of domains in the samples increased for samples with more siloxane content while the average size of domains did not change significantly. Also,

the percentage of surface areas of the siloxane domains (except 10-20 DP) increased for samples which had more siloxane content. This supports the assumption that samples with higher percent siloxane had lower surface energy resulting in a lower coefficient of friction. As it can be observed from Figs. 7 and 8, the pure epoxy sample which did not contain any siloxane, had the highest coefficient of friction since it possessed the highest surface energy.

It is important to mention that the amount of siloxane in the epoxy is not the primary factor which affects the coefficient of friction. As it is illustrated in Fig. 7, the sample with 10 percent siloxane exhibited a higher friction than the sample with 5 percent siloxane but still had a lower coefficient of friction than the control sample. Morphology results given in Table 12 show that 10-20 DP samples had the least number of the elastomeric domains and the lowest percent area of domains on the surface. This suggests that 10-20 DP sample was not as rich with the siloxane elastomer as the other samples were. Thus 10-20 DP had a higher coefficient of friction than 5-20 DP. Large number of siloxane particles in the sample, i.e., phase separation of the siloxane particles and the resulting morphology are important factors which influence the surface energy.

SEM micrographs taken at early stages of the wear track formation suggest that when wear starts and the epoxy material between the elastomeric domains is removed, the steel ball encounters the elastomeric domains and friction force smears them over the surface creating a surface rich in siloxane. This surface is then drawn along

the sliding direction as the rider passes over it. This is evident in Fig. 28, which shows the material being drawn out of the domains and smeared over the epoxy surface. A later stage of wear for tests of with and without wear debris is shown in Figs. 29 and 30, respectively. It is observed in Fig. 29 that the debris have filled up the voids produced by drawing out the domains in earlier passes. With more number of passes these voids are believed to be filled and covered with debris as shown in Fig. 31. Eventually the debris is believed to be acting like a thin film-like layer over the surface. This thin layer is speculated to be removed in later stages and this whole process is repeated (see Figs. 32, 26a).

The results in the previous chapter indicated that removal of the wear debris out of the interface increased coefficient of friction especially for 15-40 DP samples. For no-debris tests, as soon as a loose wear debris was generated it was blown out of the interface before it could interact with the slider. Thus, there was no chance for the rubbery siloxane particles with their low surface energy to be trapped under the slider to promote a slippery surface. With the removal of the debris by blowing, there was no opportunity for the siloxane material to build up in the wear track and the only source of the siloxane was the domains within the wear track.

Now let's turn to the friction coefficients for abrasive tests. For abrasive tests there was no friction transition as the contacting area of the cylindrical epoxy pin was constant. The friction coefficient remained virtually constant throughout each test. The

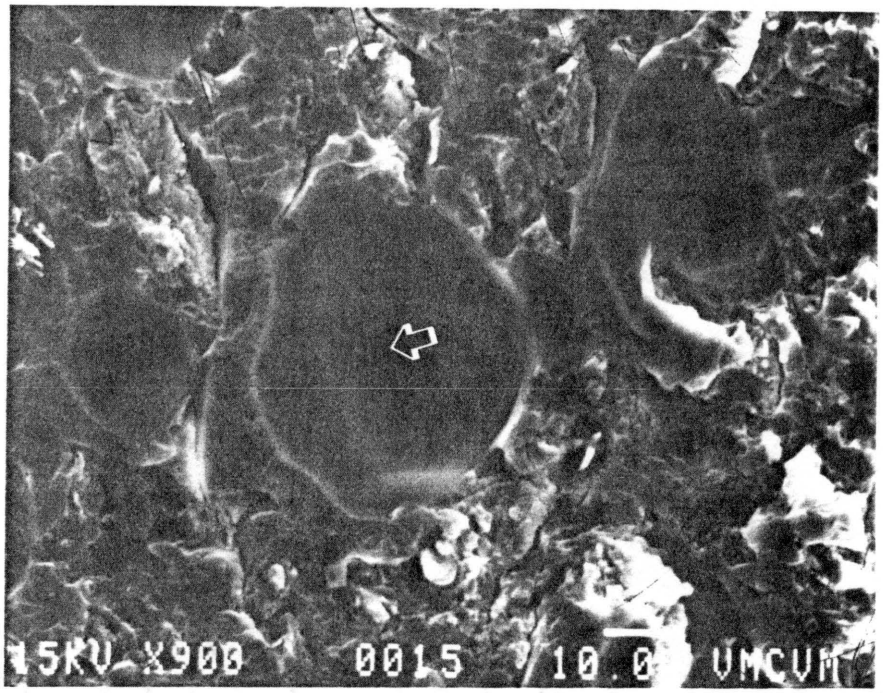

Figure 28: Wear track of 15-40DP after 8000 cycles. Arrow indicates direction of sliding.

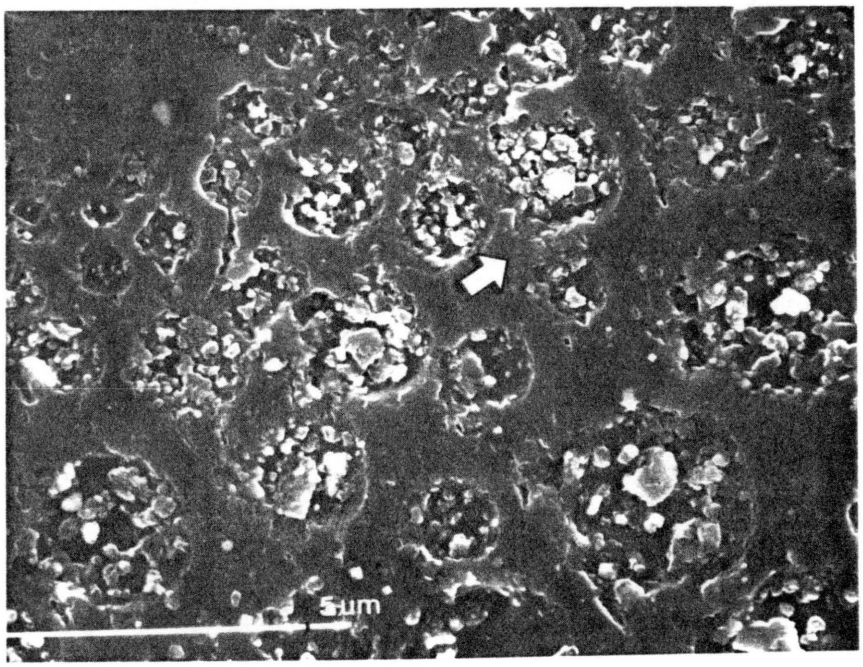

Figure 29: Wear track of 15-40DP. Arrow indicates direction of sliding.

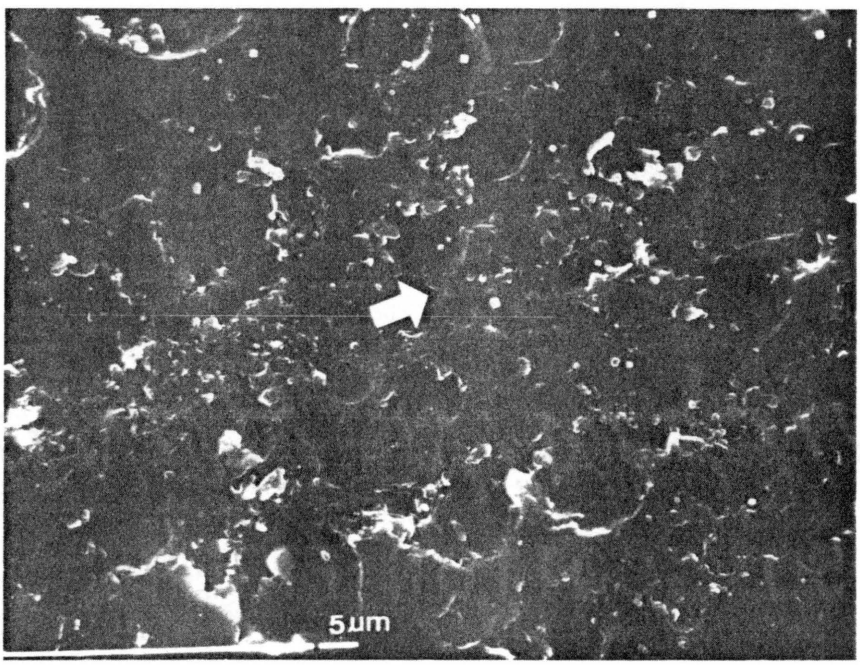

Figure 30: Wear track of 15-40DP, w/o debris. Arrow indicates direction of sliding.

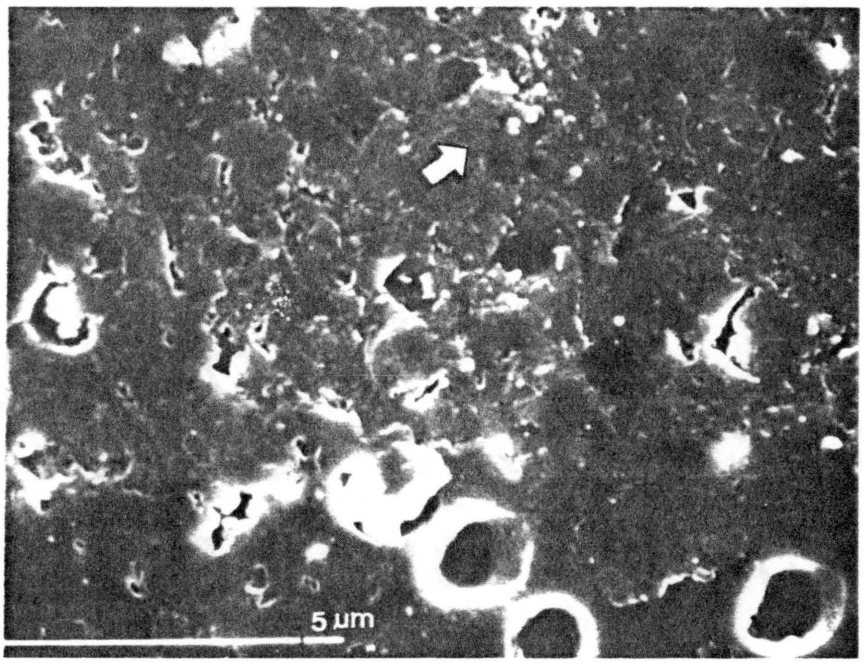

Figure 31: Wear track of 15-40DP. Arrow indicates direction of sliding.

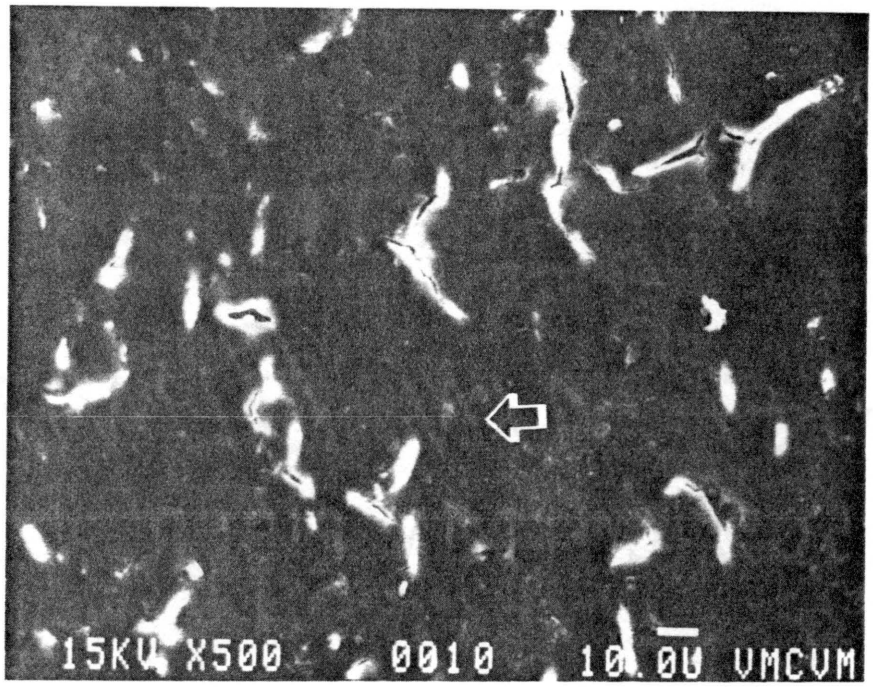

Figure 32: Wear track of 5-40DP after 14000 cycles. Arrow indicates direction of sliding.

values of friction coefficients for abrasive tests were approximately two times of those for the fatigue tests. When the epoxy pin is loaded against abrasive disk, the hard sharp asperities of the abrasive disk will penetrate into the epoxy surface. To maintain motion the interlocking asperities have to be either fractured or plastically deformed. This gives rise to energy dissipation through fracture and plastic deformation. Figures 33 and 34 show the worn surfaces of the control and 15-40 DP epoxy pins. These micrographs show parallel grooves produced by the plowing action of the hard asperities of the disk. The worn surfaces seem to be very rough. These micrographs clearly show that deformation losses were abundant. Thus, the higher values of friction coefficients for abrasive tests are attributed to the more energy dissipation through plastic deformation and fracture in comparison to those of fatigue tests.

5.2 Wear Track Formation

In order to understand the tribological responses of a system to operating conditions and material properties, it is of great importance to known how the loading conditions cause failure in the material. Therefore, before discussing the wear results, the mechanism by which the surface fails and leads to formation of wear track will be identified.

For ductile materials, the onset of plastic yielding is the failure criterion as in the von Mises criterion all three principal stresses are important. For brittle materials, however, failure occurs by fracture

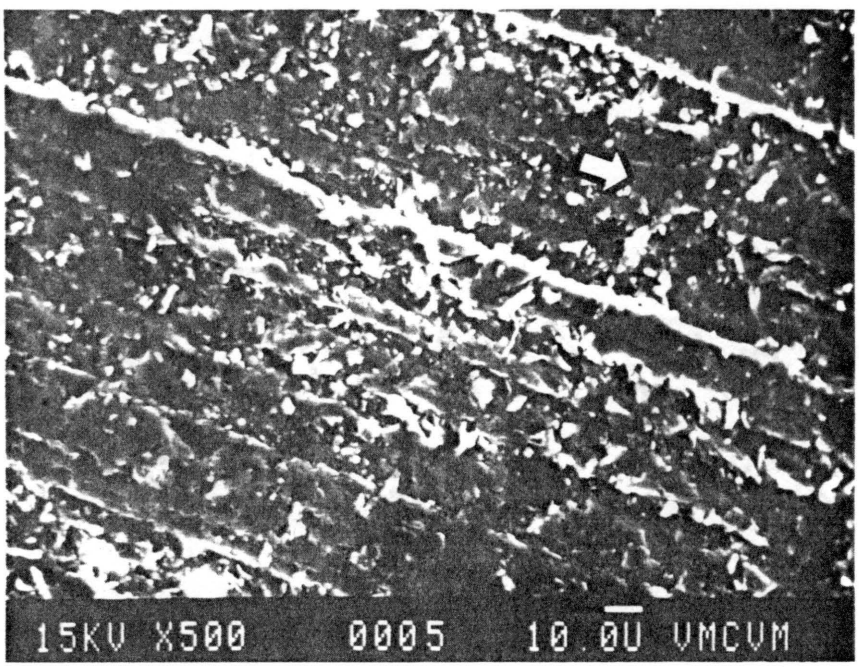

Figure 33: Abrasive wear surface of the control epoxy pin. Arrow indicates direction of sliding.

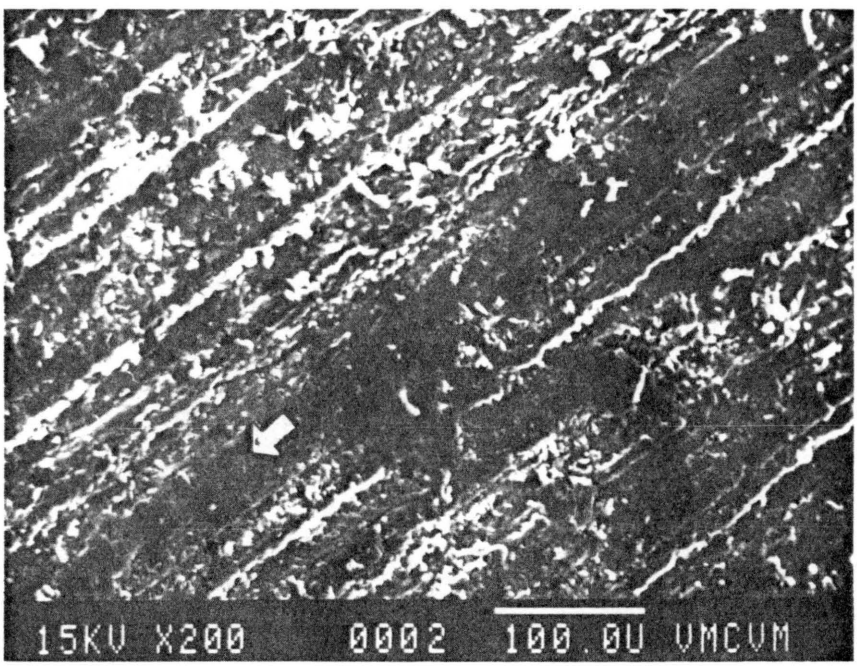

Figure 34: Abrasive wear surface of the 15-40DP pin. Arrow indicates direction of sliding.

and since brittle materials are weaker in tension, the presence of tensile stresses are important. As will be shown below, during sliding the material at the surface experiences alternating tensile and compressive stresses.

In the first test configuration (steel ball on epoxy disk) the loads involved are the applied normal force and a tangential force arising from friction. Hamilton and Goodman [52] have analyzed the stresses in a sliding circular contact region created by loading of a sliding sphere against a flat surface. Their analysis shows that two of the three principal stresses in the contact region are largely compressive in nature and the third one is tensile at the trailing edge of the contact and is compressive at the leading edge. For fracture of brittle materials due to fatigue, this stress is more important. The expression for this third stress according to [52,53] is:

$$S = -\frac{3\mu P}{2\pi a^3}\frac{x\pi(4+\nu)}{8} + \frac{3P}{2\pi a^2}\{-2\nu(a^2 - r^2)^{1/2} +$$

$$(1-2\nu)[\tfrac{1}{3}(a^2 - r^2)^{3/2} r^{-2} - \tfrac{2}{3} x^2 r^{-4}(a^2 - r^2)^{3/2} - x^2 r^{-2}(a^2 - r^2)^{1/2}$$

$$- \tfrac{1}{3} a^3 r^{-2} + \tfrac{2}{3} x^2 r^{-4} a^3]\} \qquad (1)$$

where μ is coefficient of friction, P is the normal load, ν is poisson's ratio, a is radius of Hertzian contact region (given by equations in Appendix F), $r = (x^2 + y^2)^{1/2}$, and (x,y) is the coordinate of a point of interest in the contact plane. Figure 35 shows a graph of this stress

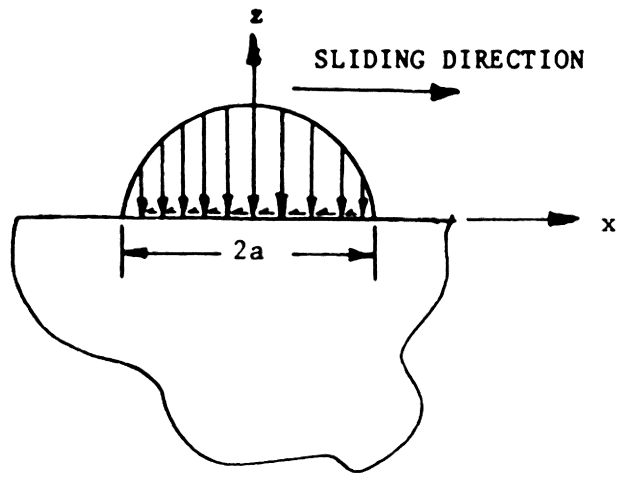

(a)

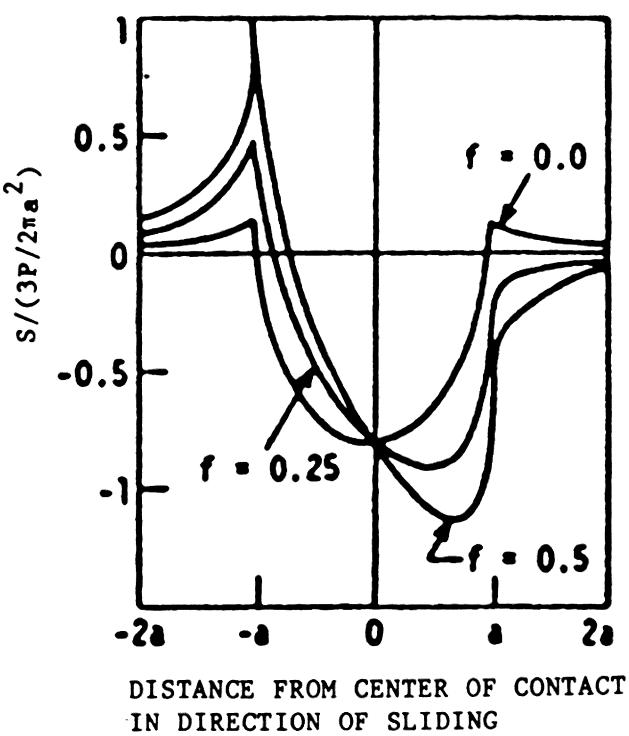

(b)

Figure 35: a) Schematic view of circular contact
b) Normalized variation of stress S in the direction of sliding and the center of contact for varying values of coefficient of friction. After reference [52].

along the centerline z = y = 0. This figure shows that even when the coefficient of friction is zero, the stress in the surface is tensile near the edge of the contact and as μ increases the tensile stress behind and the compressive stress in front of the slider increases. The maximum value of tensile stress occurs at x = -a and r = a (see Fig. 35b) and its magnitude is given by:

$$S_{max} = \frac{3P}{2\pi a^2}\left[\frac{\mu\pi}{8}(4+\nu) + \frac{1-2\nu}{3}\right] \qquad (2)$$

this equation will be used later to calculate the maximum tensile stress for each test. It should be mentioned that the thermal stress, due to frictional heating, has been neglected here.

As mentioned before, for all tests of the first configuration there was a period of 200 to 10000 cycles in which no wear occurred. Then during a few cycles, the wear track was initiated and formed. The incubation period before wear track initiation is indicative of a cumulative damage process called fatigue. The stress in direction of sliding, whose graph is shown in Fig. 35b, is thought to be responsible for the formation of surface cracks which propagate to form surface wear particles. When the contact region moves on the surface, all points at the center of the slider path, where the contact pressure is maximum, are subjected to compressive as well as tensile stresses. This stress reversal causes the cracks to form. With more number of passes, this stress reversal will propagate cracks. SEM micrographs of the partial wear tests shows these fatigue cracks. Figures 36-38 show the contact

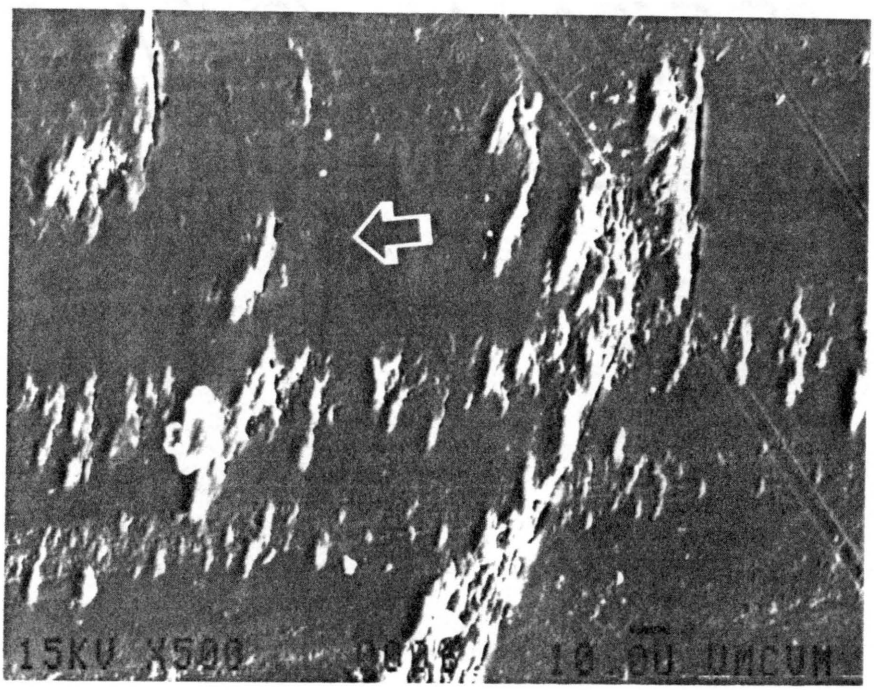

Figure 36: Contact region of control epoxy surface after 500 cycles. Arrow indicates direction of sliding.

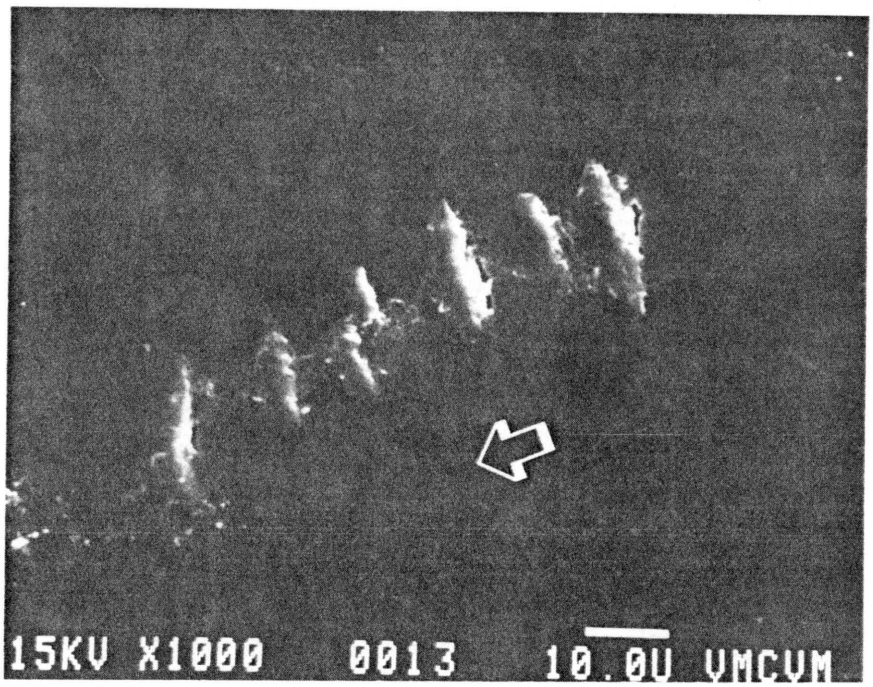

Figure 37: Contact region of control epoxy surface after 500 cycles. Arrow indicates direction of sliding.

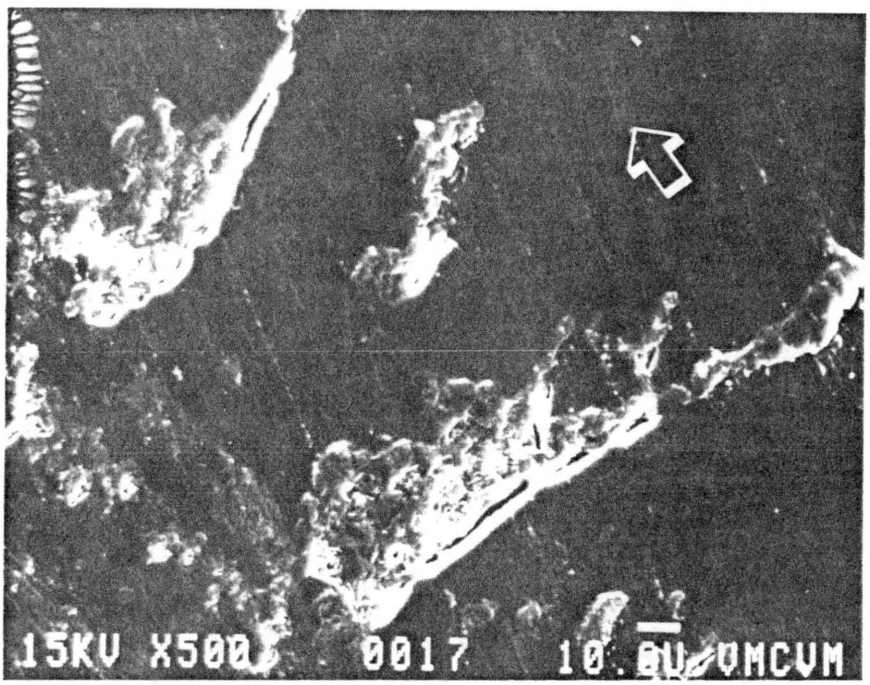

Figure 38: Contact region of control epoxy surface after 500 cycles. Arrow indicates direction of sliding.

region of control epoxy specimen after 500 cycles of loading. Notice that the cracks are perpendicular to the sliding direction. Figure 39 illustrates a fatigue crack on a CTBN rubber-modified epoxy after 600 cycles of loading. To the right of the arrow and parallel to it (i.e., in the direction of sliding) is believed to be a series of crack nucleation sites for future cracks. The cracks will propagate further as the number of cycles is increased joining the neighboring ones (Fig. 36) and eventually lead to formation of the wear particles (Fig. 26). When there was no elastomeric domains in the vicinity of cracks the epoxy fractured in a brittle manner (Figs. 40-41) and if there were numerous elastomeric domains in the path of the slider the propagation of cracks was limited to these domains as shown in Figs. 42-43. Therefore, the fracture toughness, G_{Ic}, which is the resistance of material to crack growth was postulated to be the controlling factor as far as wear was concerned.

Some of the specimens had a region in which extremely large domains ($\sim$ 200 μm) were closely packed together. In these regions, the transverse cracks initiated at the circumference of the domain because the domain acted as a stress concentrator (Figs. 46-48). The loose wear debris is thought to have first formed from the thin walls between these domains as shown in Figs. 42, 44, 45. The cracks around the domains are shown in Figs. 46-48. The magnified view of the transverse cracks of the center of Fig. 47 is shown in Fig. 48. In the regions where size of the domains were small, the appearance of the transverse cracks was different; cracks did not have sharp edges and the opposite surfaces of

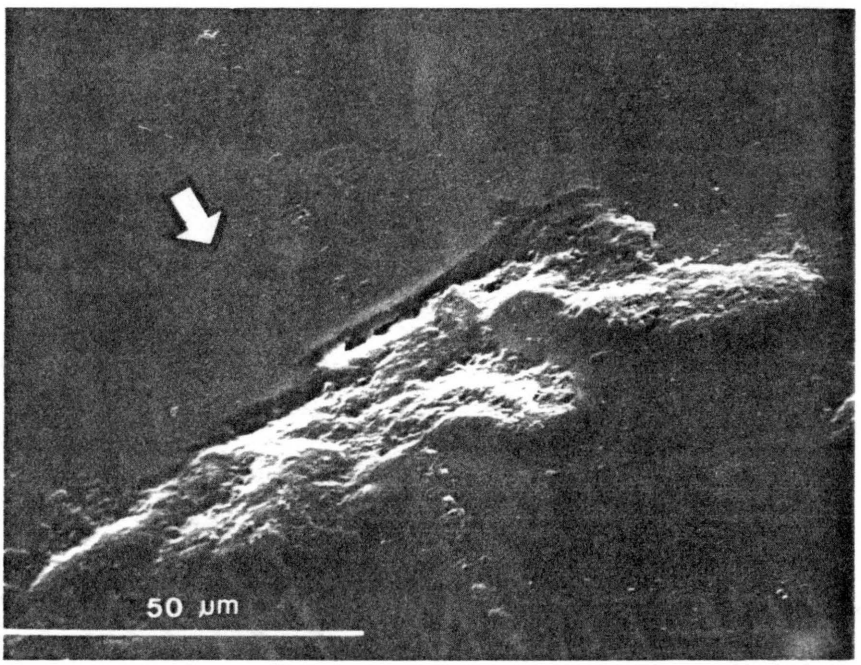

Figure 39: Contact region of a CTBN-modified epoxy after 600 cycles. Arrow indicates direction of sliding.

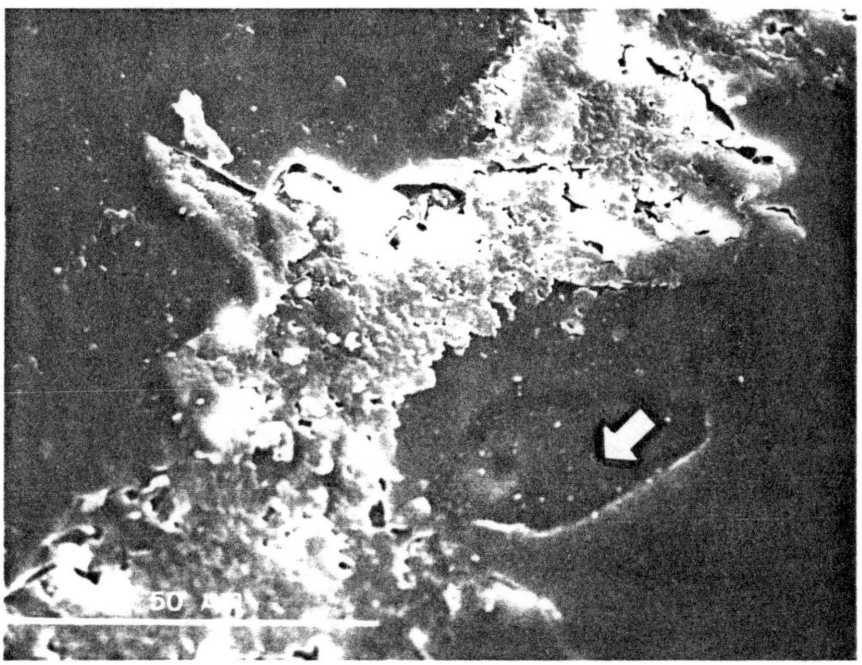

Figure 40: Contact region of 5-20DP epoxy after 600 cycles. Arrow indicates direction of sliding.

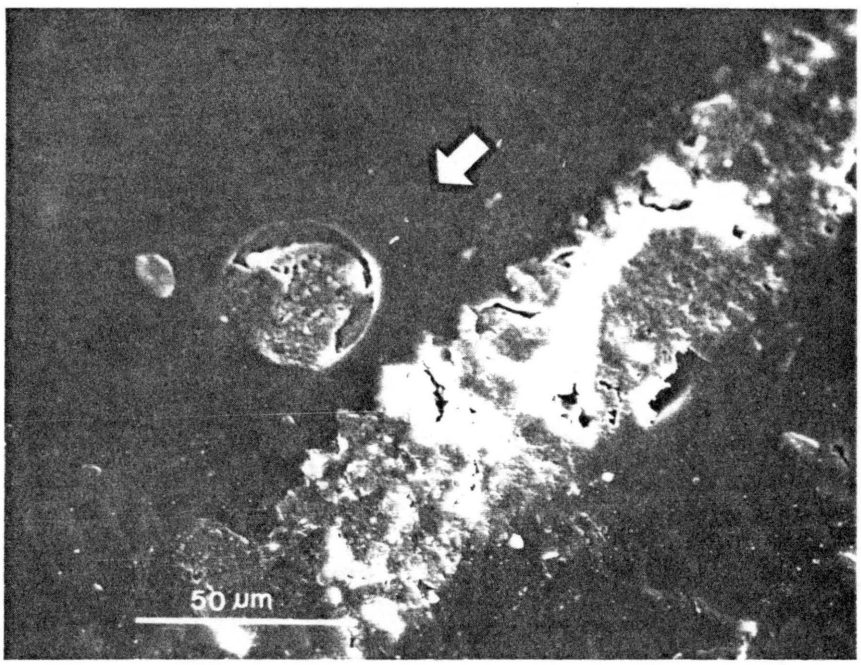

Figure 41: Wear track of 5-20DP epoxy after 600 cycles. Arrow indicats direction of sliding.

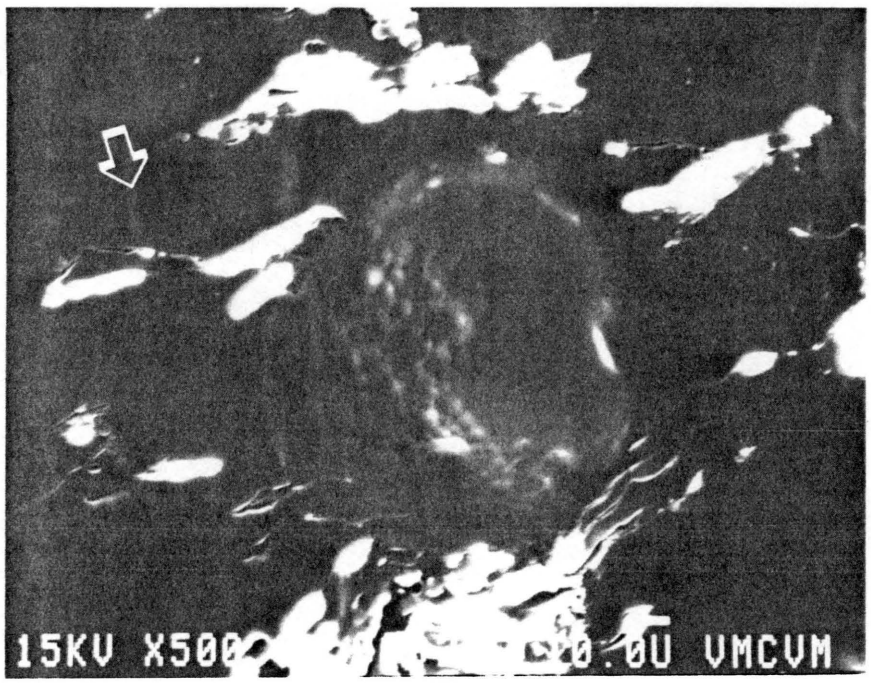

Figure 42: Contact region of 10-40DP after 3000 cycles. Arrow indicates direction of sliding.

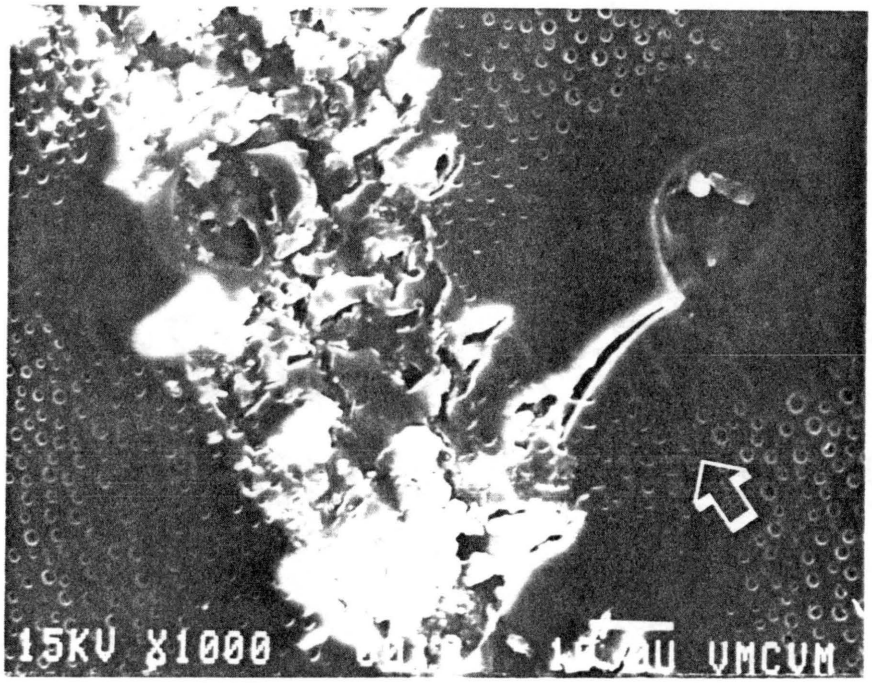

Figure 43: Wear track of 10-40DP after 1500 cycles. Arrow indicates direction of sliding.

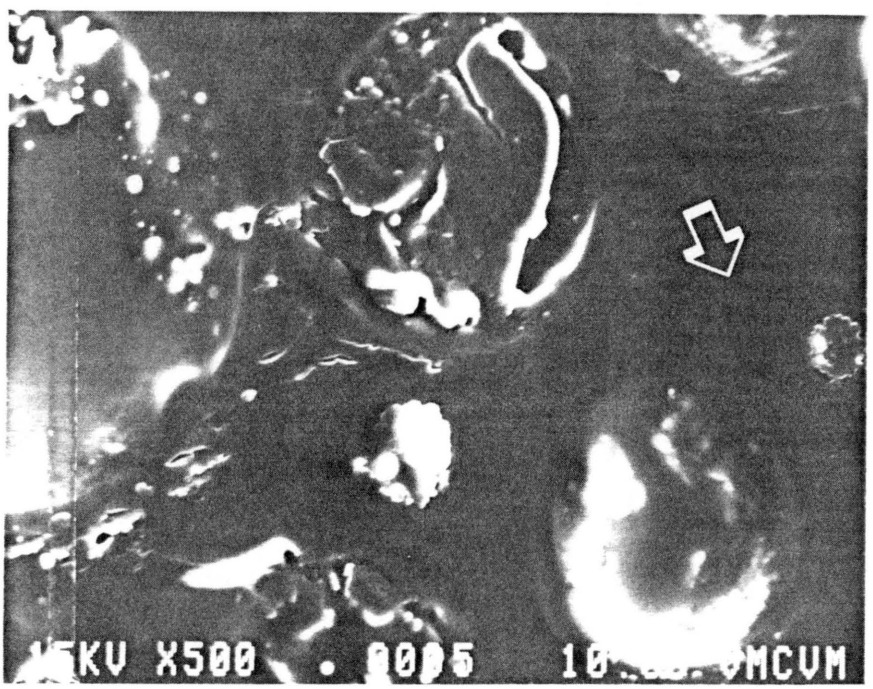

Figure 44: Contact region of 10-40DP after 2500 cycles. Arrow indicates direction of sliding.

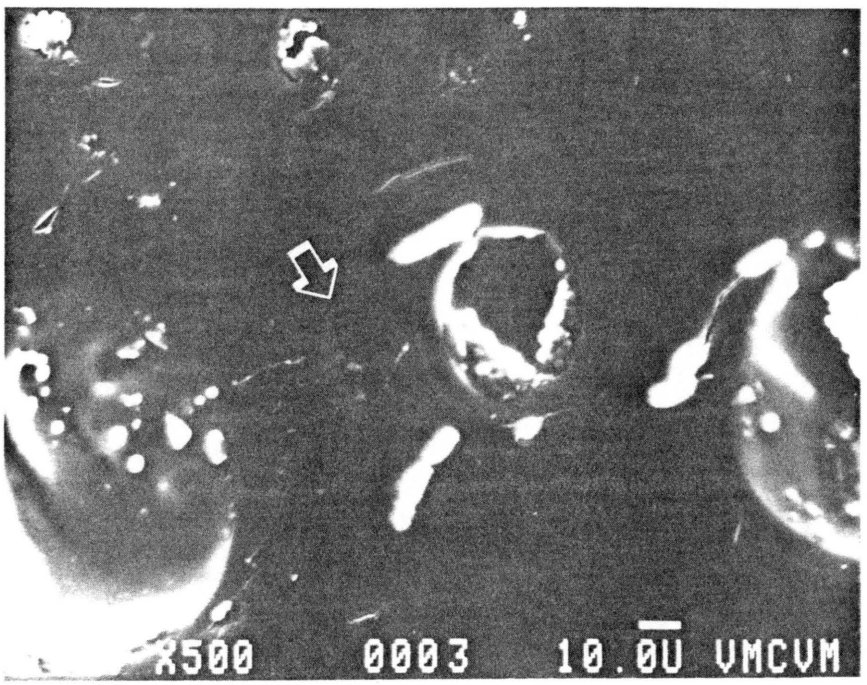

Figure 45: Contact region of 10-40DP after 1300 cycles. Arrow indicates direction of sliding.

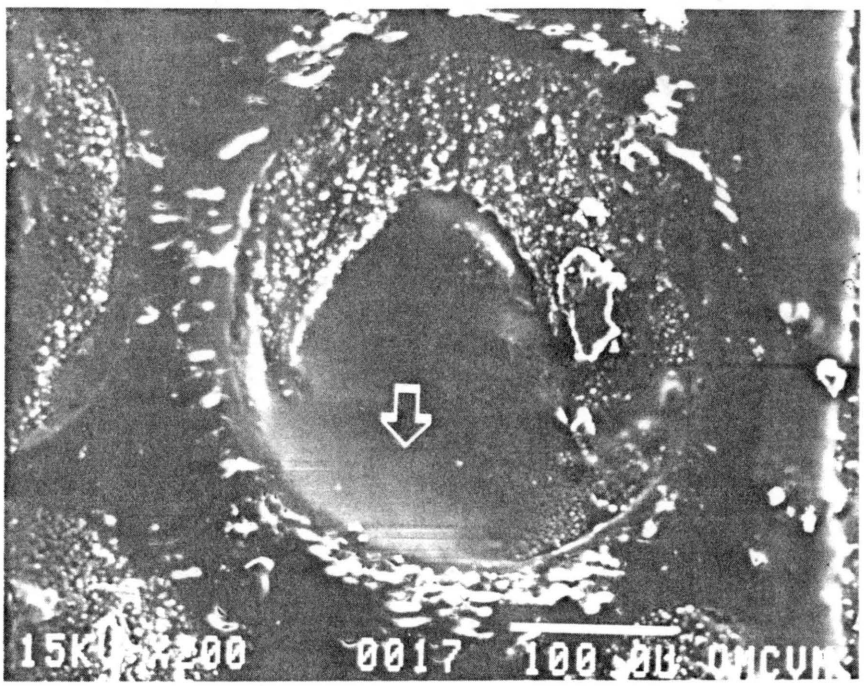

Figure 46: Contact region of 15-40DP after 1600 cycles. Arrow indicates direction of sliding.

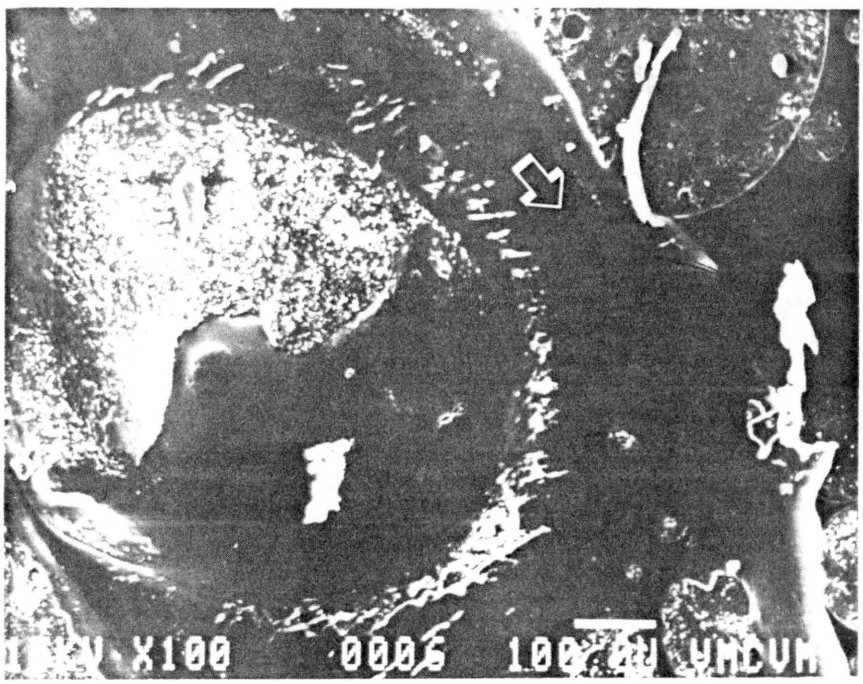

Figure 47: Contact region of 10-40DP after 3000 cycles. Arrow indicates direction of sliding.

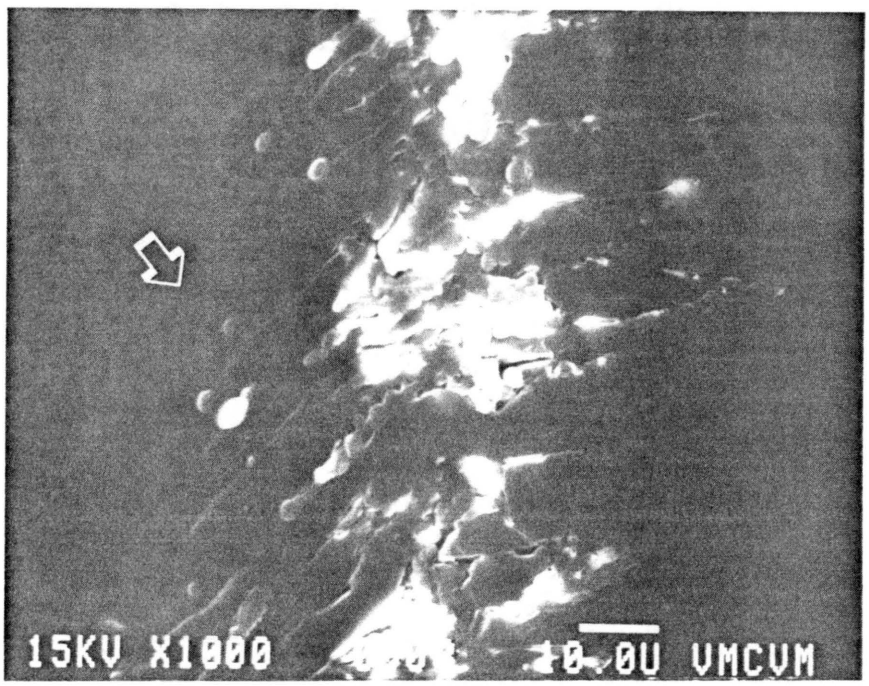

Figure 48: Contact region of 10-40DP after 3000 cycles. Arrow indicates direction of sliding.

a crack were further apart (see Fig. 49).

Finally, Figs. 50 thorugh 56 show the sequence of events during the formation of wear track. After a certain number of cycles, cracks are nucleated and propagated, joining the neighboring ones to create epoxy fragments which when trapped under the sliding ball they tear the elastomeric domains (Figs. 50, 52, the dark lines along the diameter of the domains). Later when the epoxy material between the domains is removed, the frictional force of the slider smears or draws the elastomeric domains over the surface, observe Figs. 54-56 closely, eventually when the center of sliding path has worn out the maximum tensile stress shifts to the sides of the central worn line to cause the same events; widening the wear track and in this manner the wear track is formed.

5.3 Wear

The wear results in previous chapter, Table 11, show that the unmodified epoxy had the highest wear rate and when the epoxy was modified with the elastomeric polysiloxane the wear rate decreased. For all samples, an increase in siloxane content results in a decrease in wear, except for the 10-20 DP sample. As stated in the previous section, failing of the brittle material and generation of a wear particle depends on the degree of crack resistance of that material. Although addition of elastomer will usually enhance crack resistance which in turn controls the wear, but it is not the main factor which controls wear. For brittle materials, the primary factor controlling the wear is the fracture toughness which is a measure of the ability of

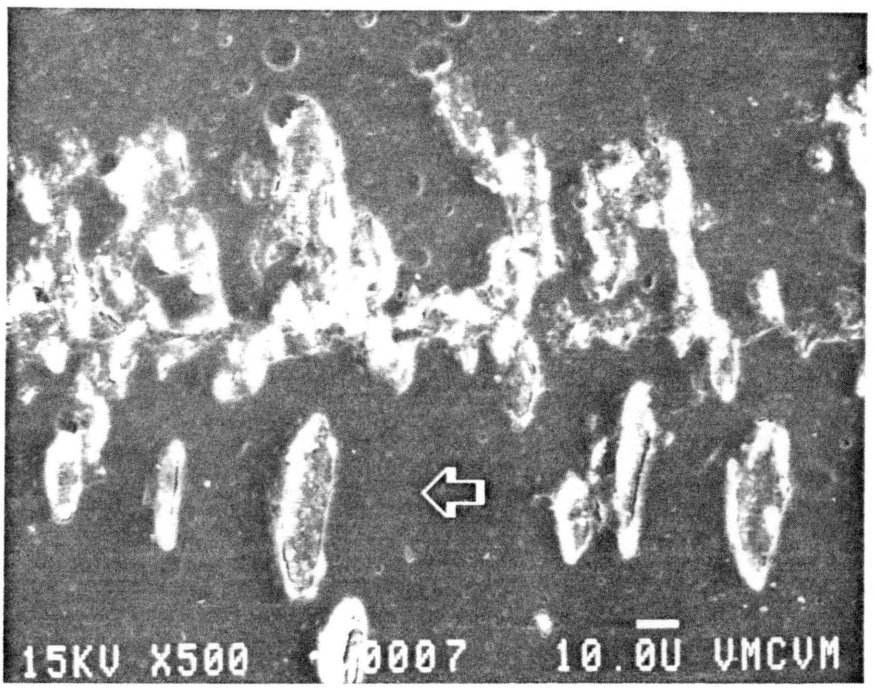

Figure 49: Contact region of 5-40DP after 600 cycles. Arrow indicates direction of sliding.

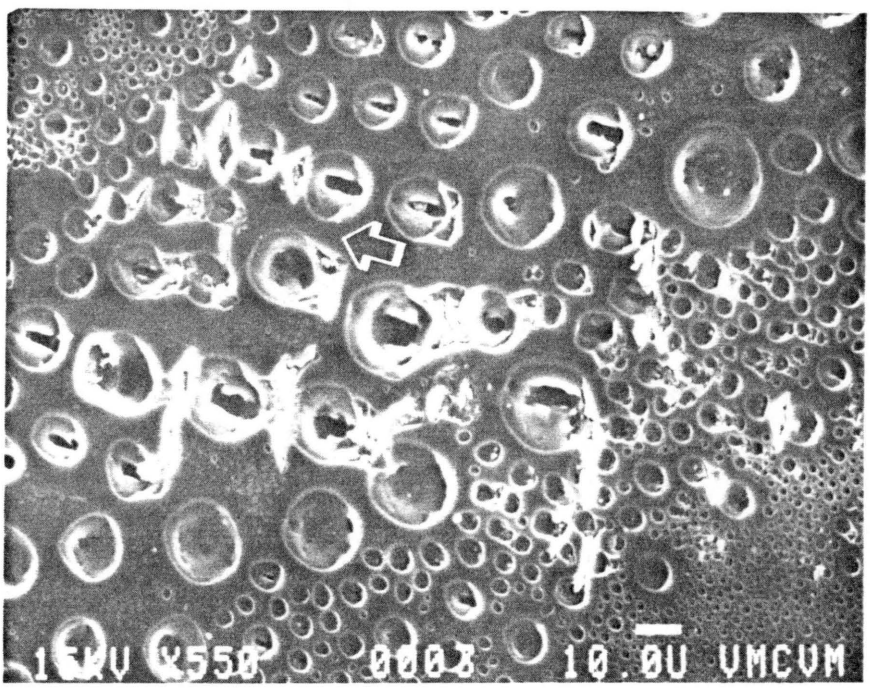

Figure 50: Contact region of 10-40DP after 10,000 cycles. Arrow indicates direction of sliding.

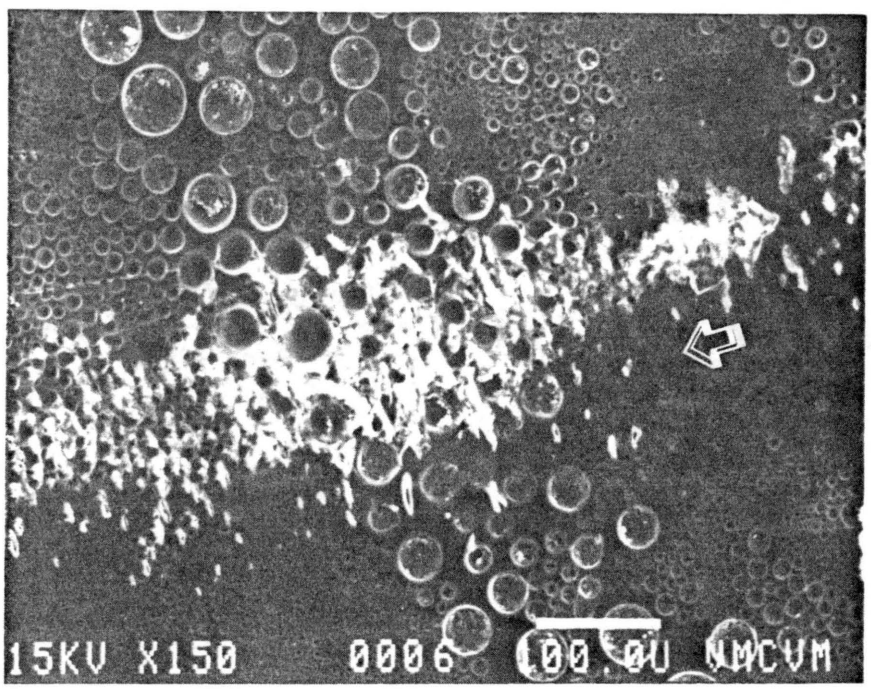

Figure 51: Partial wear track of 5-40DP after 600 cycles. Arrow indicates direction of sliding.

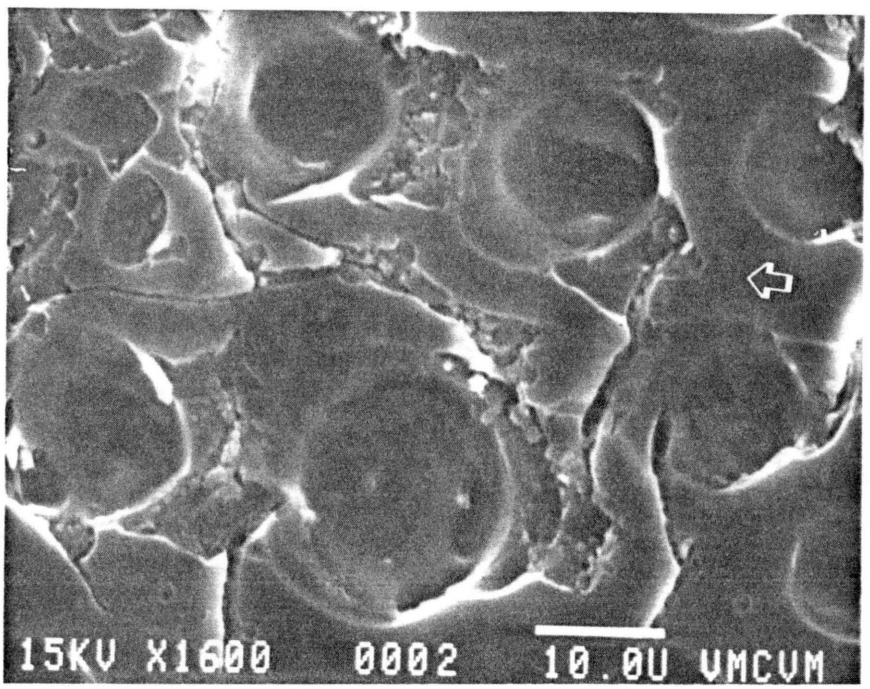

Figure 52: Fatigued surface of 10-40DP after 10,000 cycles. Arrow indicates direction of sliding.

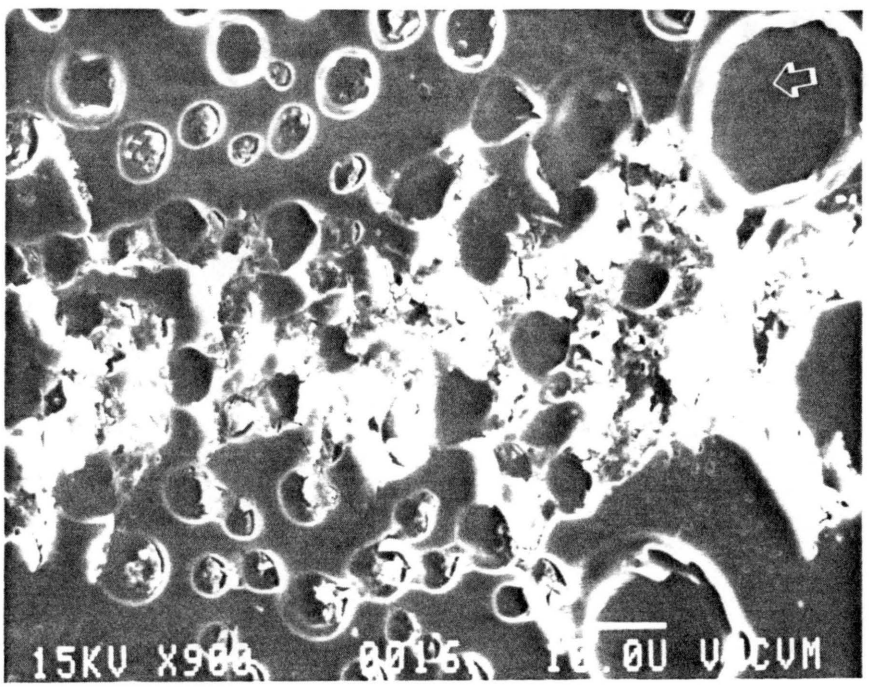

Figure 53: Contact rgion of 15-40DP after 1000 cycles. Arrow indicates direction of sliding.

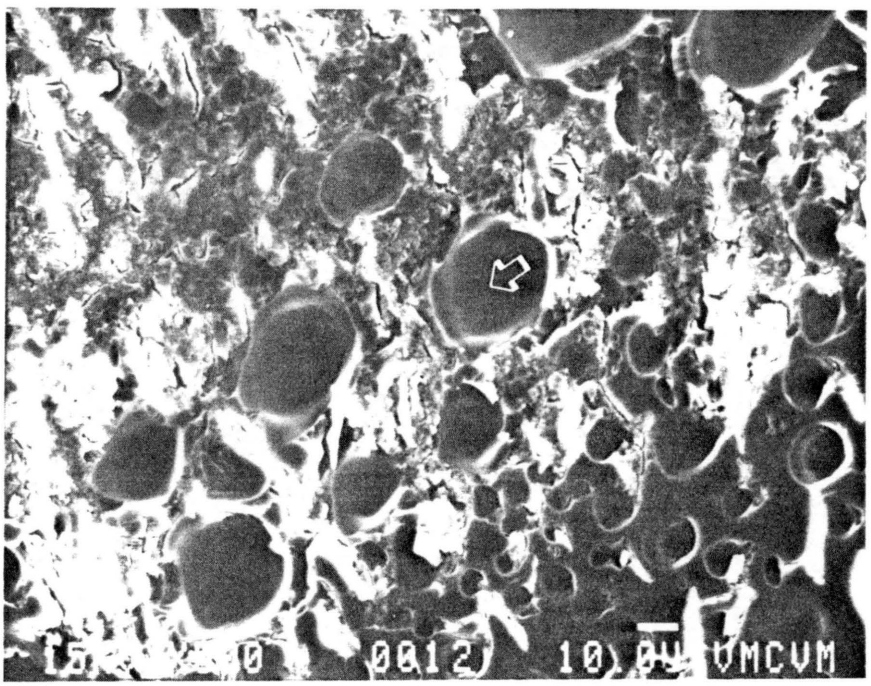

Figure 54: Contact region of 15-40DP after 8000 cycles. Arrow indicates direction of sliding.

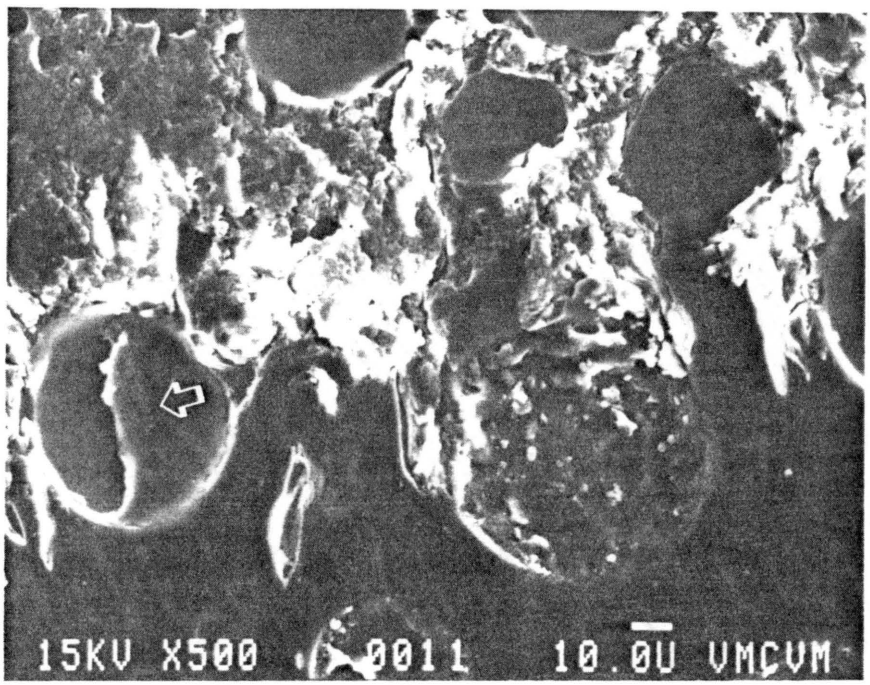

Figure 55: Contact region of 15-40DP after 1000 cycles. Arrow indicates direction of sliding.

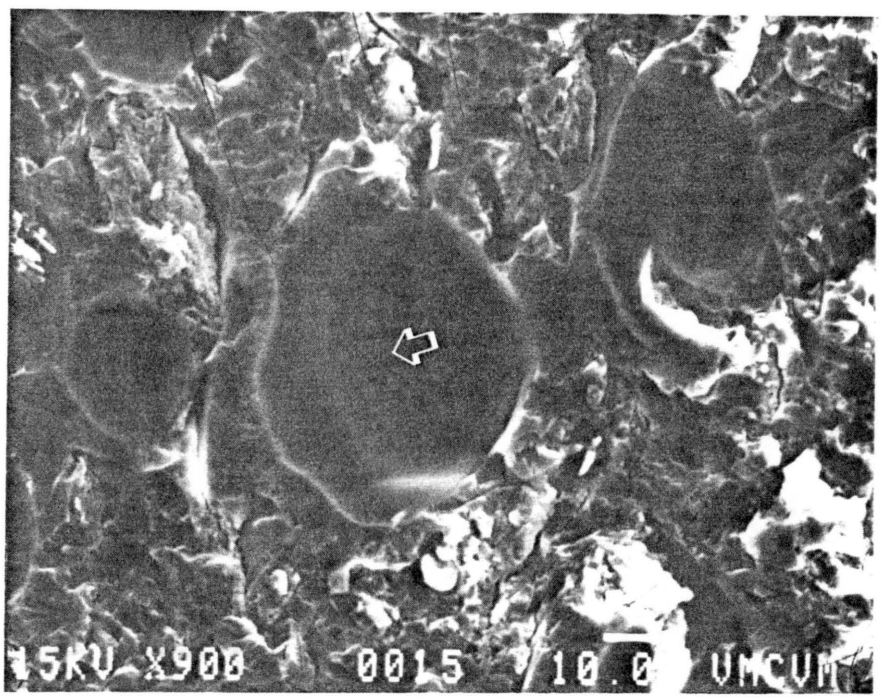

Figure 56: Contact region of 15-40DP after 8000 cycles. Arrow indicates direction of sliding.

the material to resist cracking.

Wear rates of the unmodified epoxy as well as polysiloxane- and CTBN-modified epoxies for both test configurations along with values of fracture toughness are reported in Table 14. Upon examining these values one can note that, for each type of elastomer-modified epoxy, there is a good correlation between the wear rate and fracture toughness, G_{Ic}. The values demonstrate that as fracture toughness increases, the wear rate decreases. The effect of molecular weight on fracture roughness is prominent at higher percentages of elastomer. If the molecular weight of each series at 15 percent elastomer content is compared with the corresponding values of fracture toughness, it is observed that specimens with higher molecular weight have higher fracture toughnesses. This has been reported by many investigators. Kusy et al. [54] found that G_{Ic}, which the author calls critical strain energy release rate, was strongly depended on molecular weight and reported higher G_{Ic}values for samples of higher molecular weights. Kausch [55] in study of fracture of polypropylene reported the same dependency of K_{Ic} on molecular weight.

The correlation of wear rate with fracture toughness, G_{Ic}, for all modified epoxy specimens with different molecular weights can be readily observed in Fig. 57. For samples of each type of elastomer wear rate increases with decreasing fracture toughness. It is observed here that the dependency of wear on fracture toughness is stronger at higher molecular weights.

The limited number of abrasive tests show that the pure (control)

TABLE 14

Correlation of Wear Rate to Fracture Toughness

Sample	G_{Ic} (J/m^2)	fatigue wear (cm^2/kc)	abrasive wear (mg/kc)
control	**261.8**	**12.7**	**2.10**
10-2500-20DP	352.0	11.8	—
05-2500-20DP	360.8	7.3	—
15-2500-20DP	422.7	2.6	—
05-5000-40DP	385.6	10.6	1.65
10-5000-40DP	442.2	8.4	—
15-5000-40DP	867.6	2.4	1.20
05-4000-18AN	380.3	10.5	—
10-4000-18AN	557.2	6.7	—
15-4000-18AN	729.6	2.4	—

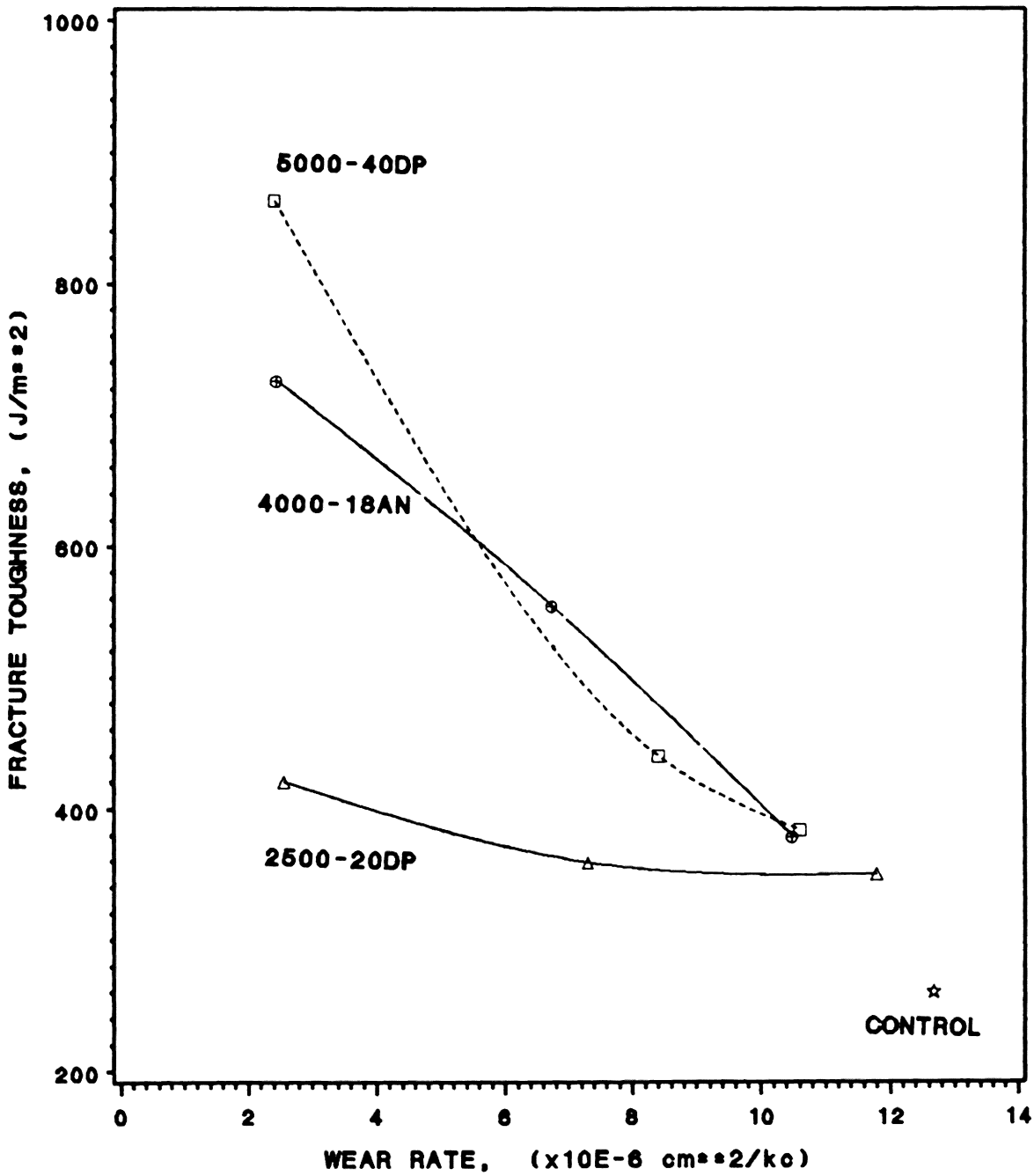

Figure 57: Correlation of wear rate to fracture toughness.

epoxy sample with the lowest fracture toughness had the highest wear rate and modified epoxies with higher fracture toughnesses had lower wear rates. Therefore, the relationship between the fracture toughness and wear rate does not seem to be very sensitive to the testing configuration. The correlation of wear with fracture toughness is in agreement with the theoretical models proposed by Zum Ghar [56,57] and Hornbogen [58]. Taking different approaches they have derived a relationship which shows wear rate is proportional to the inverse of the stress intensity factor raised to power two. The trends of Table 12 is also in agreement with the experimental work of Omar, Atkins, and Lancaster [41] who conducted wear tests on PMMA (polymethyl methacrylate), PES (polyethersulphone) in different organic liquids, and on unlubricated epoxies with different amine ratios. They reported correlation coefficients of 0.85 - 0.97. In another study, Zum Gahr [57] verified his theoretical model by performing wear tests on metals. According to his data, wear rate decreased for metals of higher K_{Ic} value. For epoxy pin-on-abrasive disk tests, the wear rates correlated with inverse of the fracture toughness this is demonstrated in Fig. 58.

There could be two reasons why 10-20 DP sample had higher wear than 5-20 DP. First, although the 10-20 DP sample was modified with more percent siloxane than 5-20 DP, for some reason its fracture toughness was not enhanced as much as 5-20 DP. Having a lower fracture toughness, it had a higher wear rate. A number of reasons can cause this lower G_{Ic} value; cure temperature, solubility of rubber, molecular weight, and

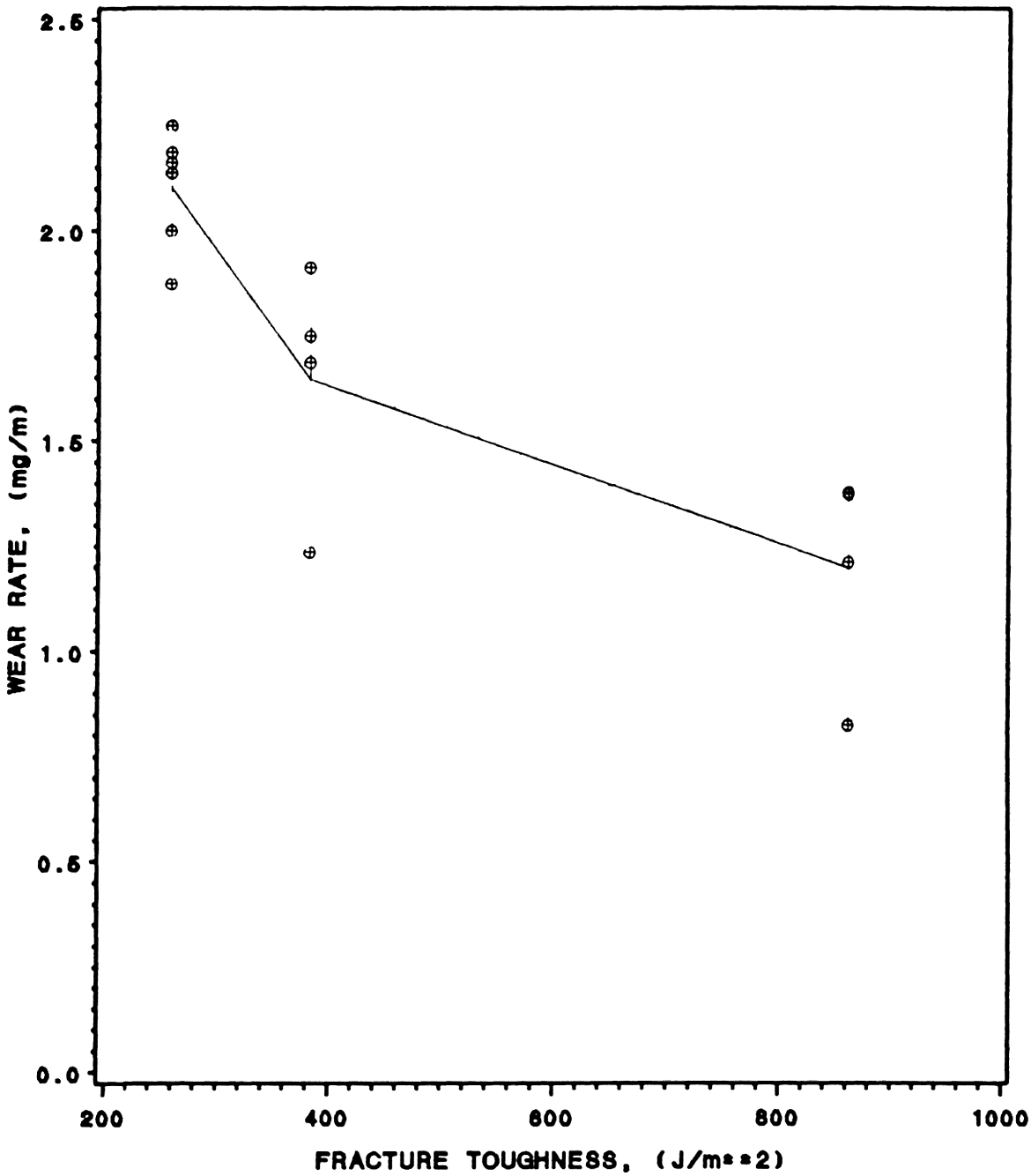

Figure 58: Correlation of wear rate to fracture toughness, abrasive tests.

morphology [21,22,35]. As reported in Table 12, 10-20 DP sample had the lowest number of elastomeric domains; less than half that of 5-20 DP. This is believed to have caused its lower-than-expected fracture toughness value.

The second reason that 20-20 DP had higher wear than 5-20 DP could be the higher stresses in the contact region. Since 10-20 DP sample had the highest tensile modulus, it had the smallest contact area for the same applied normal load. Consequently higher stresses were developed in the contact region. This was verified by calculation. As stated in previous section, the tangential stress given by Eq. (2) was responsible for crack growth which led to wear, therefore, higher tangential stresses would result in higher wear. The stress developed by Hamilton [52] in Eq. (1) is for ball on plane geometry and the premultiplier in Eq. (2) is the contact pressure. Contact pressure for ball on flat geometry and ball in groove are reported in Table 15. To a first approximation contact pressure for ball-in-groove was substituted in Eq. (2) to give the tensile stress for ball in a groove. Then the tensile stresses were calculated and are reported in Table 15. The results show that indeed 10-20 DP sample had the highest tensile stress for ball-in-groove geometry among the modified epoxies and a lower one than the control sample. This is consistent with the wear results and believed to have contributed to higher wear of 10-20 DP sample.

Conducting tests without wear debris revealed that the debris did not act as an abrasive agent. The data in Table 11 shows that at 10 and 15 percent siloxane, the removal of the debris increased the wear

TABLE 15

Calculated Contact Stresses (Mpa)

Sample	P_f †	P_s	S_f	S_s
control	**61.65**	**39.10**	**18.92**	**27.90**
05-20DP	58.40	40.93	19.66	**25.36**
10-20DP	63.25	39.27	20.11	**27.00**
15-20DP	58.60	43.00	19.63	**21.45**
05-40DP	60.60	38.76	19.58	**25.27**
10-40DP	58.80	39.97	23.31	**24.22**
15-40DP	57.10	41.44	26.74	**21.16**
5-40DP ‡	60.60	38.78	22.20	**25.50**
10-40DP	58.80	40.70	24.30	**26.20**
15-40DP	57.10	40.90	28.00	**26.30**

†*P = maximum contact pressure*
S = maximum tensile stress
$_f$ = ball on flat geometry
$_s$ = ball in groove geometry
‡ *w/o debris tests*

rate. Therefore, the debris for samples of higher siloxane content helped to lower the wear (see Fig. 13).

The tensile stresses for the no-debris tests were reported in Table 15. Upon comparison of tensile stresses for ball-in-groove geometry, S_g, for no-debris tests with those of tests with debris, it is observed that at 5 percent siloxane level, there is little difference. At higher percentages of siloxane, the difference is more pronounced. As discussed in Section 5.1, the absence of debris was in favor of friction rise, especially at higher siloxane contents. This was a hidden factor which actually caused higher contact stresses for the no-debris tests. Higher tangential stresses, responsible for crack propagation, promoted wear. Thus, the main cause of higher wear of no-debris tests is higher friction.

6. CONCLUSIONS

The incorporation of dimethyl-diphenyl siloxane into the epoxy resin enhanced the fracture toughness of the epoxy network and the effect of molecular weight of modifier on toughness was more pronounced at higher siloxane contents.

The friction coefficient was reduced by increasing the weight percent of the modifier and, at 10 and 15 percent modifier, was reduced further by increasing the diphenyl content of the siloxane. This was attributed to the low surface energy of the rubber modifier which was spread over the surface during sliding. This finding was verified by conducting tests in which the debris was blown out of the interface. The coefficient of friction was higher for abrasive tests but the samples did not rank differently as far as friction was concerned. The CTBN-modified epoxies had lower friction coefficient than epoxies modified with siloxane.

For all samples except 10-20DP, an increase in siloxane or CTBN content resulted in a decrease in wear rate. For both ball-on-epoxy and epoxy pin-on-abrasive disks experiments a positive correlation was found between the wear rates and inverse of the fracture toughness. The dependency of wear on fracture toughness was stronger for modified samples with rubber of higher molecular weights.

Removal of the wear debris increased both friction coefficient and the wear rate especially at higher siloxane contents and revealed that wear debris did not act as an abrasive agent.

Sample morphology has marked effect on both friction coefficient and wear rate. The sample with approximately the same domain size but less number of domains exhibited the highest friction coefficient and highest wear rate.

7. RECOMMENDATIONS FOR FUTURE STUDY

Friction and wear tests on samples with higher rubber contents should be conducted to find an optimum level of modifiers at which friction and wear are lowest.

More work is needed to study the effect of morphology on friction and wear. Preparing samples of the same rubber content and curing them at different temperatures should result in a different morphology. Conducting friction, wear, and fracture tests on such samples would be beneficial.

Fatigue fracture tests should be performed to obtain fatigue crack growth rate as a function of change in stress intensity factor. One is then able to determine the empirical constants of the Paris equation and predict the wear rates based on fracture data according to analysis of reference [41]. It would be interesting to see how well the predicted wear rates agree with those obtained experimentally. Bloc temperature and the resulting thermal stresses should be calculated to see if the assumption that the thermal stresses are negligible is valid.

REFERENCES

1. Potter, W. G., Epoxide Resins, Springer-Verlag, New York, 1970. TP1180 E6 P68.

2. May, C. A., "Introduction to Epoxy Resins" Epoxy Resin Chemistry and Technology, May, C. A., Tanaka, Y., (eds.), Marcel Dekker, New York, 1973, pp. 1-7. TP1180 E6 M3.

3. Bauer, R. S. (ed.), Epoxy Resin Chemistry, ACS Sym. Ser. No. 114, Am. Chem. Soc., Washington, D.C., 1979. TP1180 E6 E59.

4. Suh, N. P., Tribophysics, Prentice-Hall, New Jersey, 1986, pp. 199-208. TJ1075 S84.

5. McGarry, F. J., "Building Design with Fiber Reinforced Materials," Proc. Roy. Soc. Lond. A., Vol. 319, 1970, pp. 59-68. QA1 R75a.

6. McGarry, F. J., and J. N. Sultan, "Crack Propagation Studies in Crosslinked Glassy Polymers," 24th Ann. Tech. Conf. Reinf. Plast./Compos. Div., SP1, Sect. 11-B, 1969, pp. 1-8. TP1101 S62.

7. Sultan, J. N., and F. J. McGarry, "Effect of Rubber Particle Size on Deformation Mechanics in Glassy Epoxy," Polymr Eng. Sci., Vol. 13, 1973, pp. 29-34. TP986 A1 S5732.

8. Riew, C. K., E. H. Rowe, and A. R. Siebert, "Rubber Toughened Thermosets," Toughness and Brittleness of Plastics, Deanin, R. D. and A. M. Crugnola (eds.), Adv. Chem Ser. no. 154, Am. Chem. Soc., Washington, D.C., 1976, pp. 326-343. QD1 A355.

9. Donald, A. M., and E. J. Kramer, "The Competition Between Shear Deformation and Crazing in Glassy Polymers," J. Matter. Sci., Vol. 17, 1982, pp. 1871-1879. TA401 J673x.

10. Kinloch, A. J., and R. J. Young, Fracture Behavior of Polymers, Applied Science, London, 1983. TA455 p. 58 K5.

11. Creed, K. E., Jr., " Aging in CTBN Modified Epoxy Resin Stocks," INIS Atomindex, Vol. 11, 1980, Abst. No. 517048, p. 2478. Ref. Z5160 I54.

12. Okamoto, Y., "Thermal Aging Study of Carboxyl-Terminated Polybutadiene and Poly(butadiene-Acrylonitrile)-Reactive Liquid Polymers," Polym. Eng. Sci., Vol. 23, 1983, pp. 222-225. TP986 A1 S5732.

13. Warrick, E. L., O. R. Pierce, K. E. Polmanteer, J. C., Saam, "Silicone Elastomer Developments 1967-1977," Rubber Them. Tech., Vol. 52, 1979, pp, 437-490, TS1870 R75.

14. Cush, R. J., H. W. Winnan, "Silicone Rubbers," in Developments in Rubber Technology - 2, Whelan, A., K. S. Lee, (eds.), Applied Science, London, 1981, pp. 203-231. TS1890 D49.

15. Riffle, J. S., I. Yilgor, A. K. Banthia, C. Tran, G. L. Wilkes, J. E. McGrath, "Elastomeric Polysiloxane Modifiers for Epoxy Networks: I., Synthesis of Functional Oligomers and Network Formation Studies," Epoxy Resin Chemistry II, Bauer, R. S. (ed.), ACS Symp. Ser. no. 221, Am. Chem. Soc., Washington, D.C. 1983, pp. 21-54. TP1180 E6 E588.

16. Yorkgitis, E. M., C. Tran, N. S. Eiss, Jr., T. Y. Hu, I. Yilgor, G. L. Wilkes, J. E. McGrath, " Siloxane Modifiers for Epoxy Resins," Rubber-Modified Thermoset Resins, Riew, C. K., and J. K. Gillham, (eds.), Adv. Chem. Ser. no. 208, Am. Chem. Soc., Washington, D.C., 1984, pp. 137-161. QD1 A355.

17. Eiss, N. S., Jr., and H. Czichos, "Tribological Studies on Rubber-Modified Epoxies: Influence of Material Properties and Operating Conditions, Wear, Vol. 111, 1986, pp. 347-361. TA401 W4.

18. Lancaster, J. K., "Basic Mechanisms of Friction and Wear of Polymers," Plastics and Polymers, Vol. 41, 1973, pp. 297-306. TP1101 P52.

19. Hertzberg, R. W., and J. A. Manson, Fatigue of Engineering Plastics, Academic Press, New York 1980, pp. 34-39. TA455 P5 H45.

20. Kinloch, A. J., S. J. Shaw, D. A. Tod, and D. L. Hunston, "Deformation and Fracture Behavior of a Rubber-Toughened Epoxy: 1. Microstructure and Fracture Studies," Polymer, Vol. 24, 1983, pp. 1341-1354. QD380 P62.

21. Levita, G., A. Marchetti, and E. Butta, "Influence of the Temperature of Cure on the Mechanical Properties of ABTN/Epoxy Blends," Polymer, Vol. 26, 1986, pp. 1110-1116. QD380 P62.

22. Butta, E., G. Levita, A. Marchetti, and A. Lazzeri, "Morphology and Mechanical Properties of Amine-Terminated Butadiene-Acrylonitrile/Epoxy Blends," Polymer Eng. Scie., Vol. 26, 1986, pp. 63-73. TP986 A1 S5732.

23. Kunz, S. C., J. A. Sayre, and R. A. Assink, "Morphology and Toughness Characterization of Epoxy Resins Modified with Amine and Carboxyl Terminated Rubbers," Polymer, Vol. 23, 1982, pp. 1897-1905. QD380 P62.

24. Rowe, E. H., A. R. Siebert, and R. S. Drake, "Liquid Rubber for Toughening Thermoset Resins," Modern Plastics. Vol. 47, 1970, pp. 110-119. TP986 Al M6.

25. Bascom, W. D., R. Y. Ting, R. J Moulton, C. K Riew, and A. R. Siebert, "The Fracture of an Epoxy Polymer Containing Elastomeric Modifiers," J. Matter. Sci., Vol. 16, 1981, pp. 2657-2664. TA401 J673x.

26. Riew, C. K., "Amine Terminated Reactive Liquid Polymers: Modification of Thermoset Resins," Rubber Chem. Technol., Vol. 54, 1981, pp. 374-402. TS1870 R75.

27. Daly, J., R. A. Pethric, P. Fuller, A. V. Cunliffe, P. K. Datta, "Rubber-Modified Epoxy Resins: 1. Equalibrium Physical Properties," Polymer, Vol. 22, 1981, pp. 32-36. QD380 P62.

28. Bucknall, C. B., Toughened Plastics, Applied Science, London, 1977. TP1177 B83.

29. Yee, A. F., and R. A. Pearson, "Toughening Mechanisms in Elastomer-modified Epoxies, Part 1 Mechanical Studies," J. Matter. Sci., Vol. 21, 1986, pp. 2462-2474. TA401 J673x.

30. Pearson, R. A., and A. F. Yee, "Toughening Mechanisms in Elastomer-Modified Epoxies, Part 2 Microscopy Studies," J. Mater. Sci., Vol. 21, 1986, pp. 2475-2488. TA401 J673x.

31. Kinloch, A. J., S. J. Shaw, and D. L. Hunston, "Deformation and Fracture Behavior of Rubber-Toughened Epoxy: 2 Failure Criteria," Polymer, Vol. 24, 1983, pp. 1355-1363. QD380 P62.

32. Sayre, J. A., S. C. Kunz, and R. A. Assink, "Effect of Rubber Cross-link Density and Tear Energy on the Toughness of Rubber-Modified Epoxies," Rubber-Modified Thermoset Resins," Riew, C. K., J. E. Gillham, (eds.), Adv. Chem. ser. no. 208, Am. Chem. Soc., Washington, D.C., 1984, pp. 215-234. QD1 A355.

33. Kinloch, A. J., and J. G. Williams, "Crack Blunting Mechanism in Polymers," J. Mater. Sci., Vol. 15, 1980, pp. 987-996. TA401 J673x.

34. Yamini, S., and R. J. Young, "The Mechanical Properties of Epoxy Resins, Part 1: Mechaisms of Plastic Deformation," J. Mater. Sci., Vol. 15, 1980, pp. 1814-1822. TA401 J673x.

35. Nae, H. N., S. Reich, and Z. Nir, "Rubber-Modified, Flame-Retardant, High Glass Transition Temperature Epoxy Resins," Rubber-Modified Thermoset Resins, Riews, C. K., J. K. Gillham, (eds.), Adv. Chem. Ser. no. 208, Am. Chem. Soc., Washington, D.C., 1984, pp. 281-191. QD1 A355.

36. Kirshenbaum. S. L., S. Gazit, and J. P. Bell, "An Alternative Liquid Rubber for Epoxy Resin Toughening," Rubber-Modified Thermset Resins, Riew, C. K., J. K. Gilham, (eds), Adv. Chem. Ser. no. 208, Am. Chem. Soc., Washington, D.C., 1984, pp. 164-177. QD1 A355.

37. Manzione, L. T., J. K. Gillham, and C. A. McPherson, "Rubber-Modified Epoxies: I. Transitions and Morphology," J. Appl. Polym. Sci., Vol. 26, 1981, pp. 889-906. TP156 P6 J6.

38. Chitsaz-Zadeh, M. R., and N. S. Eiss, "Friction and Wear of Polyimide Thin Films, Wear, Vol. 110, 3, 1986, pp. 359-368. TA401 W4.

39. Hanmin, Z., H. Guoren, and Y. Guicheng, "Friction and Wear of Poly(phenylene sulphide) and Its Carbon Fiber Composites: I Unlubricated," Wear, Vol. 116, 1987, pp. 59-68. TA401 W4.

40. Thomas, S., "Scanning Electron Microscopy Studies on Wear Properties of Blends of Plasticized Poly(vinyl Chloride) and Thermoplastic Polyester Elastomer," Wear, Vol. 116, 1987, pp. 201-209. TA401 W4.

41. Omar, M. K., A. G. Atkins, and J. K. Lancaster, "The Role of Crack Resistance Parameters in Polymer Wear," Journal of Physics D, Vol. 19, 1986, pp. 177-195. QC1 I548.

42. Subramanian, C., P. Asaithambi, and Kishore, "Friction and Wear of Epoxy Resin Containing Graphite," J. Reinf. Plast. Compos., Vol. 5, 1986. pp. 200-208. TA455 P55 J68.

43. Hu, T. Y., N. S. Eiss, Jr., E. M. Yorkgitis, G. L. Wilkes, C. Tran, I. Yilgor, and J. E. McGrath, "Elastomeric Polysiloxane Modifiers: III, Friction and Wear," Proc. ACS Division of Polymeric Materials Science and Engineering, Vol. 49, 1983, pp. 508-512. QD380 A5.

44. Lee, L. H., "Fracture Energetics and Surface Energetics of Polymer Wear," in Polymer Wear and Its Control, Lee, L. H., (ed.), ACS Symp. Ser. no 287, Am. Chem. Soc., Washington, D.C., 1985, pp. 27-38. QD380 P6537.

45. Eiss, N. S., Jr. and J. R. Potter, III, "Fatigue Wear of Polymers," Polymer Wear and Its Control, Lee, L. H., (ed.), ACS Symp. Ser., No. 287, Am. Chem. Soc., Washington, D.C., 1985, pp. 59-66. QD380 P6537.

46. Yorkgitis, E. M., N. S. Eiss, Jr., C. Tran, G. L. Wilkes, and J. E. McGrath, "Siloxane-Modified Epoxy Resins," Epoxy Resins and Composites I, Dusek, K., (ed.), Springer-Verlag, New York, 1985, pp. 79-109.

47. Knott, J. F., Fundamentals of Fracture Mechanics, Wiley, New York, 1973. TA409 K66.

48. Eiss, N. S., Jr., and S. C. Milley, "The Effect of Asprity Curvature on Polymer Wear," Wear of Materials, Ludema, K. C., (ed.), ASME, New York 1983, pp. 650-656. TA418.4 A46a.

49. Madakson, R. B., "The Frictional Behavior of Materials," Wear, Vol. 87, 1983, pp. 191-206. TA401 W4.

50. Friedrich, I. K., "Friction and Wear of Polymer Composites," Fortschritt-Berichte Der VDI Zeitschriften, Reihe 18, No. 15, 1985, pp. 13-17.

51. Czichos, H., "Contact Deformation and Static Friction of Polymers: Influence of Viscoelasticity and Adhesion," in Polymer Wear and Its Control, Lee, L. H., (ed.), ACS Sym. Ser. no., 287, Am. Chem. Soc., Washington, D.C., 1985, pp. 3-26. QD380 P6537.

52. Hamilton, G. M., and L. E. Goodman, "The Stress Field Created by Circular Sliding Contact," J. of Applied Mechanics, Vol. 33, 1986, pp. 371-376. TA1 J6.

53. Jain, V. K., and S. Bahadur, "Development of a Wear Equation for Polymer-Metal Sliding in Terms of Fatigue and Topography of the Sliding Surfaces," Wear, Vol. 60, 1980, pp. 237-247. TA401 W4.

54. Kusy, R. P., and D. T. Turner, "Infuence of Molecular Weight of Poly(methyl methacrylate) on Fracture Surface Energy in Notched Tension," Polymer, Vol. 17, 1976. pp. 161-166. QD380 P62.

55. Kausch, H., Polymer Fracture, 2nd ed., Springer-Verlag, Berlin, 1987, pp. 375-377. TA455 P58 K38.

56. Zum Gahr, K. H., "How Microstructure Affects Wear Resistance," Metal Progress, Vol. 116, 1979, pp. 46-52. TS200 M36.

57. Zum Gahr, K. H., "Relation Between Abrasive Wear Rate and Microstructure of Metals," in Wear of Materials, Ludema, K. C. (ed.), ASME, New York, 1979, pp. 266-274. TA418.4 A46a.

58. Hornbagen, E., "The Role of Fracture Toughness in Wear of Metals," Wear, Vol. 33, 1975, pp. 251-259. TA401 W4.

59. Timoshenko, S. P., and N. J. Goodier, Theory of Elasticity, 3rd ed., McGraw-Hill, New York, 1970, pp. 420-427. QA931 T54.

APPENDIX A

A. Sample Mechanical Property Measurements

Modified epoxy samples were machined out of molded plates into standard dog-bone specimens (3.5 mm width, 2 mm thickness, 13 mm gauge length). They were pulled to break in Model 1122 Instron tester at a cross-head speed of 5mm/min. A typical load-elongation curve is shown in Fig. 59. The mechanical properties were measured from the curves as follows:

1. Ultimate tensile strength -- the load (kgf) at break multiplied by gravitational acceleration (g) and then divided by the original cross-sectional area of the specimen.
2. Modulus of elasticity -- the initial slope of the load-elongation curve multiplied by the original specimen length and gravitational acceleration (g) and divided by the product of the original cross-sectional area.
3. Strain to break -- the elongation at break divided by the original specimen length.
4. Energy-to-rupture parameter -- approximated by the product of ultimate tensile strength and strain to break.

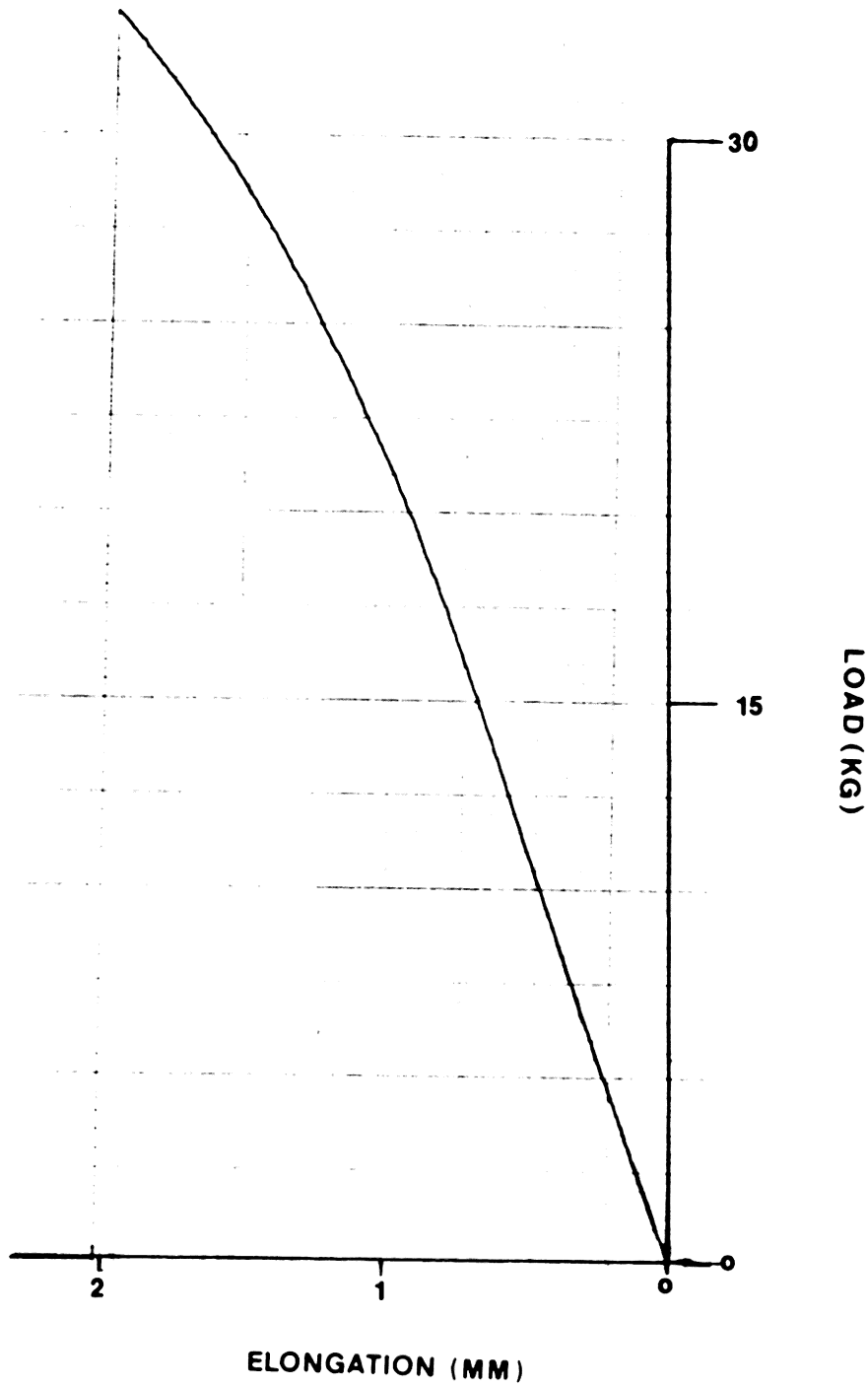

Figure 59: Typical load-elongation curve.

APPENDIX B

B. Fracture and Flexural Modulus

Two types of sample geometry were prepared for flexural modulus and fracture toughness measurements, both designed to be tested utilizing a three-point bend apparatus in an Instron machine. The apparatus consists of two bars attached to the Instron which is fitted with a tensile load cell. The two side bars remain stationary above the sample as the central bar below the sample moves upward. The cross-head speed for the flexural testing was 1.0 mm/min and for fracture testing was 0.5 mm/min. The following formula was used to calculate the flexural modulus:

$$E_f = 40.2 \cdot \frac{P}{wt^3 Y} \quad \text{(GPa)} \qquad \text{(B1)}$$

where P = mass (kg), w = width (mm), t = thickness (mm), and Y = displacement (mm). Dimensions of the sample are shown in Fig. 60a.

Figure 60b shows sample geometry, its dimensions, and the location of the crack and crack notch for fracture testing. Into the indicated notch was placed a sharp, one-sided razor blade which was lightly tapped to make a short pre-crack. The cross-head speed was 0.5 mm/min. After fracture, pre-cracks were enlarged with a magnifying glass, the length measured with digital calipers, and calculated as the average of side, center, and side values. The calculation of stress intensity factor and fracture toughness is reported in section 3.2.

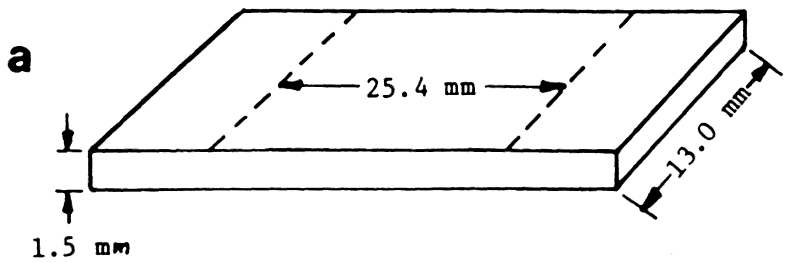

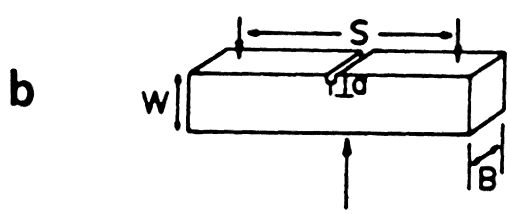

W = 6.4 mm

S = 25.4 mm

B = 3.2 mm

a ≃ (2-4) mm

Figure 60: a) Flexural modulus test specimen.
b) Fracture toughness test specimen.

APPENDIX C

C. Calibration Procedure for Friction Apparatus

Friction force caused a deflection of the cantilever beam to which the pin was attached. The deflection was measured by a proximity transducer whose output was recorded on an X-Y plotter. The gap between the beam and transducer was adjusted so as to give a linear friction scale. The scale on the friction axis was obtained in the following manner:

A tangential force was supplied by means of weights on a hanger. Using the definition of the friction coefficient which is the tangential force divided by normal force, the weight necessary to give a friction coefficient of 0.1 was computed to be that of 102 gram mass for a normal load of 10N. For each reading on the friction axis, an additional 100 gram mass was placed on the hanger and the corresponding friction coefficient was marked. This was successively done until the friction axis was graduated to a value of 0.5.

APPENDIX D

D. Morphology Analysis

The modified epoxy disks of different compositions were examined in a Ziess SEM Image Processing System (IPS). For each sample composition three regions of the surface (labeled a, b, and c in Figs. 61-66) were analyzed in the IPS to give the domain size distributions, average domain size, and the number of domains in the image area. The actual image area for all analyses was 2376 μm^2. The output of each analysis is shown in Figs. 61-66.

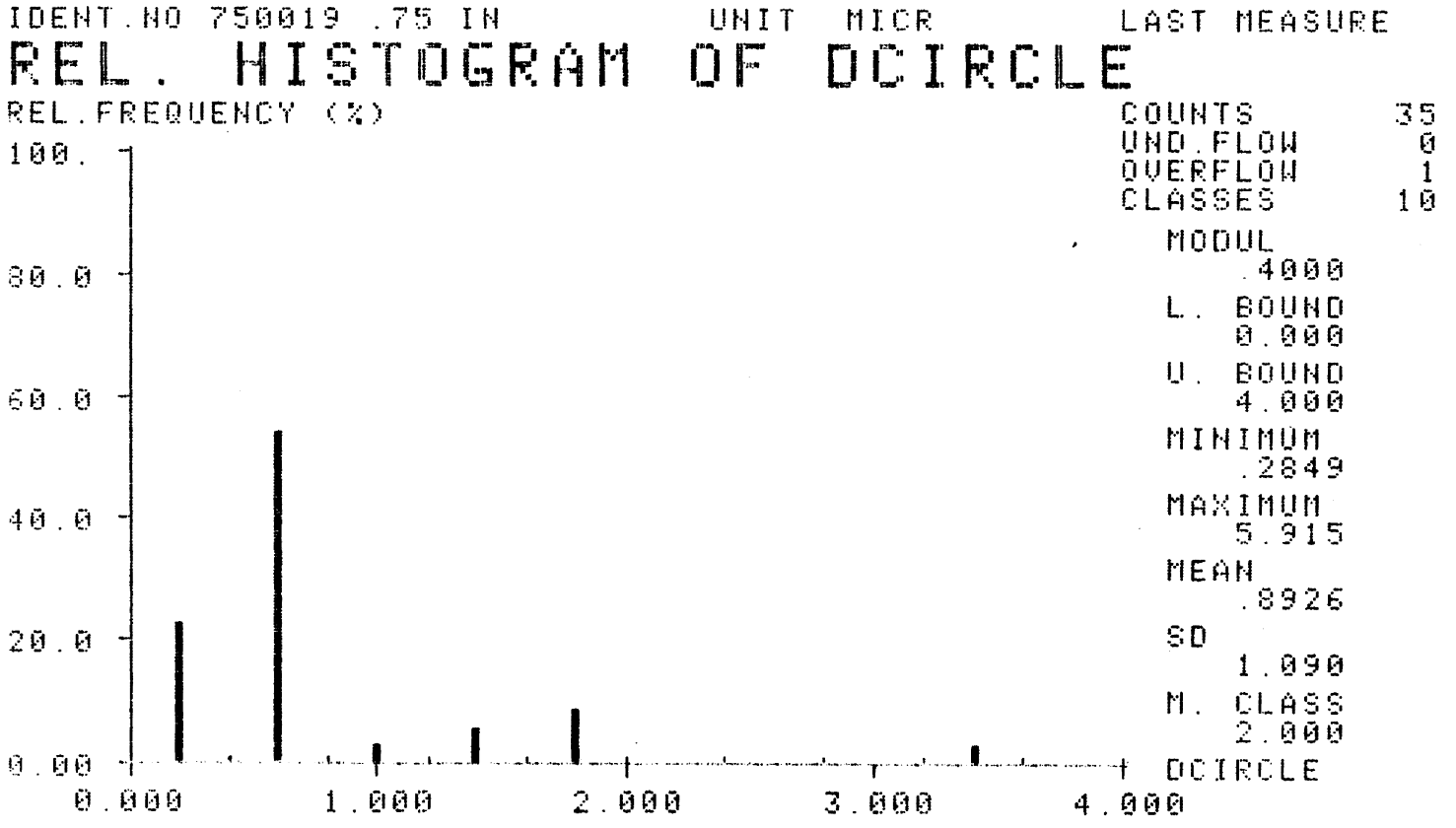

Figure 61a: Domain size distribution, 5-20DP

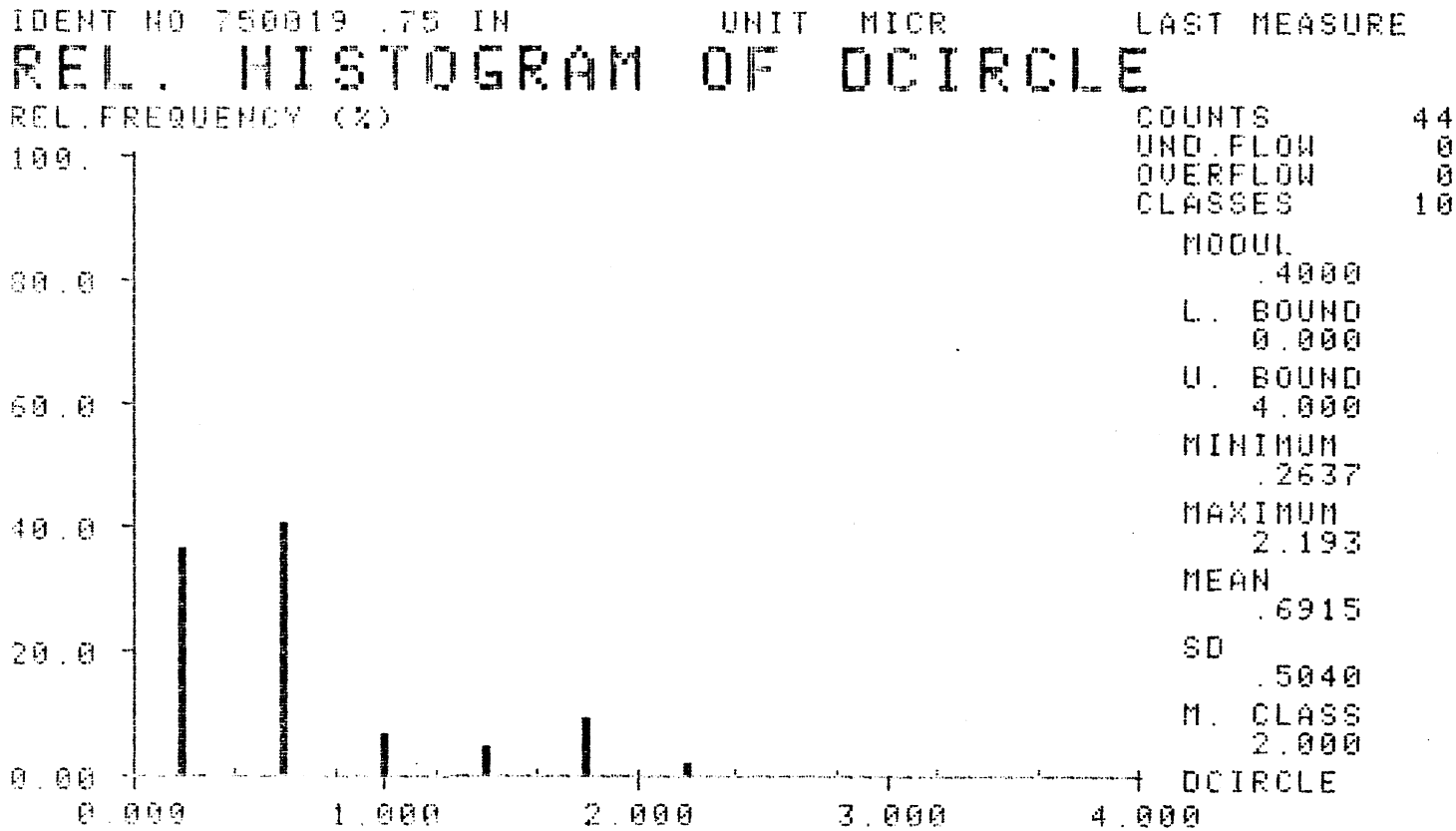

Figure 61b: Domain size distribution, 5-20DP

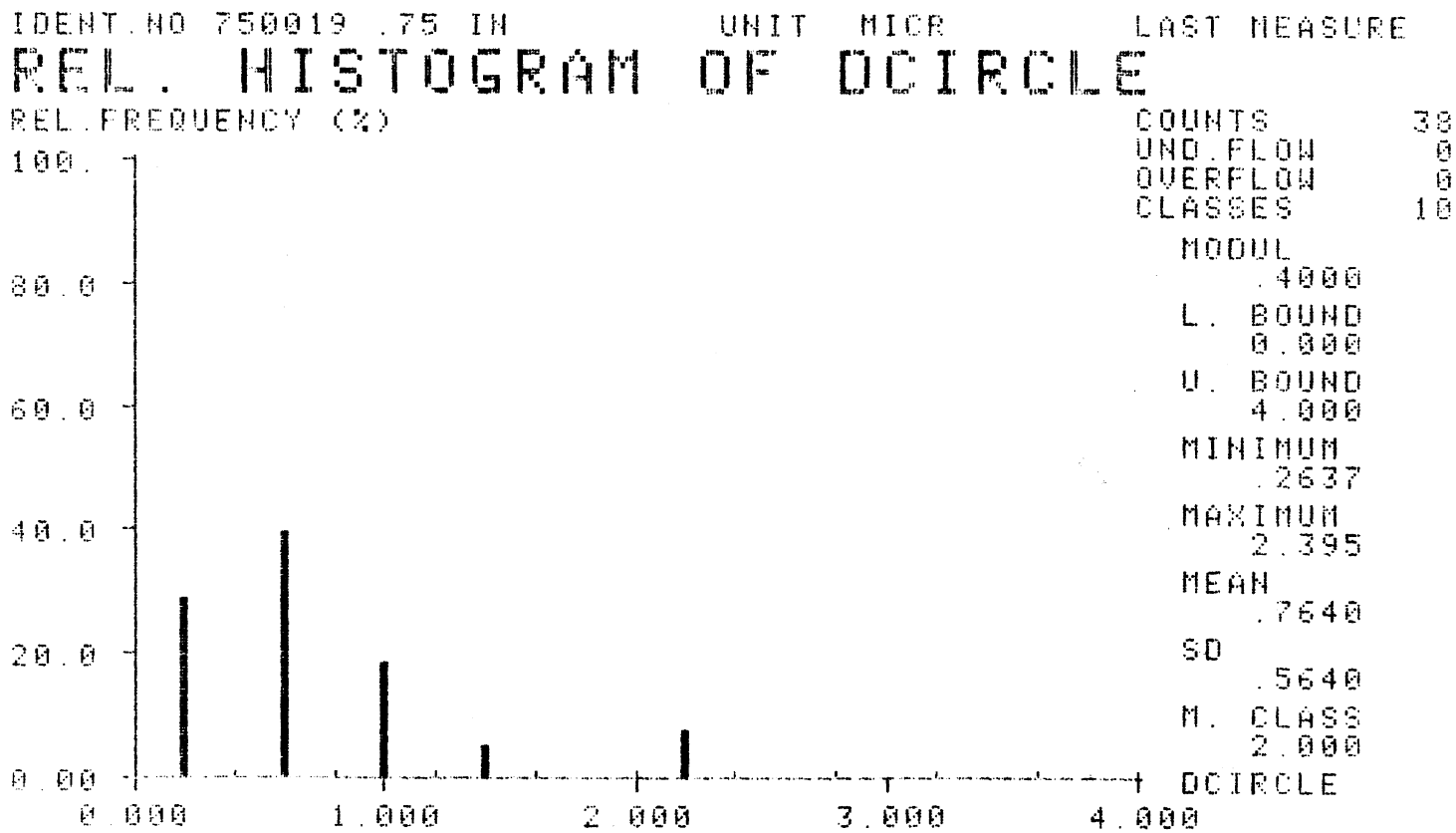

Figure 61c: Domain size distribution, 5-20DP

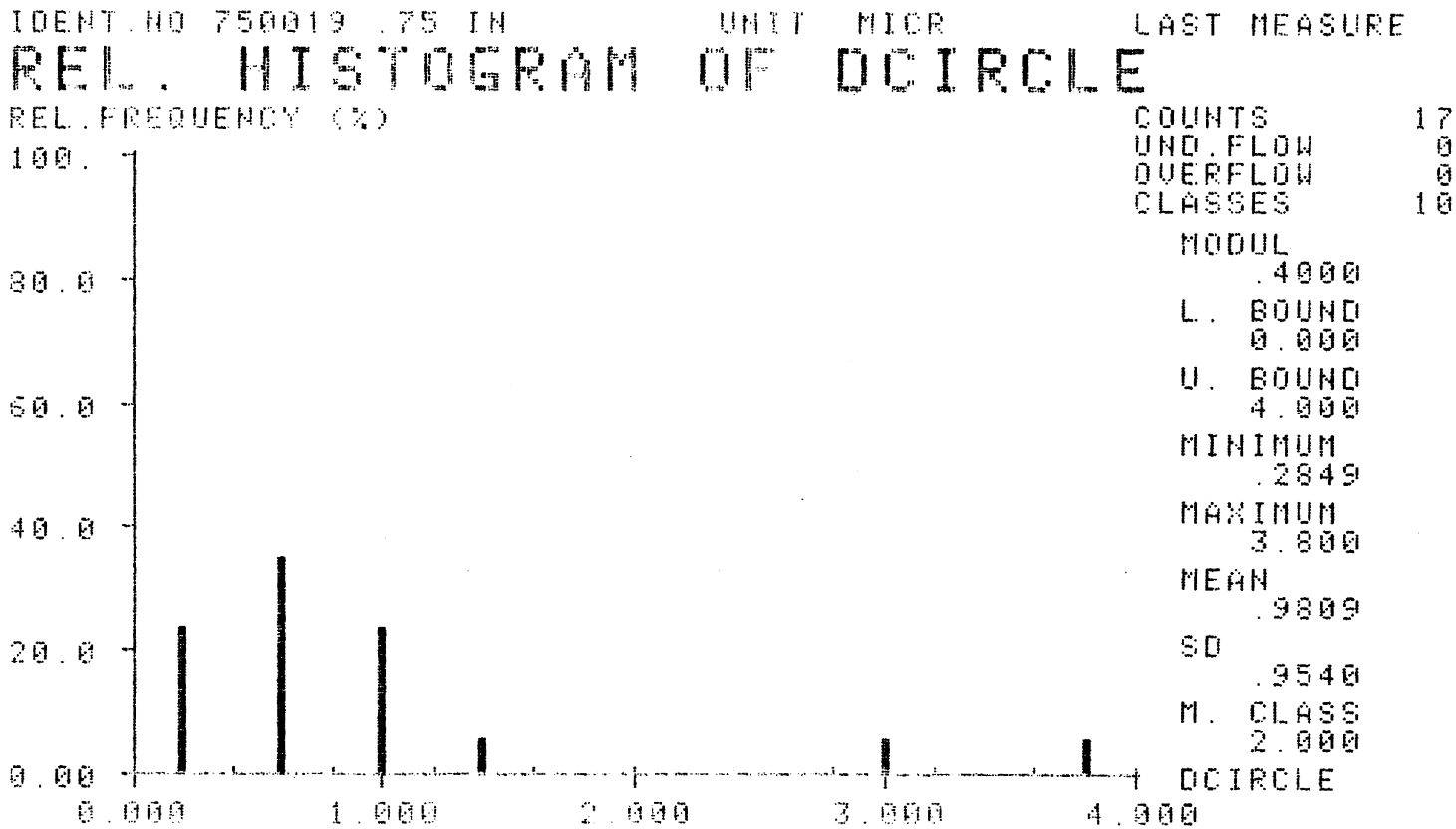

Figure 62a: Domain size distribution, 10-20DP

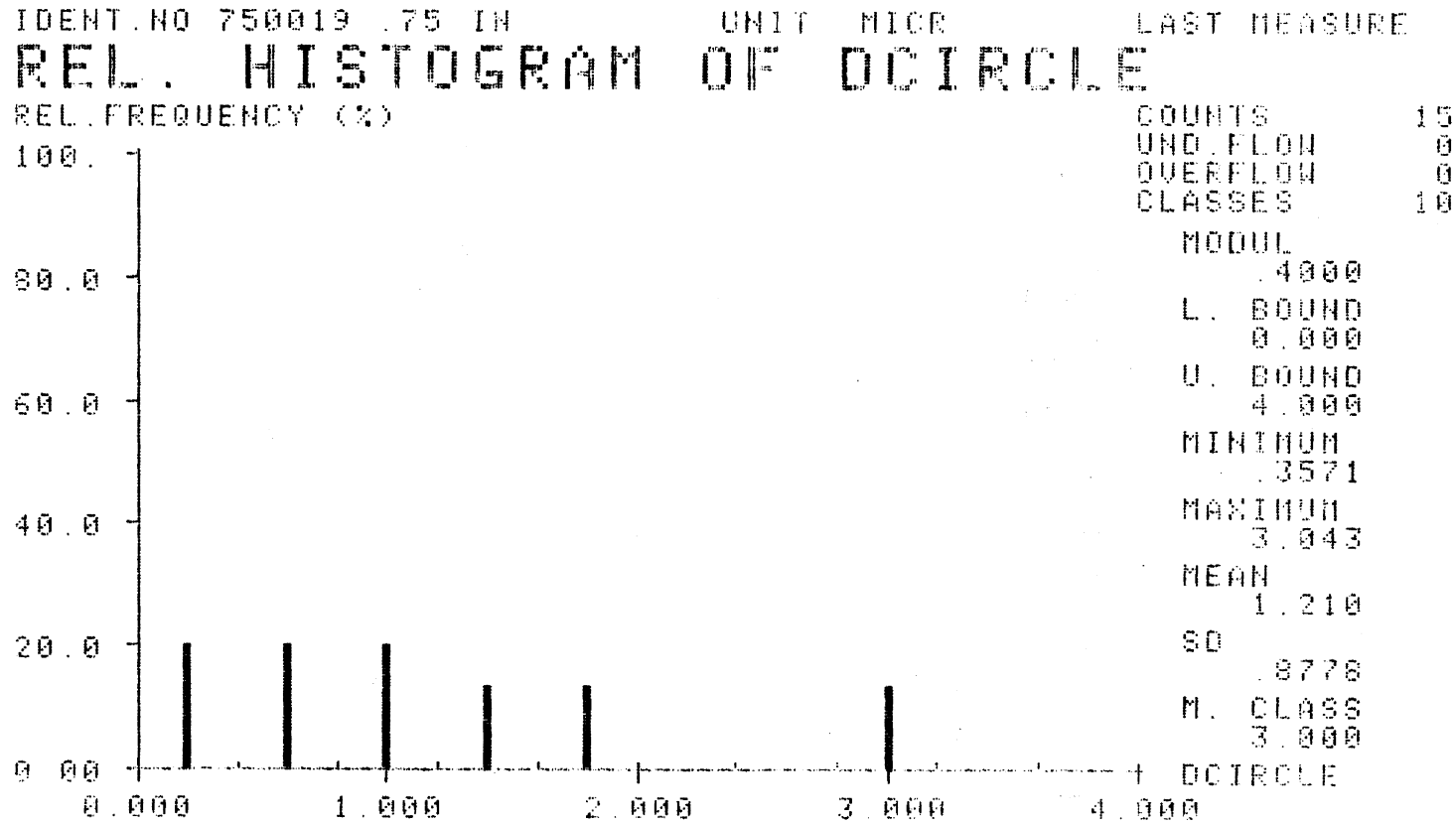

Figure 62b: Domain size disbribution, 10-20DP

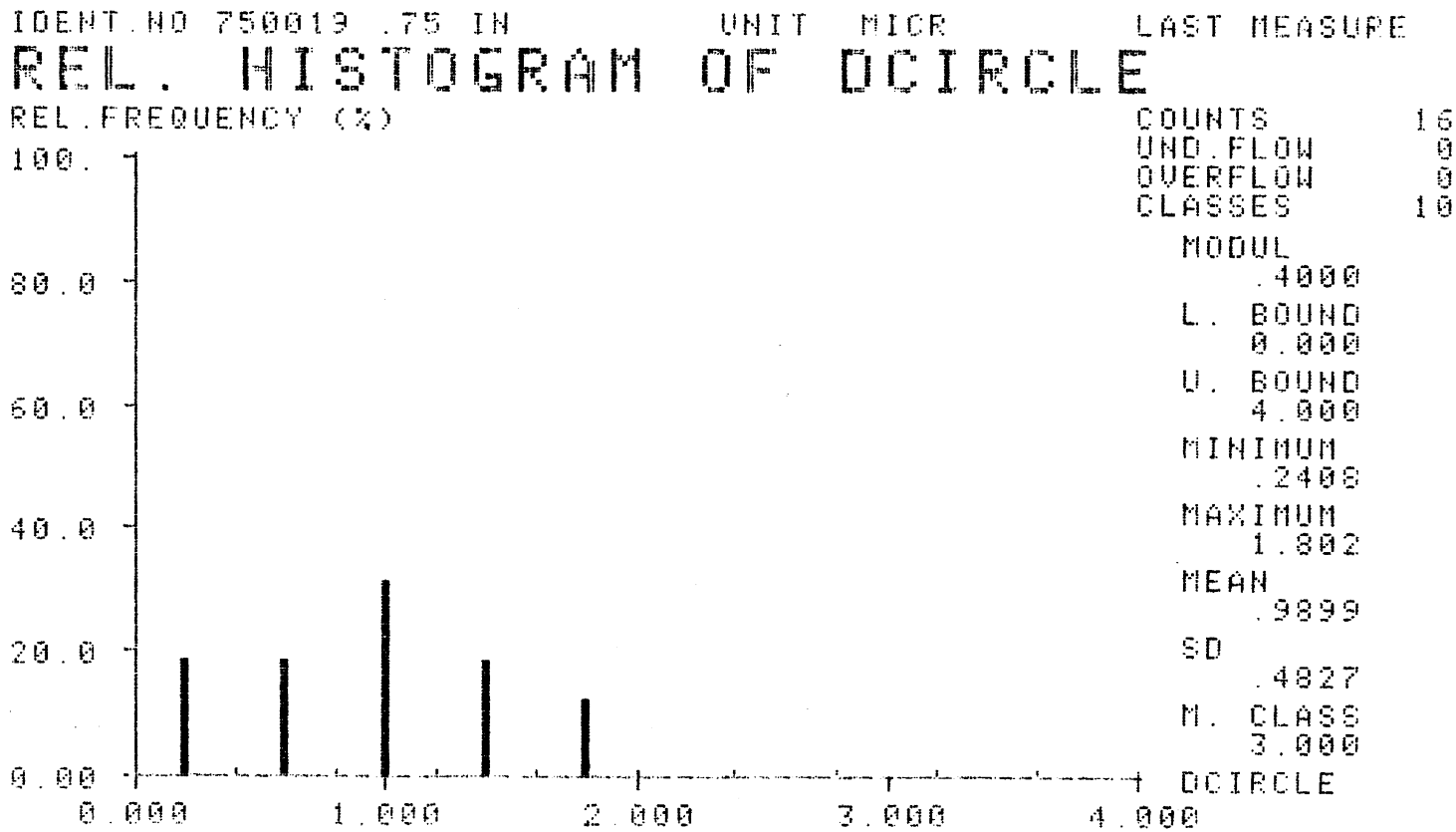

Figure 62c: Domain size disbribution, 10-20DP

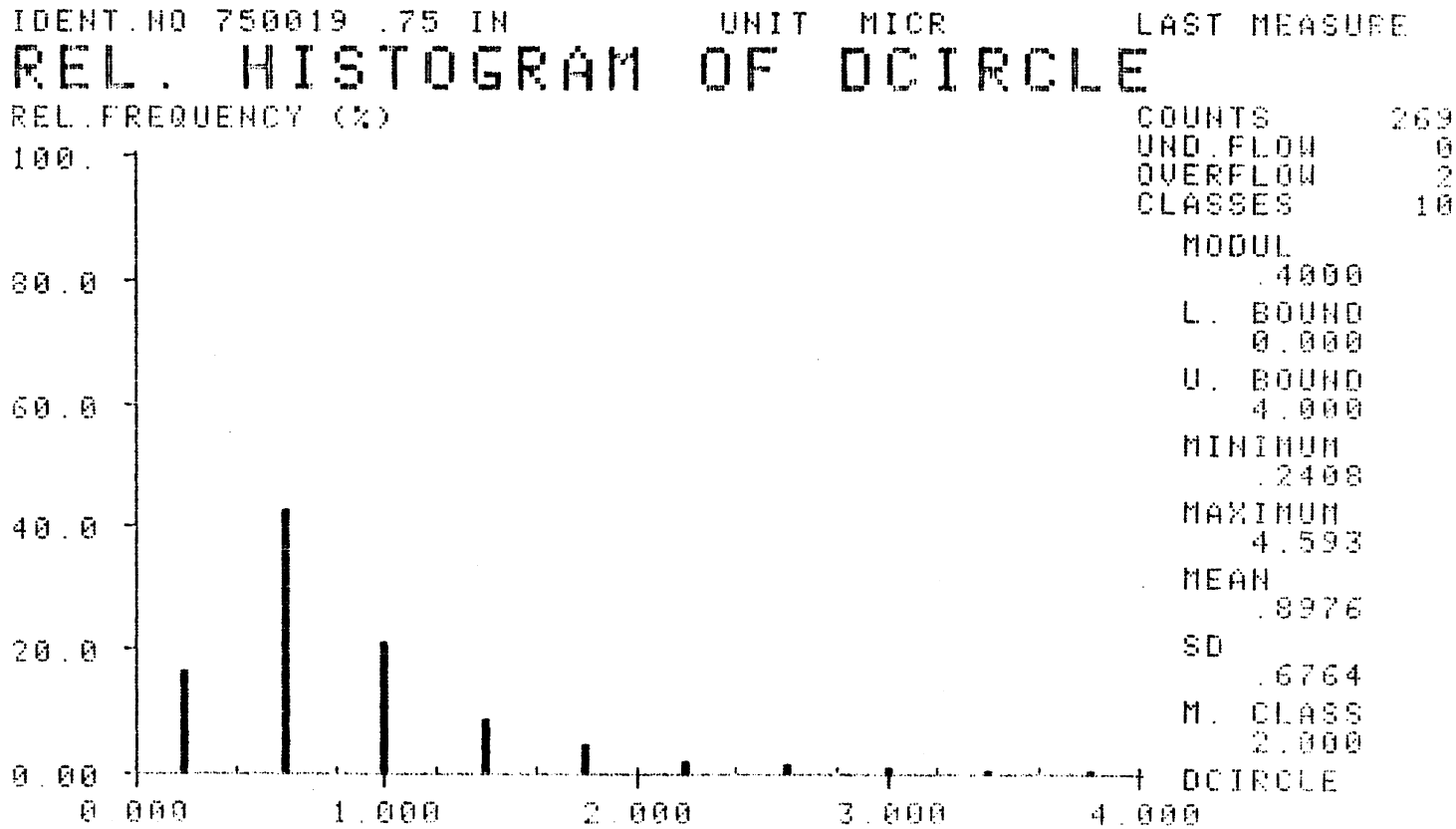

Figure 63a: Domain size distribution, 15-20DP

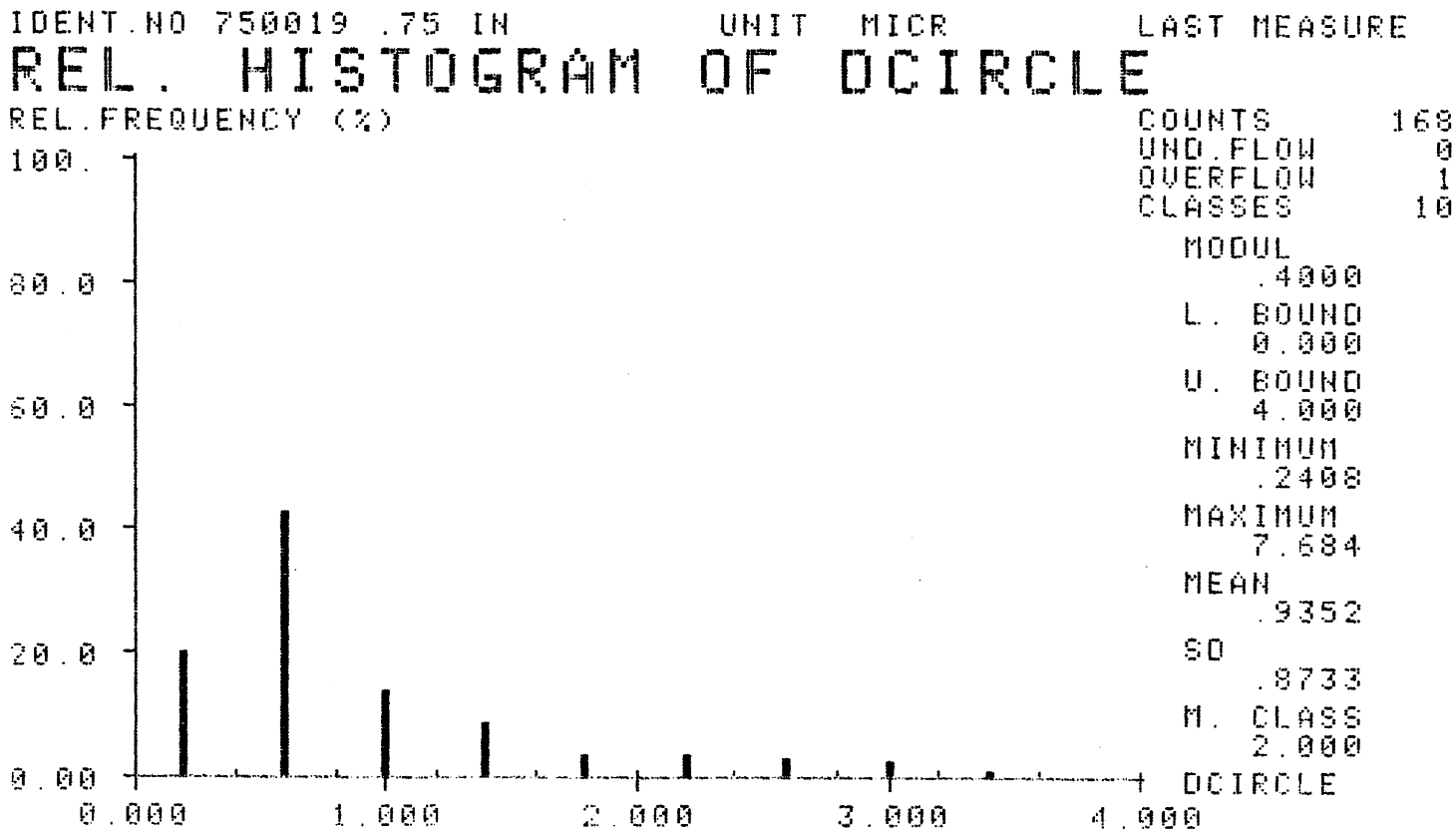

Figure 63b: Domain size distribution, 5-20DP

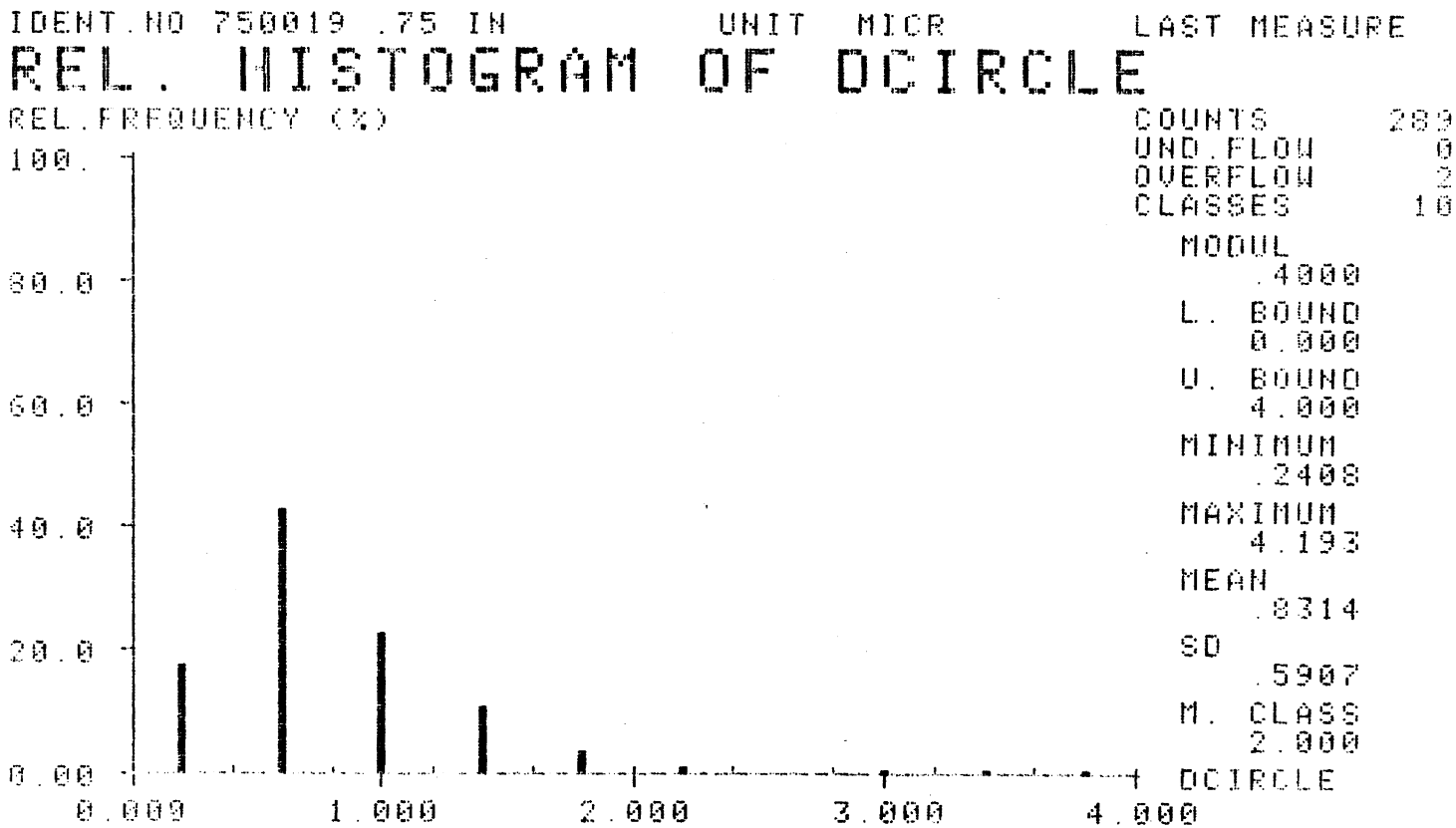

Figure 63c: Domain size distribution, 15-20DP

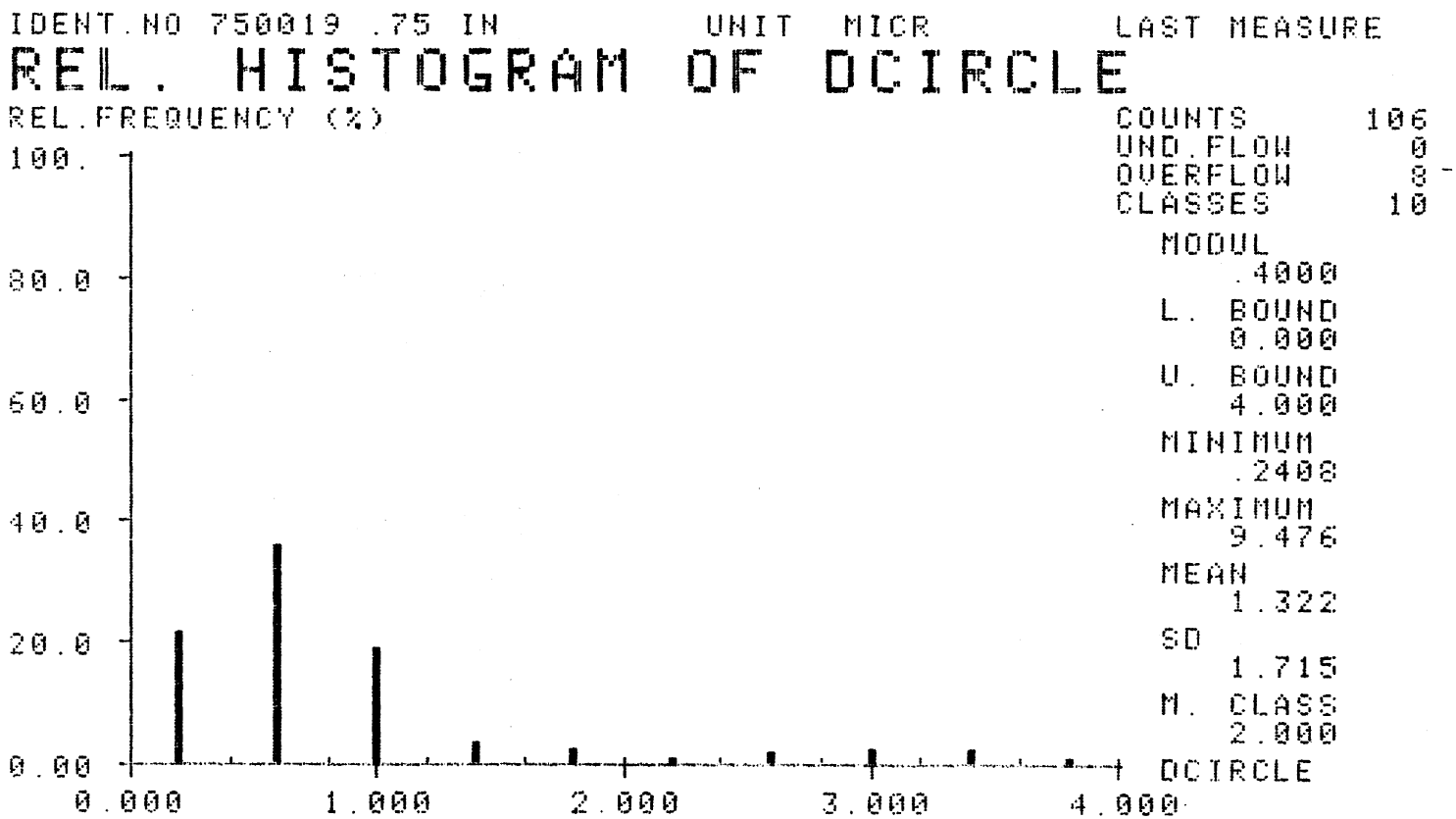

Figure 64a: Domain size distribution, 5-40DP

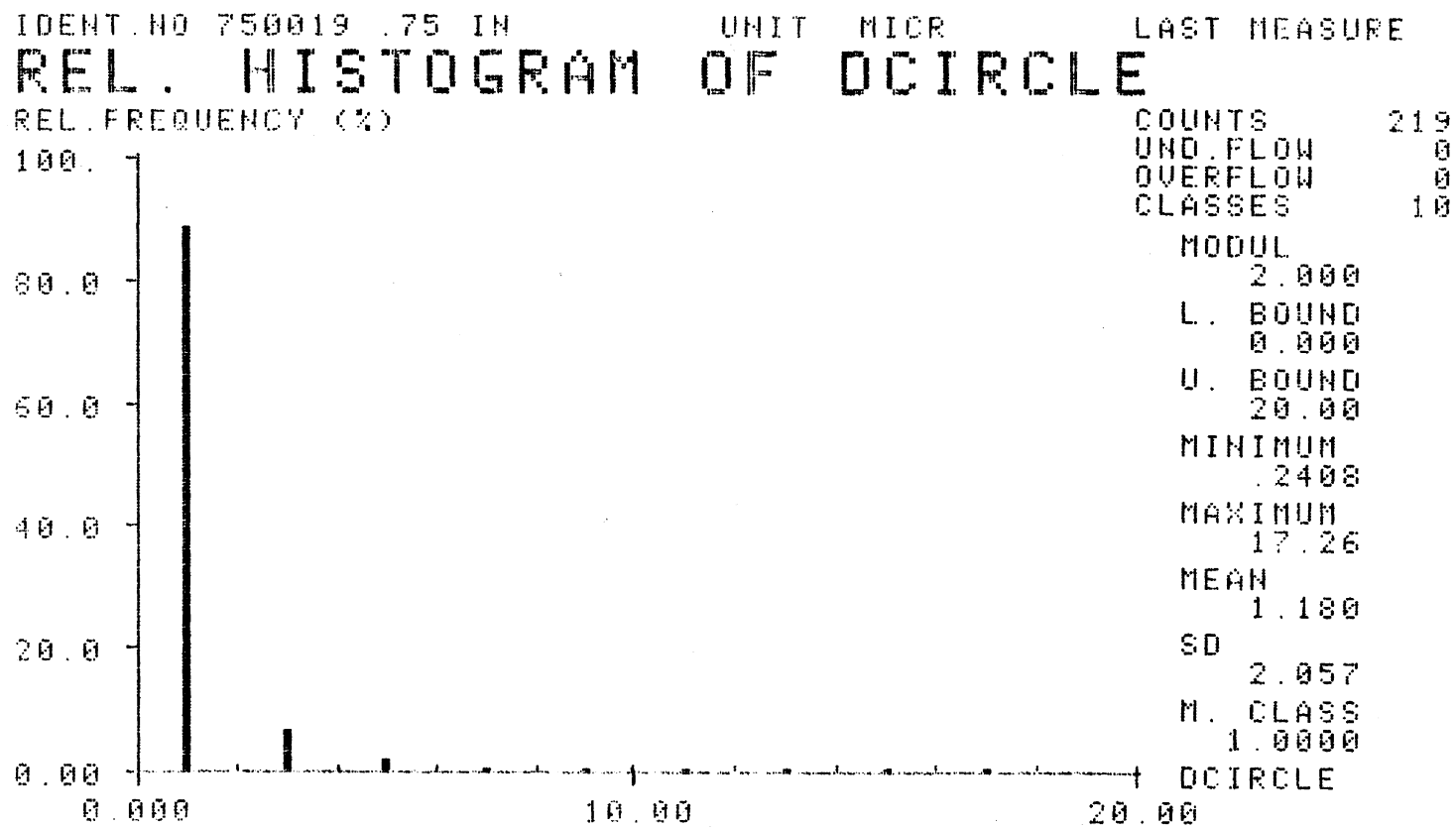

Figure 64b: Domain size distribution, 5-40DP

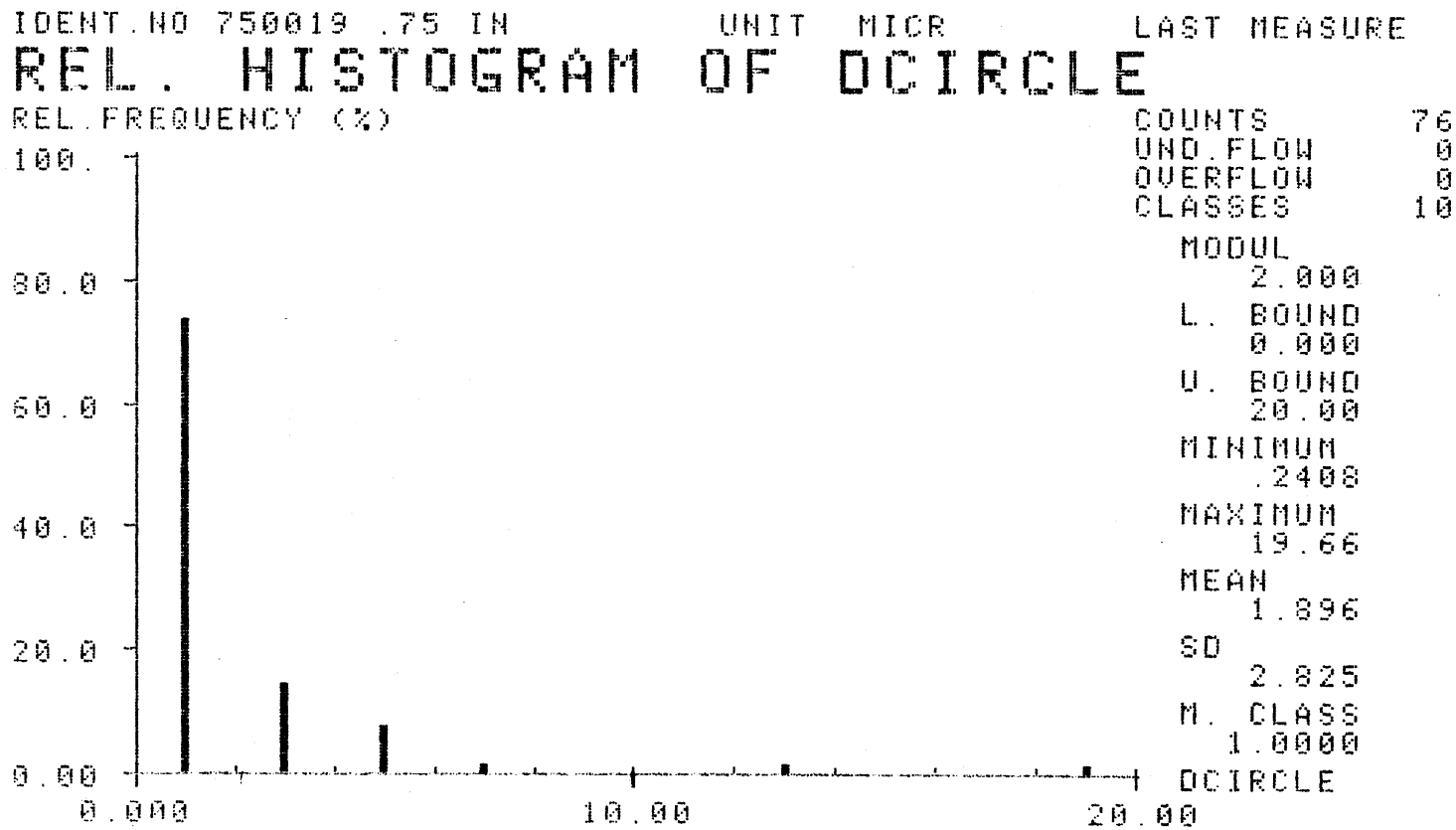

Figure 64c: Domain size distribution, 5-40DP

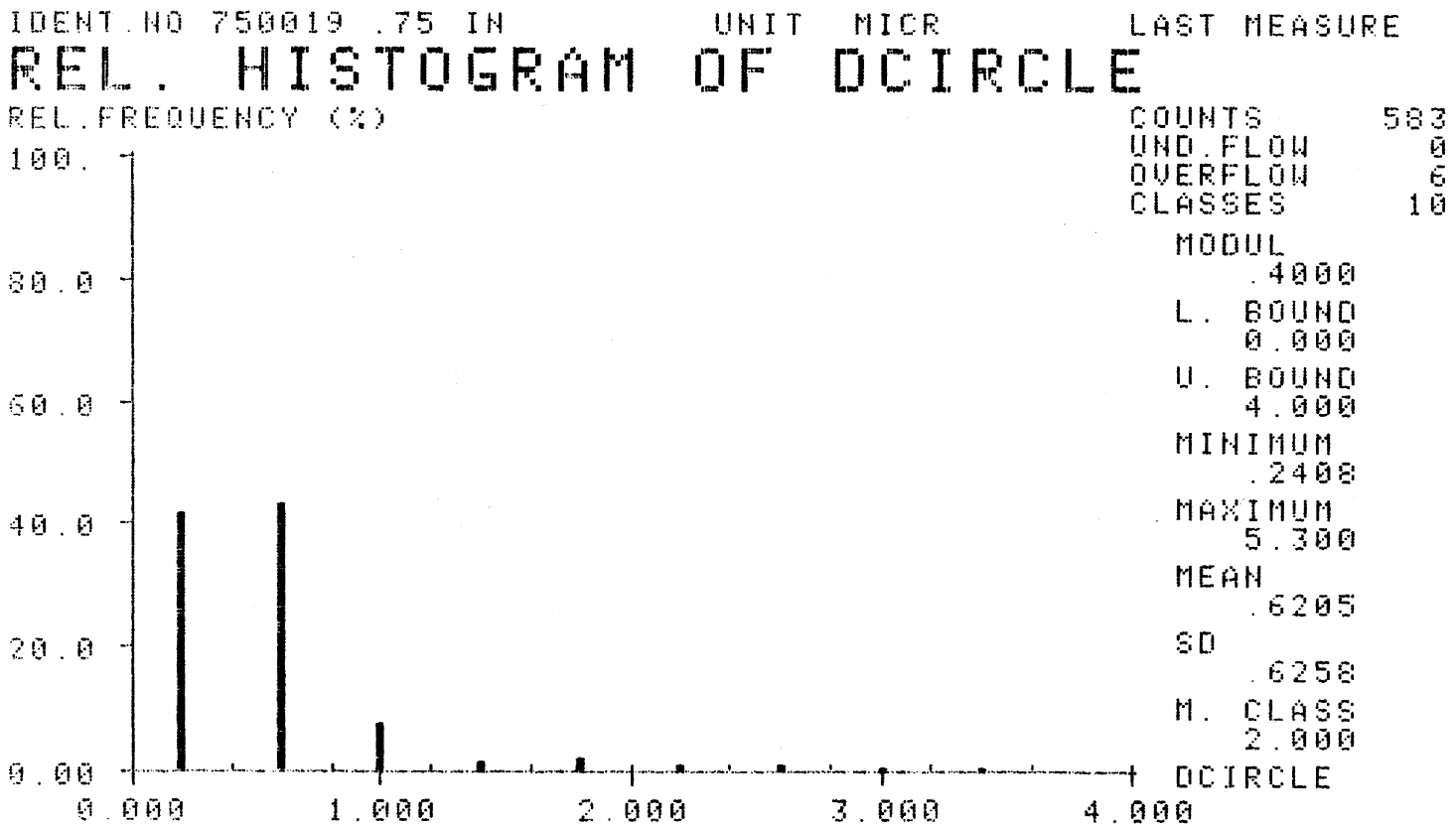

Figure 65a: Domain size distribution, 10-40DP

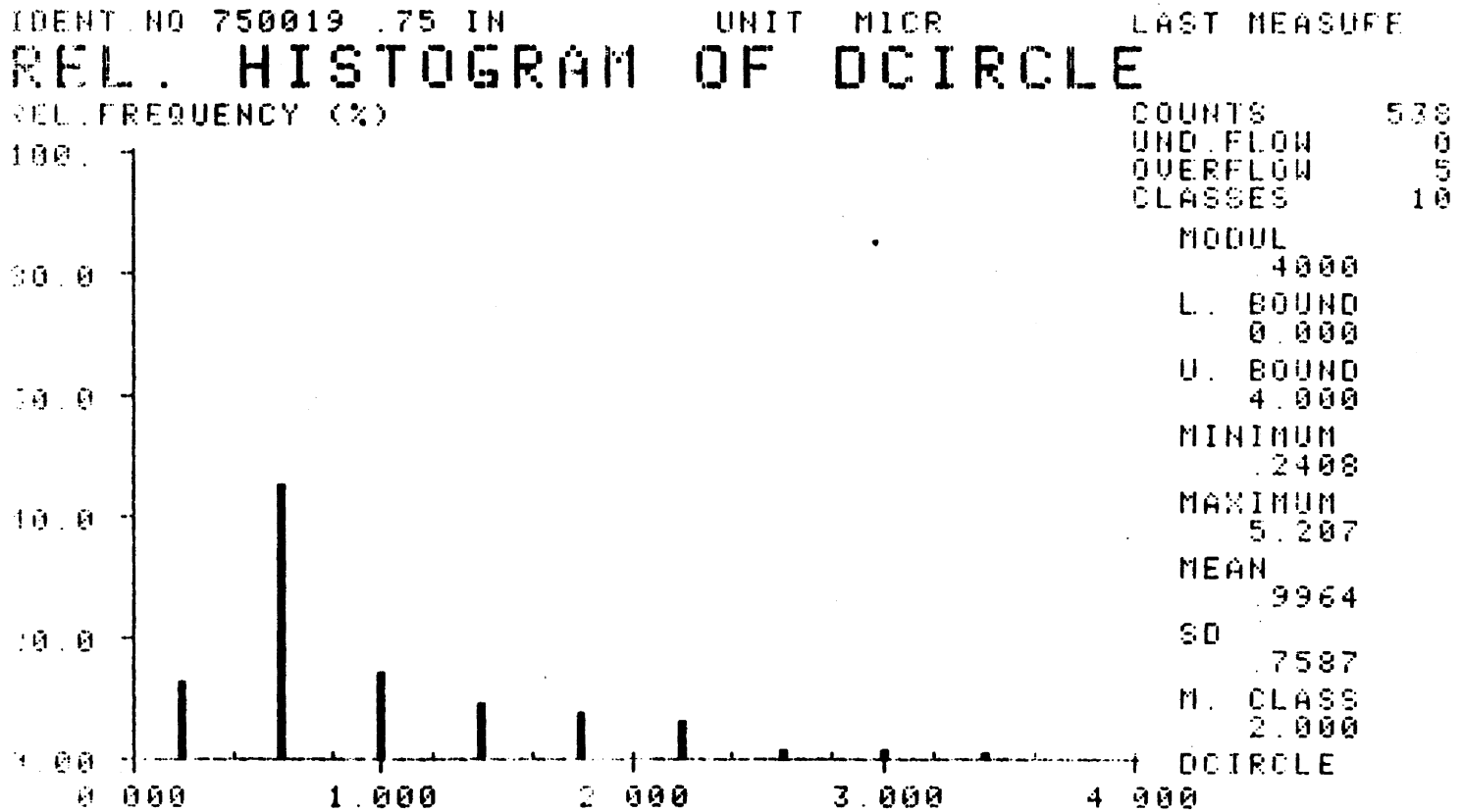

Figure 65b: Domain size distribution, 10-40DP

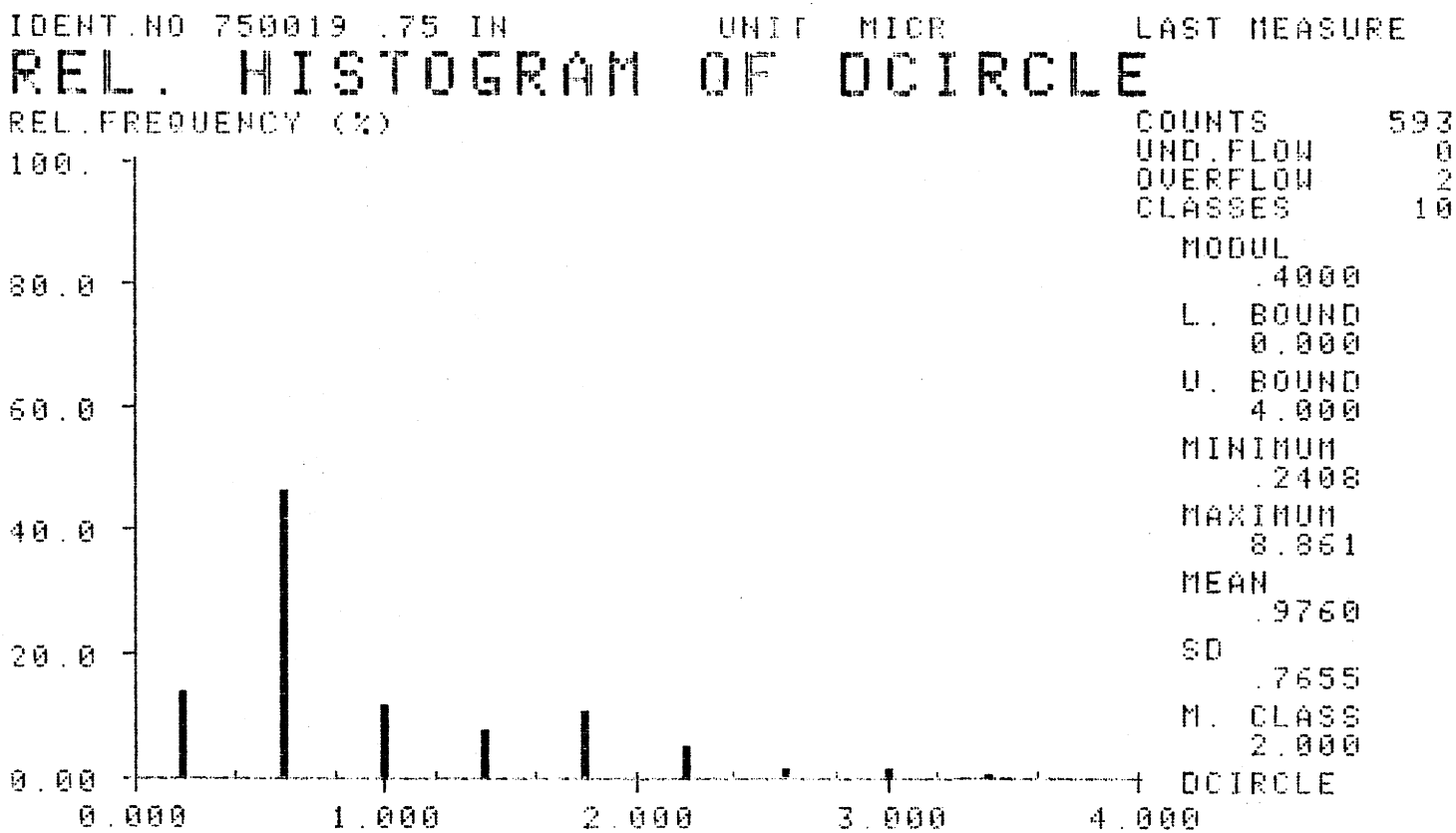

Figure 65c: Domain size distribution, 10-40DP

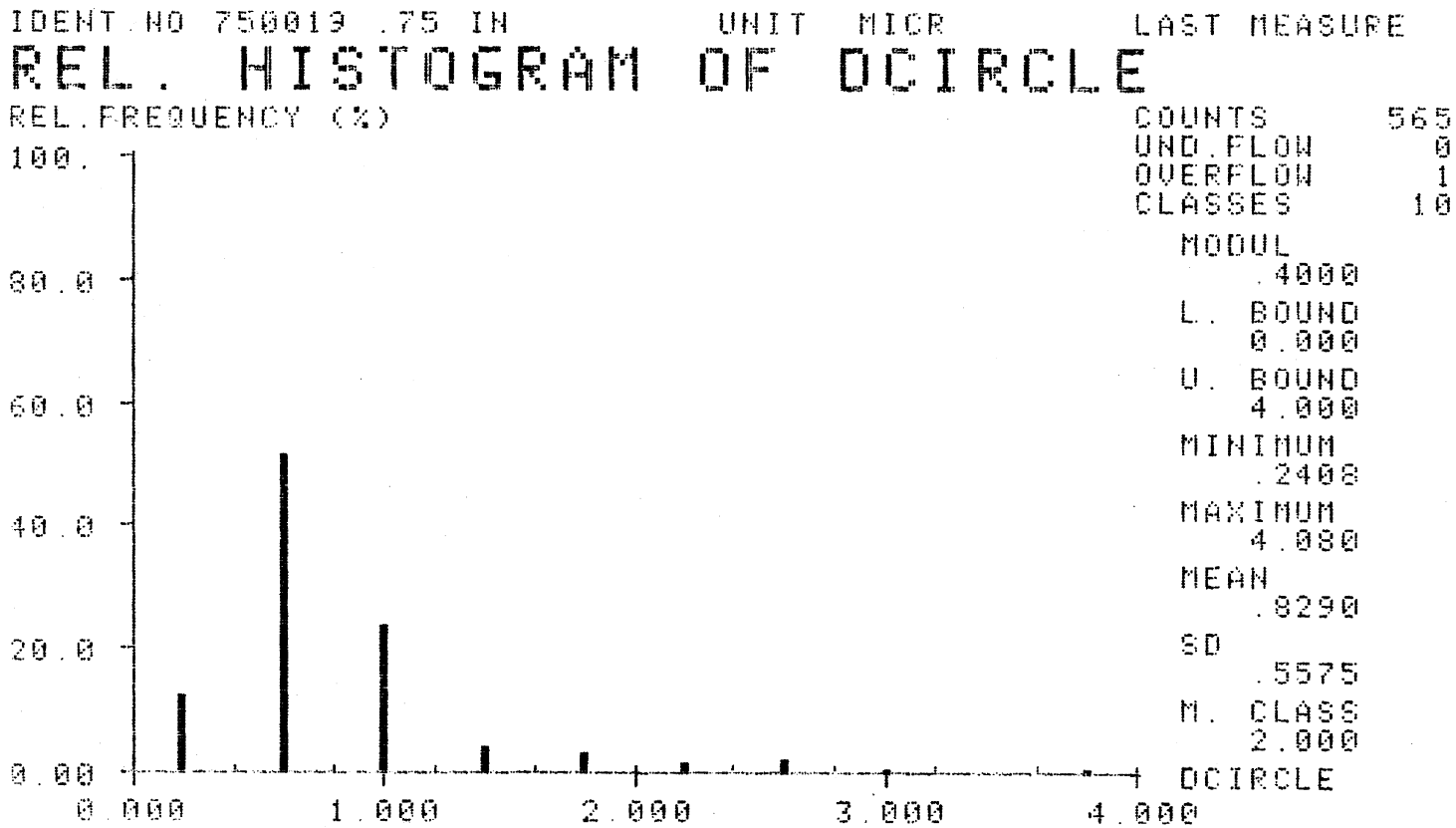

Figure 66a: Domain size distribution, 15-40DP

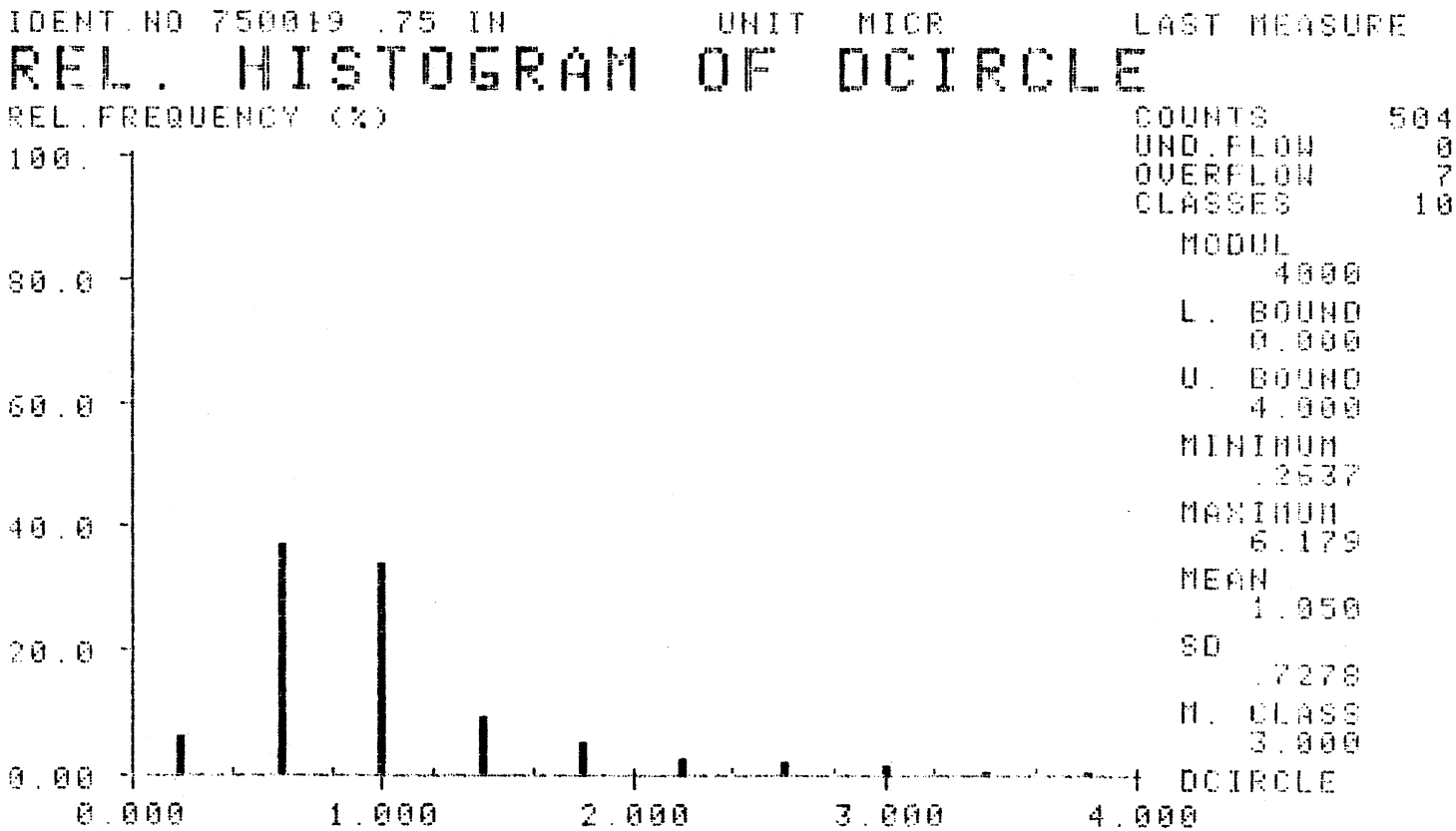

Figure 66b: Domain size distribution, 15-40DP

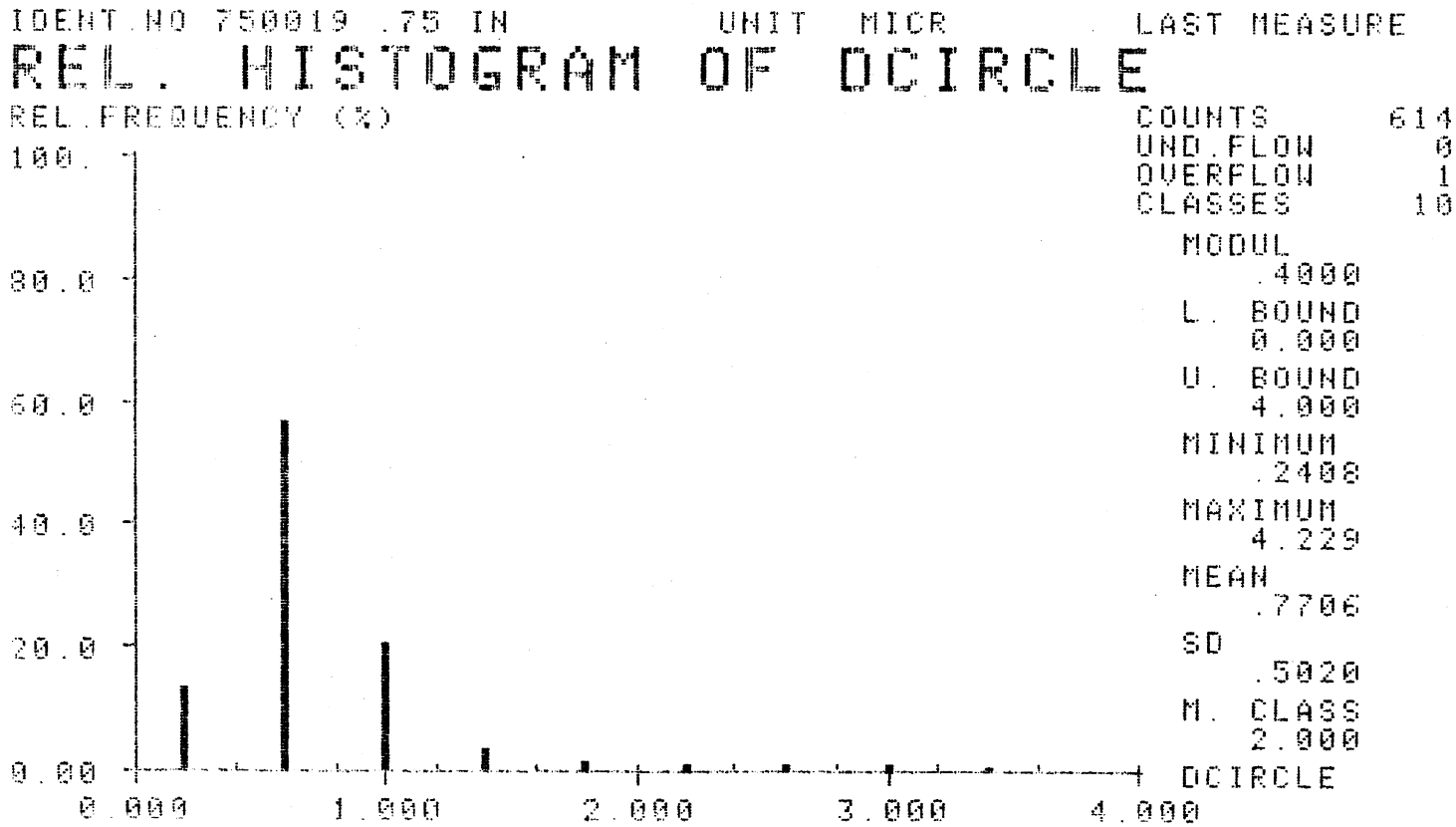

Figure 66c: Domain size distribution, 15-40DP

APPENDIX E

E. Contact Area Equations

The contact area for a ball on plane was estimated using Hertzian contact theory [59]. The area of contact, A, calculated to be

$$A = \pi a^2 \tag{E1}$$

where a is given by Eq. (3). The contact area for ball in a cylindrical groove, A_g, was also estimated using Hertzian contact theory. The area is given by Eq. (E2) below.

$$A_g = \pi a \cdot b \tag{E2}$$

$$a = m\left[\frac{3F}{4} \cdot \frac{k_1 + k_2}{A + B}\right]^{1/3} \tag{E3}$$

$$b = a(n/m)$$

$$m,n = f(\cos\theta) \text{ given in reference 59}$$

$$k_1 = \frac{1 - \nu_1^2}{E_1}$$

$$k_2 = \frac{1 - \nu_2^2}{E_2}$$

$$\cos\theta = \frac{B - A}{B + A}$$

$$A + B = \frac{2}{D_1} - \frac{1}{D_2}$$

$$B - A = \frac{1}{D_2}$$

where,

D_1 = diamter of the ball

D_2 = diameter of the groove

F = applied normal force

ν_1 = Poisson's ratio of the ball material

ν_2 = Poisson's ratio of the epoxy material

E_1 = elastic modulus of the ball material

E_2 = elastic modulus of the epoxy material

APPENDIX F

F. Friction and Wear Data

In the following tables (16-23) friction coefficient, μ, cross-sectional area of wear track, W(cm^2), and diameter of the wear groove, D(mm), are reported at each 2000 cycles (W.R. = wear rate). A linear correlation on diameter of wear grooves versus number of cycles was performed. Correlation coefficients are shown as the last entry under the diameter of wear grooves. Friction and wear data for abrasive tests are reported in Table 24.

TABLE 16

Friction and Wear Data, control

kc	W (cm^2)	μ	d (mm)
4	43.42	0.36	3.85
6	76.44	0.37	4.28
8	108.72	0.37	3.90
10	142.56	0.38	4.22
12	162.87	0.38	4.48
14	171.62	0.38	4.10
			0.23
	W.R. = 13.34×10^{-6} cm^2/kc		
4	45.00	0.35	3.63
6	69.60	0.35	3.80
8	100.00	0.36	3.24
10	119.40	0.36	4.15
12	134.90	0.36	3.65
14	151.10	0.36	3.83
			0.07
	W.R. = 10.66×10^{-6} cm^2/kc		

TABLE 16 (con' t)

Friction and Wear Data, Control

kc	W (cm^2)	μ	d (mm)
4	51.50	0.35	3.90
6	77.61	0.35	4.53
8	113.66	0.36	4.26
10	144.25	0.35	4.86
12	170.45	0.36	4.67
14	195.37	0.37	4.37
			0.28
	W.R. = 14.69×10^{-6} cm^2/kc		
4	48.75	0.35	3.67
6	72.69	0.36	4.34
8	98.60	0.38	4.05
10	119.70	0.38	4.12
12	140.19	0.37	3.66
14	169.75	0.37	4.37
			0.07
	W.R. = 13.30×10^{-6} cm^2/kc		

TABLE 16 (con' t)

Friction and Wear Data, Control

kc	W (cm^2)	μ	d (mm)
4	42.69	0.37	3.59
6	77.70	0.37	3.50
8	104.12	0.36	3.84
10	113.84	0.37	3.98
12	143.40	0.38	3.78
14	160.19	0.38	3.73
			0.27

W.R. = 11.60×10^{-6} cm^2/kc

TABLE 17

Friction and Wear Data, 5-20DP

kc	W (cm^2)	μ	d (mm)
4	18.73	0.32	4.09
6	37.45	0.32	4.22
8	53.30	0.33	4.56
10	81.00	0.35	4.07
12	102.60	0.37	4.22
14	120.30	0.37	4.10
			0.02
	W.R. = 10.44×10^{-6} cm^2/kc		
4	23.07	0.30	5.14
6	52.33	0.31	4.27
8	75.38	0.32	4.16
10	90.68	0.32	4.65
12	101.23	0.33	3.97
14	111.91	0.33	4.63
			0.14
	W.R. = 8.66×10^{-6} cm^2/kc		

TABLE 17 (con' t)

Friction and Wear Data, 5-20DP

kc	W (cm^2)	μ	d (mm)
4	33.50	0.32	----
6	41.10	0.30	----
8	48.40	0.29	----
10	74.40	0.28	----
12	80.40	0.29	----
14	87.30	0.29	----
	W.R. = 5.89×10^{-6} cm^2/kc		
4	34.70	0.28	4.85
6	54.50	0.28	5.10
8	64.90	0.27	3.35
10	65.50	0.26	5.31
12	76.94	0.27	5.10
14	94.11	0.27	4.62
			0.004
	W.R. = 5.21×10^{-6} cm^2/kc		

TABLE 17 (con' t)

Friction and Wear Data, 5-20DP

kc	W (cm^2)	μ	d (mm)
4	17.90	0.30	4.96
6	45.80	0.30	4.91
8	59.30	0.31	5.42
10	69.56	0.31	4.62
12	74.55	0.30	4.76
14	85.12	0.29	4.47
			0.36

W.R. = 6.20×10^{-6} cm^2/kc

TABLE 18

Friction and Wear Data, 10-20DP

kc	W (cm^2)	μ	d (mm)
4	76.40	0.35	----
6	99.90	0.35	----
8	139.30	0.35	----
10	163.30	0.35	----
12	185.10	0.36	----
14	235.40	0.36	----
	W.R. = 15.80×10^{-6} cm^2/kc		
4	53.12	0.36	4.20
6	92.53	0.37	3.78
8	116.03	0.37	3.80
10	134.10	0.38	3.98
12	155.60	0.37	3.73
14	188.50	0.38	3.98
			0.13
	W.R. = 12.63×10^{-6} cm^2/kc		

TABLE 18 (con' t)

Friction and Wear Data, 10-20DP

kc	W (cm^2)	μ	d (mm)
4	69.70	0.35	4.42
6	86.70	0.34	4.28
8	107.00	0.35	4.11
10	111.30	0.34	3.66
12	118.22	0.35	3.90
14	137.30	0.34	3.67
			0.80
	W.R. = 7.80×10^{-6} cm^2/kc		
4	46.14	0.34	4.14
6	70.70	0.33	4.39
8	90.91	0.34	3.67
10	110.64	0.35	4.00
12	123.28	0.36	4.10
14	164.10	0.35	3.64
			0.30
	W.R. = 10.34×10^{-6} cm^2/kc		

TABLE 18 (con' t)

Friction and Wear Data, 10-20DP

kc	W (cm^2)	μ	d (mm)
4	79.70	0.35	4.14
6	135.75	0.35	4.12
8	134.10	0.34	3.81
10	160.30	0.34	3.76
12	164.50	0.36	3.82
14	204.80	0.36	3.51
			0.80

W.R. = 12.75×10^{-6} cm^2/kc

TABLE 19

Friction and Wear Data, 15-20DP

kc	W (cm^2)	μ	d (mm)
4	13.00	0.24	----
6	20.60	0.23	4.81
8	24.75	0.23	5.22
10	42.87	0.28	4.60
12	57.20	0.28	4.49
14	65.40	0.29	4.57
			0.40
	W.R. = 5.57×10^{-6} cm^2/kc		
4	12.65	0.22	----
6	15.30	0.23	----
8	16.10	0.23	----
10	19.04	0.23	----
12	18.60	0.23	----
14	20.90	0.23	----
	W.R. = 0.80×10^{-6} cm^2/kc		

TABLE 19 (con' t)

Friction and Wear Data, 15-20DP

kc	W (cm^2)	μ	d (mm)
4	20.10	0.20	5.91
6	19.62	0.20	4.45
8	24.70	0.21	5.07
10	31.40	0.21	5.27
12	32.00	0.21	5.40
14	35.40	0.21	4.61
			0.12
	W.R. = 2.23×10^{-6} cm^2/kc		
4	11.05	0.25	5.34
6	16.00	0.23	4.87
8	20.50	0.23	5.60
10	22.90	0.24	5.34
12	26.40	0.24	5.85
14	28.70	0.25	4.80
			0.00
	W.R. = 1.66×10^{-6} cm^2/kc		

TABLE 20

Friction and Wear Data, 5-40DP

kc	W (cm^2)	μ	d (mm)
4	26.40	0.32	3.92
6	27.56	0.35	3.65
8	56.20	0.33	3.73
10	70.57	0.30	4.04
12	81.97	0.31	3.56
14	103.10	0.32	3.97
			0.006
	W.R. = 6.90×10^{-6} cm^2/kc		
4	53.80	0.34	3.65
6	105.10	0.35	4.27
8	126.30	0.35	3.70
10	150.70	0.35	3.63
12	164.60	0.35	3.79
14	195.00	0.35	3.64
			0.11
	W.R. = 12.90×10^{-6} cm^2/kc		

TABLE 20 (con' t)

Friction and Wear Data, 5-40DP

kc	W (cm^2)	μ	d (mm)
4	87.80	0.32	4.16
6	121.10	0.31	4.36
8	147.20	0.32	4.52
10	171.10	0.32	4.46
12	192.00	0.32	4.51
14	225.40	0.32	4.38
			0.35
	W.R. = 13.20×10^{-6} cm^2/kc		
4	78.70	0.30	4.27
6	96.20	0.30	4.41
8	122.40	0.30	4.16
10	138.70	0.30	4.03
12	152.70	0.30	4.37
14	174.30	0.30	4.23
			0.03
	W.R. = 9.48×10^{-6} cm^2/kc		

TABLE 21

Friction and Wear Data, 10-40DP

kc	W (cm^2)	μ	d (mm)
4	76.10	0.30	4.99
6	89.60	0.31	5.19
8	108.70	0.32	5.28
10	132.20	0.32	4.65
12	154.00	0.32	4.67
14	165.90	0.32	5.00
			0.20
	W.R. = 9.51×10^{-6} cm^2/kc		
4	15.10	0.28	5.47
6	32.20	0.29	4.84
8	52.30	0.30	5.16
10	76.70	0.31	4.62
12	95.80	0.32	4.52
14	112.50	0.32	4.58
			0.7
	W.R. = 10.0×10^{-6} cm^2/kc		

TABLE 21 (con' t)

Friction and Wear Data, 10-40DP

kc	W (cm^2)	μ	d (mm)
4	36.30	0.30	4.65
6	43.90	0.31	4.05
8	58.40	0.31	4.21
10	68.44	0.32	4.42
12	75.90	0.31	3.96
14	86.50	0.32	4.07
			0.30

W.R. = 5.71×10^{-6} cm^2/kc

TABLE 22

Friction and Wear Data, 15-40DP

kc	W (cm^2)	μ	d (mm)
4	21.70	0.20	4.43
6	22.50	0.20	4.98
8	26.00	0.22	4.87
10	26.53	0.24	4.63
12	32.60	0.24	3.50
14	35.40	0.25	4.21
			0.30
	W.R. = 1.28×10^{-6} cm^2/kc		
4	27.10	0.26	5.17
6	29.10	0.26	4.66
8	36.30	0.26	4.16
10	44.80	0.26	4.35
12	45.90	0.25	4.64
14	48.90	0.25	4.56
			0.2
	W.R. = 2.41×10^{-6} cm^2/kc		

TABLE 22 (con' t)

Friction and Wear Dtat, 15-40DP

kc	W (cm^2)	μ	d (mm)
4	26.70	0.25	5.17
6	37.50	0.24	5.46
8	38.80	0.24	5.40
10	43.53	0.24	4.92
12	50.00	0.24	5.37
14	53.60	0.24	5.18
			0.00
	W.R. = 2.52×10^{-6} cm^2/kc		
4	19.10	0.24	5.63
6	29.00	0.24	5.49
8	34.20	0.24	5.44
10	38.80	0.24	4.97
12	46.20	0.25	5.29
14	55.80	0.25	4.78
			0.7
	W.R. = 3.43×10^{-6} cm^2/kc		

TABLE 23

Friction and Wear Data, w/o Debris Tests 5-40DP

kc	W (cm^2)	μ	d (mm)
4	56.70	0.33	3.47
6	86.10	0.32	3.84
8	124.40	0.33	4.14
10	147.53	0.34	3.65
12	158.90	0.35	3.62
14	191.40	0.34	3.61
			0.01
	W.R. = 13.1×10^{-6} cm^2/kc		
4	60.90	0.32	4.00
6	75.20	0.32	3.73
8	104.10	0.32	3.48
10	135.50	0.33	3.89
12	157.10	0.33	3.99
14	183.40	0.34	3.63
			0.03
	W.R. = 12.7×10^{-6} cm^2/kc		

TABLE 23 (con' t)

Friction and Wear Data, w/o Debris Tests 5-40DP

kc	W (cm^2)	μ	d (mm)
4	-----	----	----
6	29.80	0.31	5.37
8	62.16	0.32	4.47
10	83.40	0.33	4.49
12	110.90	0.32	4.46
14	120.20	0.33	----
			0.6

W.R. = 11.5×10^{-6} cm^2/kc

TABLE 23 (con' t)

Friction and Wear Data, w/o Debris Tests 10-40DP

kc	W (cm^2)	μ	d (mm)
4	57.90	0.31	4.98
6	100.80	0.30	4.63
8	125.00	0.31	4.80
10	165.23	0.32	4.03
12	186.00	0.31	4.29
14	221.00	0.33	4.02
			0.7
	W.R. = 15.7×10^{-6} cm^2/kc		
4	47.15	0.32	4.97
6	73.60	0.33	4.68
8	114.20	0.33	4.65
10	136.20	0.32	4.50
12	161.20	0.33	4.11
14	187.00	0.33	4.43
			0.7
	W.R. = 14.1×10^{-6} cm^2/kc		

TABLE 23 (con' t)

Friction and Wear Data, w/o Debris Tests 15-40DP

kc	W (cm^2)	μ	d (mm)
4	35.90	0.31	4.96
6	51.40	0.30	4.73
8	66.90	0.31	4.58
10	94.23	0.31	4.92
12	93.30	0.32	4.74
14	131.10	0.32	5.14
			0.008
	W.R. = 9.07×10^{-6} cm^2/kc		
4	38.05	0.32	5.06
6	58.10	0.33	4.74
8	78.60	0.34	4.68
10	99.10	0.34	4.76
12	115.10	0.35	4.24
14	135.70	0.36	4.50
			0.6
	W.R. = 9.71×10^{-6} cm^2/kc		

TABLE 24

Friction and Wear Data, Abrasive Tests, control

cycles	M (mg)	M (mg)	M (mg)
50	10.90	10.54	10.09
100	20.46	19.78	19.46
150	29.62	28.54	28.72
200	38.69	37.05	37.73
250	47.56	45.45	46.23
300	56.40	53.74	54.16
350	64.96	61.97	61.94
$\mu =$	0.71	0.72	0.70
W.R. = (mg/m)	2.25	2.14	2.16
50	10.19	9.27	10.54
100	19.61	17.47	19.64
150	28.61	24.99	27.86
200	37.17	32.51	35.68
250	45.57	40.63	43.51
300	53.97	47.64	51.28
350	63.46	53.84	59.07
$\mu =$	0.73	0.70	0.72
W.R. = (mg/m)	2.19	1.87	2.0

TABLE 24 (con' t)

Friction and Wear Data, Abrasive Tests

upper: 5-40DP, lower: 15-40DP

cycles	M (mg)	M (mg)	M (mg)	M (mg)
50	5.0	9.30	9.61	8.56
100	10.0	17.15	19.83	16.18
150	14.6	24.65	27.93	23.66
200	19.8	31.64	34.20	30.37
250	25.0	38.40	41.64	36.86
300	29.5	44.95	48.83	43.04
350	34.5	51.44	55.37	49.34
μ =	0.66	0.66	0.65	0.67
W.R. = (mg/m)	1.24	1.75	1.91	1.69
50	3.60	6.47	8.95	8.86
100	6.7	11.73	15.77	15.55
150	10.25	16.66	21.12	21.09
200	13.60	21.42	26.86	27.21
250	17.40	26.06	32.23	31.94
300	20.17	30.79	37.21	37.54
350	23.70	35.70	42.60	41.81
μ =	0.63	0.62	0.62	0.61
W.R. = (mg/m)	0.825	1.21	1.37	1.37

The vita has been removed from the scanned document